CRANFIELD UNIVERSITY

D. Y. LEE

WAKE AFFECTED BOUNDARY LAYER FLOWS WITHIN AN EMBEDDED STAGE OF A MULTI-STAGE AXIAL COMPRESSOR

SCHOOL OF MECHANICAL ENGINEERING

MPhil THESIS

CRANFIELD UNIVERSITY

SCHOOL OF MECHANICAL ENGINEERING

MPhil THESIS

Academic Year 2000-2001

D. Y. LEE

WAKE AFFECTED BOUNDARY LAYER FLOWS WITHIN AN EMBEDDED STAGE OF A MULTI-STAGE AXIAL COMPRESSOR

Supervisors: **Professor Robin L. Elder**
Dr. Ian Bennett

June 2001

This thesis is submitted in partial fulfilment of the requirements for the degree of MPhil in Turbomachinery

ABSTRACT

Boundary Layer Flows in turbomachines have been recognised to crucially influence the stability and performance of gas turbine components particularly the compressor since its function is to provide a pressure rise through diffusion that is accompanied by an adverse pressure gradient. This brings about the danger of separation of flow and thus understanding the behaviour and control of the boundary layer is of great importance. The interaction between stationary and rotating blade rows inevitably make the flow environment within a multi-stage axial compressor unsteady, Dean (1959). Stator blades are subjected to periodic wakes from upstream rotor rows, which initiate transition that is very much unlike those encountered in a steady state (clean) flow conditions.

This thesis describes the third stage of the fundamental research on boundary layer flows in turbomachinery at Cranfield University. The feature that makes this experimental work unique is that with constant temperature hot-wire anemometry (CTA) as the principal tool, detailed boundary layer surveys have been carried out within real turbomachinery environment of Cranfield University's world renowned four-stage low-speed research compressor facility (LSRC). This is a considerable step from the flat plate and wind tunnel arrangement employed in the previous stages of this research programme. Two-dimensional flow field measurements taken downstream of an embedded rotor stage complement the boundary layer survey experiment to contribute toward a better understanding of the unsteady wake affected boundary layer flows that occur in turbomachinery. The current study was conducted with particular reference to a low speed 3 D end bend controlled diffusion blade design.

X-array hot-wire measurements of the unsteady flow field have captured the strong wake features exhibiting periodic variations in thickness, which indicates blade loss fluctuations. This is more prominent at Near Stall conditions. Strong variations are present in the end-wall regions where corner stall and corner vortex and tip clearance

flows dominate. Radial migration of flow deviation was also detected with each passage of a rotor wake indicating significant radial asymmetries in velocity profiles.

Periodic fluctuation of the suction surface boundary layer on a stator blade has been detected starting from the first leading edge measurement location (i.e. 15%) until 37% chord where imminent separation was evident at design flow conditions. Different states of boundary layer flows exist at different heights of a fixed chord position, indicating that the inlet conditions to the stator vary throughout the span. This periodic alternating between laminar and turbulent of the boundary layer appeared to be primarily dependent on the state of the boundary layer itself rather than the wake passing frequency.

Results from this first ever attempt of detailed boundary layer survey within turbomachinery environment at Cranfield, though qualitative, has shown that transitional flows occupy up to approximately 40% of the stator blade suction surface. Total separation of the flow, which had been detected at 65% chord in this investigation was not anticipated as the design of the current blading was aimed at delaying if not eliminating any separation until or near the trailing edge.

ACKNOWLEDGEMENTS

The author wishes to express his sincere gratitude to the staff within the University, in particular to Prof. Robin Elder for his continuous support and guidance, and Dr. Ian Bennett who provided important advice and suggestions concerning all aspects of the experimental work.

The experimental phase of this study required significant engineering support. For this the author would like to thank Mr. Peter Timmis for his CAD/CAM expertise and the technical staff of the department at the test area, headed by Mr. Bernard Charnley, for their invaluable assistance.

The joint scholarship awarded in the first year by the Department of Trade and Industry and Cranfield University is gratefully acknowledged.

Finally the author would like to thank his parents and fiancée for the unimaginable sacrifices, which made the author's study at Cranfield possible.

"Komapsumnida"

D. Y. LEE

CONTENTS

	Page
ABSTRACT	i
ACKNOWLEDGEMENTS	iii
CONTENTS	iv
LIST OF TABLES AND FIGURES	viii
NOMENCLATURE	xiii
CHAPTER 1 INTRODUCTION	
1.1. Introduction	1
1.2. The Gas Turbine	1
1.3. Compressors and their Applications	2
1.4. The Role of Turbomachinery Aerodynamics	5
1.4.1 Unsteady Flow	6
1.4.2 End wall Boundary Layer	6
1.4.3 Tip Clearance Flow	7
1.4.4 Scraping Vortex	7
1.4.5 Shock Waves	7
1.4.6 Blade Boundary Layers and Wakes	7
1.5. This Research: Wakes and Behaviour of Boundary Layers	8
1.5.1 Motivation	8
1.5.2 Aim of the Project	9
1.6. Outline of Thesis	10

CHAPTER 2 REVIEW OF PAST WORK

2.1. Introduction 12

2.2. Brief Introduction to the Concept of the Boundary Layer 13

2.2.1 Boundary Layer over a Flat Plate 14

2.2.2 Transition 16

2.3. Boundary Layer Properties 16

2.3.1 Displacement thickness δ^* 16

2.3.2 Momentum thickness θ 18

2.4. The Role of Laminar Turbulent transition in Gas Turbines 19

2.5. Transition Processes 21

2.5.1 Natural Transition 21

2.5.2 Bypass Transition 22

2.5.3 Separated-Flow Transition 23

2.5.4 Turbulent Spot Theory 24

2.6. Wakes and Transition 26

2.6.1 Turbulence and Unsteadiness 26

2.6.2 The Concept of the Becalmed Region 28

2.7. The Effect of Stator/Rotor Indexing 29

2.8. Summary 30

CHAPTER 3 EXPERIMENTAL ARRANGEMENT AND MEASUREMENT TECHNIQUES

3.1. Introduction 31

3.2. Comparisons of Different Testing Arrangements 31

3.2.1 Wind tunnel Arrangement with Flat Plate/Cascades 32

3.2.2 Single and Multi-Stage Compressor Facilities 33

3.2.3 High-Speed Compressor Rigs 34

3.2.4 Low-Speed Compressor Rigs 35

3.3. The Low Speed Research Compressor (LSRC) 36

3.4. Blading 37

3.5. Instrumentation 40

3.5.1 Thermal Anemometry 40

3.5.2 The Hot-Wire Flow Measurement Probes 42

3.5.3 Calibration of Hot-Wires 43
3.5.4 Single Sensor 45
3.5.5 X array Dual Sensor 45
3.6. Area Traverse Measurement 45
3.7. Stator Blade Suction Surface Boundary Layer Survey 46
3.8. Data acquisition, Stepper Motor Control & Processing System 48
3.9. Hot film Anemometry 49
3.10. Other Instrumentation 50

CHAPTER 4 HOT WIRE INVESTIGATION OF THE FLOW FIELD
4.1. Introduction 51
4.2. Experimental Test Programme 52
4.3. Hot Wire Measurement Techniques 55
4.3.1 X Array Probe Calibration 55
4.3.2 Application 58
4.4. Data Reduction 60
4.5. Results and Discussion 61
4.5.1 Circumferentially Averaged Data 61
4.5.2 Unsteady Area Traverse Data 66
4.5.3 Contour Plots of Flow Field 69
4.5.4 Accuracy of Results 70
4.6. Conclusions 71

CHAPTER 5 BOUNDARY LAYER SURVEY ON THE SUCTION SURFACE OF STATOR
5.1. Introduction 81
5.2. Design of the Traverse 82
5.2.1 The Concept 82
5.2.2 Traverse Control System 85
5.3. Measurement Method 87
5.4. Difficulties Encountered 89
5.4.1 Positioning of Measurement Probe 90
5.4.2 Accuracy of Measurements 92

5.4.3 Proximity Effects 93
5.5. Results 94
5.6. Conclusions 95

CHAPTER 6 CONCLUSIONS AND SUGGESTIONS FOR FUTURE WORK
6.1. Introduction 105
6.2. Conclusions 106
6.3. Suggestions for Future Work 107

BIBLIOGRAPHY 109

APPENDIX A
HOT WIRE CALIBRATION AND MEASUREMENT TECHNIQUES 119
A.1. Introduction 119
A.2. Hot-Wire Anemometry 119
A.2.1 Principles 119
A.3. Calibration of Hot-wires 122
A.3.1. Single Sensor 124
A.3.2. Dual Sensor 124
A.4. Examples of Hot Wire Calibration 125
A.4.1 Single Sensor Probe 125
A.4.2 X Array Dual Sensor Probe 127
A.5. The Effect of Fluid Temperature 136

APPENDIX B
DISCUSSION ON PROXIMITY EFFECTS ON HOT WIRE READINGS 138
B.1 Introduction 138
B.2 Brief Review of Literature 139
B 3 The Present Correction Method 142

APPENDIX C
BL TRAVERSE MECHANISM TECHNICAL DRAWINGS 145

LIST OF TABLES AND FIGURES

Tables

Table		Page
3.1	General Specifications and Operating Conditions of the LSRC	38
4.1	Mean Exit Flow Angles Downstream of Rotor 3	53
5.1	Measurement Locations where Data have been Successfully Collected	94
A.1	Calibration Data for Single Sensor Probe	125
B.1	The ratio of the thermal conductivity, k_w, of wall materials to the Thermal conductivity of air, (k =0.02559 W m^{-1} K^{-1}) (Turan et al. 1987)	139

Figures

Figure		Page
1.1	Velocity Diagrams for an Axial Compressor Stage	4
1.2	Fundamental Problems in a Modern Compressor Flow Field	5
2.1	Boundary Layer on a Flat Plate (from Massey, 1989)	14
2.2	Typical Velocity Profiles on a Flat Plate at Zero Incidence for Laminar and Turbulent BoundaryLayers (from Young, 1989).	15
2.3	Boundary Layer Displacement Thickness	18
2.4	Reynolds Number Variation through a Medium-Sized Gas Turbine Engine (Hourmouziadis, 1989)	20
2.5	Idealised Sketch of Tollmien-Schlichting and Bypass Transition (from White, 1974)	22
2.6	Separated Flow Transition with Separation Bubble shaded (after Walker 1975)	23
2.7	Schematic of 'Dependence' and 'Propagation' Cone of a point P in Time and Space (Emmons 1951)	24
2.8	Emmons' Turbulent Spot (After Milton Van Dyke)	25
2.9	Geometry of a Turbulent Spot as Measured by Schubauer and Klebanoff (1955) and Simplified by Chen and Thyson (1971)	25

2.10 The Choppping of Wakes by Downstream Blade Rows. 27
3.1a Schematic Diagram of the Four-Stage Low Speed Compressor 37
3.1b Photograph of the LSRC Facility 37
3.2 Typical Performance Map of the VRB3.5 Build 39
3.3 Traverse Location for the Flow Field Measurements (from Ivey & Swoboda, 1998) 40
3.4a Dual X array Probe used in Flow Field Investigation (DANTEC) 42
3.4b Single Sensor Probes used for BL Surveys (DANTEC) 42
3.5 Block diagram of a Constant Temperature Anemometer (Lomas, 1986) 44
3.6 General Layout of the Experimental Facility 46
3.7 Traverse Gear with DANTEC 55P05 BL Probe 47
3.8 Traverse Assembly Mounted on the LSRC Facility 47
3.9 Data Acquisition Scheme Used During Calibration and Testing 48
4.1 X Array Hot Wire Traverse Plane Downstream of Rotor Three (after Lockwood, 1999) 52
4.2 Dual Sensor Probe Circumferential Traverse Location in the Axial Gap (Not to Scale) 54
4.3 Measurement Matrix of Hot-Wire Area Traverse 54
4.4 Datum Position of X Array Probe during Calibration. 55
4.5 New 'Confidence Zone' Due to Prong Effects 56
4.6 Axial Velocity at Peak Efficiency Design Flow Conditions 60
4.7 Comparison of Circumferentially Averaged Absolute Flow Angles at Near Stall Condition Downstream of Rotor 3 61
4.8 Comparison of Circumferentially Averaged Relative Flow Angle at Design Condition Downstream of Rotor 3 62
4.9 Spanwise Distributions of Absolute Flow Angle Downstream of Rotor 3 64
4.10 Spanwise Distributions of Axial Velocity Downstream of Rotor 3 64
4.11 Spanwise Distributions of Absolute Velocity Downstream of Rotor 3 65
4.12 Spanwise Distributions of Relative Flow Angle Downstream of Rotor 3 65
4.13 Selected Hot-Wire Measurement Locations Downstream of Rotor 3 67
4.14 Hot-Wire Measurement Traces at Design Mass Flow at Locations Shown in Figure 4.13 67

4.15 Contour Plots of Absolute Flow Angles Downstream of Rotor three at Design Flow Conditions 73
4.16 Contour Plots of Absolute Flow Angles Downstream of Rotor three at Near Stall Flow Conditions 74
4.17 Contour Plots of Absolute Velocity Downstream of Rotor three at Design Flow Conditions 75
4.18 Contour Plots of Absolute Velocity Downstream of Rotor three at Near Stall Flow Conditions 76
4.19 Contour Plots of Axial Velocity Downstream of Rotor three at Design Flow Conditions 77
4.20 Contour Plots of Axial Velocity Downstream of Rotor three at Near Stall Flow Conditions 78
4.21 Contour Plots of Relative Flow Angle Downstream of Rotor three at Design Flow Conditions 79
4.22 Contour Plots of Relative Flow Angle Downstream of Rotor three at Near Stall Flow Conditions 80
5.1a Initial Traverse Concept Drawing (Leading Edge) 83
5.1b Initial Traverse Concept Drawing (Trailing Edge) 83
5.2 Three Probe 'Rake' Arrangement 84
5.3 Traverse Assembly Fitted with VRB 3.5 Blades 84
5.4 Traverse Cassette Assembly Without Stator Blades 86
5.5 Designated Chord Positions for Boundary Layer Survey Measurements 88
5.6 Technical Drawing Illustrating Probe Orientation 89
5.7 Time Averaged Plots of Velocity Profiles at 15% Chord & 15% Height 97
5.8 Time Averaged Plots of Velocity Profiles at 15% Chord & 50% Height 98
5.9 Time Averaged Plots of Velocity Profiles at 26% Chord & 50% Height 99
5.10 Time Averaged Plots of Velocity Profiles at 37% Chord & 50% Height 100
5.11 Time Averaged Plots of Velocity Profiles at 65% Chord & 15% Height 101
5.12 Time Averaged Plots of Velocity Profiles at 65% Chord & 50% Height 102
5.13 Time Averaged Plot of Velocity Profile at 65% Chord & 15% Height 102
5.14 Boundary Layer Traverse at Design Conditions (26% chord). 103
5.15 Initial Unsteady Plots of Data Using the Log Law 104

A.1 Block diagram of a Constant Temperature Anemometer (Lomas, 1986) 120
A.2 Calibration Curve of Hot-wire Probe type 55P01 (single sensor) 126
A.3 Linearised Calibration Curve 126
A.4 DANTEC's' Miniature' and 'Gold Plated' X Array Probes 127
A.5 Datum Position of X Array Probe 130
A.6 Voltage Map of X Array Probe 55P62 (Miniature) 130
A.7 Voltage Map of X Array Probe 55P52 (Gold Plated) 131
A.8 Characteristic Plot of Probe 55P62 Inner Wire 132
A.9 Characteristic Plot of Probe 55P52 Inner Wire 132
A.10 Characteristic Plot of Probe 55P62 Outer Wire 133
A.11 Characteristic Plot of Probe 55P52 Outer Wire 133
A.12 Polynomial Curve fit for Outer wire of 55P52 Probe 134
A.13 Polynomial Curve fit for Inner wire of 55P52 Probe 134
A.14 Reduction in Measurement Area Due to Probe Interference 135
A.15 Effect of Air Temperature On a Wire Calibration 136
B.1 Correction to Measured Values of $Re_w^{0.45}$ for Proximity to Wall (after Wills 1962) 140
B.2 Numerical and Experimental Values of the Velocity Correction Factor C_U for Different Temperature Loadings (after Lange et al, 1998) 143
C1 Probe Holder Bracket 146
C2 Brass Bush 147
C3 Clamp Element No.1 148
C4 Clamp Element No.2 149
C5 Stepper Motor Support Plate 150
C6 Main Support Plate (Rod hole & Slot Position) 151
C7 Main Support Plate (2 BA tapped hole positions) 152
C8 Support Rods 153
C9 Traverse Shaft and End Piece No.1 154
C10 Traverse Shaft and End Piece No.2 155
C11 Spigot Base for Motor Location 156
C12 Spigot Shaft and End Piece 157
C13 Traverse Tube 158

C14 Traverse Shaft Hole Locations 159
C15 Dowel Holes for Location of Stator Blade 160
C16 Support Rods Positioning Holes 161
C17 Traverse Assembly 162

NOMENCLATURE

A	King's Law Constant
a	Overheat Ratio
C	King's Law Constant
C_U	Correction factor for proximity effects
c	Blade chord
E_0	Hot wire output voltage at zero flow
E	Hot wire output voltage
k	Yaw factor constant from champagne's law
	Thermal conductivity of air
k_w	Thermal conductivity of wall material
N	Number of blades, number of ensembles
Re	Reynolds number
t	Time
Tu	Turbulence intensity
u	Velocity
U_τ	Friction velocity
U^+	Normalized velocity quantity
U_∞	Free stream velocity
U_{eff}	Effective velocity
V_a	Axial velocity
U_{eff}	Effective velocity on Hot Wire
Y^+	Normalised distance
y	Distance from wall
U	Blade speed
U_y	Local velocity

Greek Symbols

α	Absolute Flow angle
β	Relative Flow angle
δ	Boundary layer thickness
δ^*	Boundary layer displacement thickness
τ	Shear stress
τ_w	Shear stress at the wall
$\varnothing$	Flow coefficient V_a/U
ρ	Density
ν	Dynamic viscosity
μ	Viscosity
θ	Momentum thickness

CHAPTER 1

Introduction

1.1. Introduction

This chapter will introduce the reader to the gas turbine and one of its main components, the axial compressor, the flow in which is the main concern of this investigation. Different flow structures are briefly discussed and the main objectives will be stated followed by the outline of the thesis.

1.2. The Gas Turbine

Soon after the introduction of the gas turbine in the nineteen thirties it was discovered that its superior power to weight ratio and absence of balancing problems made it ideally suited for application in aircraft propulsion. It rapidly replaced the piston engine and has been used as a turbojet, turboprop or turbofan engine. The gas turbine began to compete successfully in other fields only in the mid-nineteen fifties, but since then it has made a progressively greater impact in an increasing variety of applications where shaft power is desired. For example in combined cycle power plants where the gas turbine contributes about two thirds of the total power output and helps to increase the overall plant efficiencies close to, or beyond 60 percent.

Competition between manufacturers of aircraft engines and within the electrical power generation industry as well as strict global environmental regulations are driving further research on gas turbines to develop more efficient, reliable, quiet and powerful gas turbines. The market for civil air transport is highly competitive and the engine manufacturers are constantly striving for permanent improvement. This does not require justification considering the fact that nearly half of the operational costs of an airline stem from costs related to the engine, most of which are direct fuel costs. In addition the international standards concerning emissions and noise at take-off are becoming increasingly stringent and have to be met in order to obtain engine certification. All these add to the sophistication of the design process, which demands

the highest level of contributions from various key fields of engineering research, primarily thermodynamics, material sciences and aerodynamics.

1.3. Compressors and their Applications

A compressor is defined as "a device that transfers energy to a gaseous fluid, air in our case, for the purpose of raising the pressure of the fluid as in the case where the compressor is the prime mover of the fluid through the process" (Gresh, 1991). In the case of other gases the purpose may also include raising the pressure and temperature to a desired level to enhance a chemical reaction in the process.

Devices that develop a pressure rise of less than 5 psig (345 millibars) are usually classified as fans or blowers. Pumps are very similar to compressors but are primarily used for dealing with incompressible hydraulic fluids, whereas compressors generally are used for gaseous fluids (both in compressible and incompressible conditions) such as air (Gresh, 1991). There are two basic types of compressors: the Positive Displacement and Dynamic type. Examples of Positive Displacement compressors are:

- Piston compressor
- Screw compressor
- Vane compressor
- Lobe compressor

In these cases compression is achieved by the entrapment of a volume of gas and further reducing the volume. The Dynamic type of compressors mainly uses the motion to transfer energy from the compressor to the working gas. Unlike the positive displacement types, there is no entrapment of the gas. Examples of these are the

- Centrifugal compressor
- Axial compressor

Both the centrifugal compressor, also known as a radial compressor, and the axial compressor have an axis of symmetry along which lies a shaft to which the impeller or the rotor blades are attached. The shaft drives the compressor providing the work input. At the exit of the compressor, the working fluid possesses a higher pressure and momentum. Depending upon the application the momentum may not be of further use.

A centrifugal or radial compressor consists of an impeller rotating within a casing and a diffuser. The flow is such that the fluid enters axially through the eye of the casing and is drawn in by the impeller blades, and is whirled tangentially and radially outward until it leaves through all the circumferential parts of the impeller into the diffuser part of the casing. The fluid gains both velocity and pressure while passing through the impeller and the diffuser located within the scroll casing decelerates and further increases the pressure. The centrifugal compressor is popular in applications of low mass flows and high pressure ratios and has an advantage in terms of relative simplicity and cost.

Since the early stage of the history of the gas turbine, the potential of the axial compressor for aerospace applications was recognised particularly due to the much larger flow rate possible for a given frontal area. This allowed an appropriate pressure ratio and efficiency to be obtained compared to the centrifugal compressor. In an axial compressor stage, the fluid essentially passes almost axially through alternate rows of moving rotor and fixed stator blades. In this arrangement, depending on the reaction, the stator blades are the primary diffusing stage where there occurs an increase in static pressure. The process is repeated in as many stages as are necessary to obtain the required overall pressure ratio. Multi-stage axial compressors may have as many as twenty stages in some applications, making the machine rather lengthy (Dixon, 1975). The incompressible-flow assumption is frequently used because the pressure rise per stage is usually small. The combination of moving and stationary blades makes the flow fundamentally unsteady, which is responsible for much of the complexity of the flow within axial compressors.

Figure 1.1 below shows the velocity vectors and the associated velocity diagram for a typical stage of an axial compressor. The air from a previous stage (or from the guide vanes) approaches the rotor with a velocity $\mathbf{V_1}$ at an angle α_1 from the axial direction.

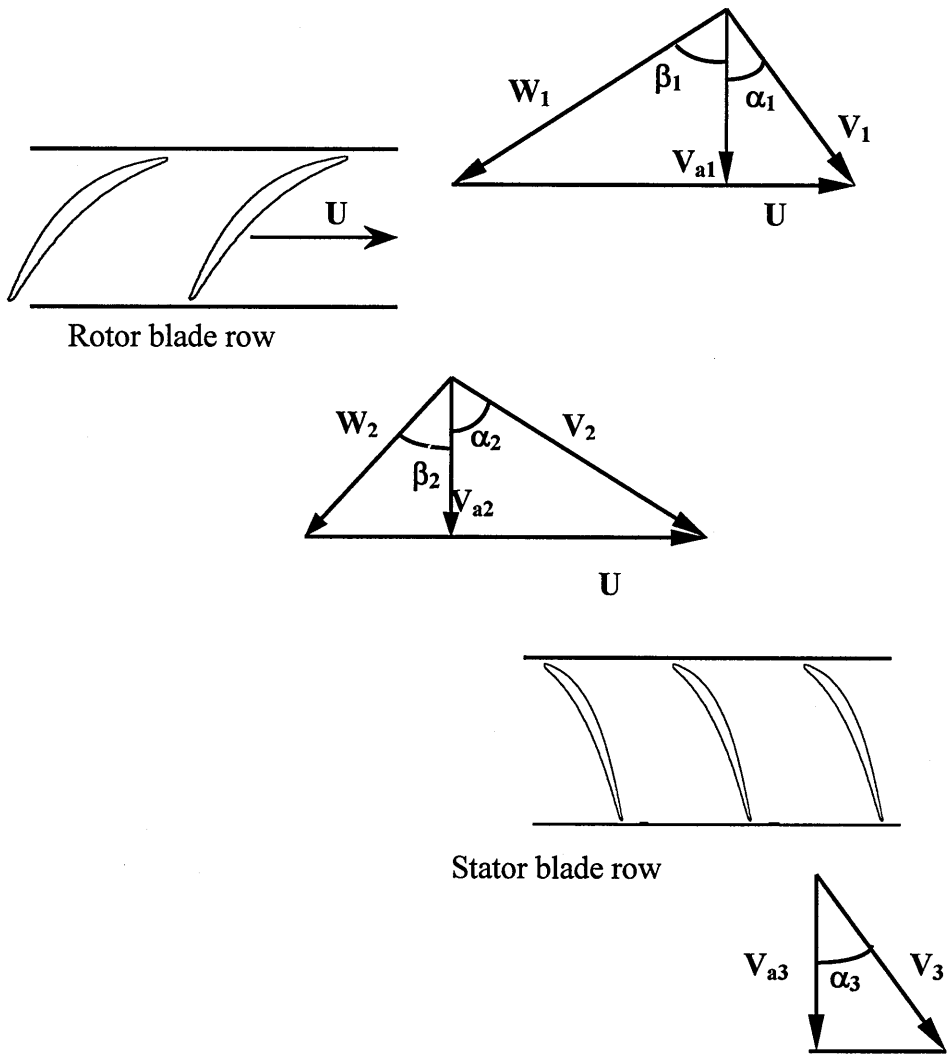

Figure 1.1 Velocity Diagrams for an Axial Compressor Stage

Combining $\mathbf{V_1}$ vectorially with the blade speed $\mathbf{U}$ gives the inlet relative velocity $\mathbf{W_1}$ at angle β_1 (the axial direction is the datum for all angles). The absolute velocity of the air increases after passing through the rotor and relative to the blades of the rotor, the flow is turned to the direction β_2 at the outlet with a relative velocity $\mathbf{W_2}$. Assuming that the design of the compressor is such that the axial velocity $\mathbf{V_a}$ remains constant, it can clearly be seen that by adding vectorially the blade speed $\mathbf{U}$ on to $\mathbf{W_2}$ gives the

absolute velocity from the rotor, V_2 at angle α_2. The air leaving the rotor is deflected towards the axis by the stator blades where it is diffused to a velocity V_3 at angle α_3. For the normal stage the typical design is such that $V_3 \cong V_1$ and $\alpha_3 \cong \alpha_1$ so that the air is ready for entry to another similar stage. It can be seen from Figure 1.1 that both the relative velocity in the rotor and the absolute velocity in the stator are diffused. This relative amount of diffusion of kinetic energy in the rotor and the stator rows significantly influences the stage efficiency (Dixon, 1975).

1.4. The Role of Turbomachinery Aerodynamics

The flow within turbomachines is inevitably unsteady due to the interaction between rotating and stationary blades. The complexities that exist within the flow of a typical axial compressor are shown schematically in Figure 1.2.

Axial compressors rely fundamentally on aerodynamic diffusion to achieve pressure rise. This diffusion brings about adverse pressure gradients, which become strong at the high-loading level of modern compressor designs, which lead the boundary layers to thicken. The conditions of these boundary layers crucially influence the probability of separation and by consequence, the loss of stability and performance. The present investigation will mainly be concerned with the boundary layer flows,

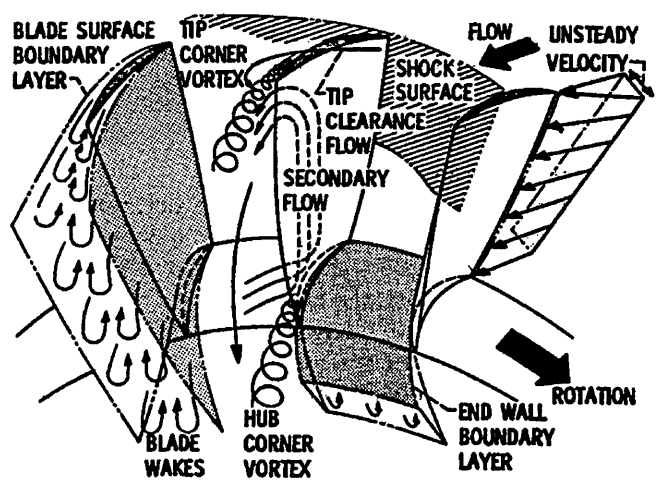

Figure 1.2 Fundamental Problems in a Modern Compressor Flow Field (McNally & Sockol 1982)

which exist within turbomachines, particularly those on multi-stage compressor blades that are affected by the wakes shed by previous stages.

Although this study is primarily concerned with the boundary layer in compressor blades, it would be artificial and naïve to consider this in isolation from the other flows that exist within the compressor. The different flow structures or even the existence of a particular flow phenomenon is invariably dependent on the individual compressor geometry as well as the free stream conditions. Therefore, the following give brief descriptions of some of the flow phenomena illustrated in Figure 1.2.

1.4.1 Unsteady Flow

In general, the flow within a turbomachine is unsteady (Dean, 1959) and turbulent with various coherent structures of vorticity. Many parameters affect the conditions of the boundary layer such as the instability in the free stream and background turbulence. Acoustic noise, mechanical vibrations as well as surface roughness and dimensional accuracy of the solid walls of the flow passage can also be considered as important parameters that affect the boundary layer flow. These phenomena are more apparent in multistage machines due to the interaction of the consecutive stages, which generate a highly perturbed flow environment.

1.4.2 End wall Boundary Layer

The flow phenomena occurring in the end wall regions (hub and casing) are considered vitally important but also one of the least well understood parts of the compressor flows. The flow is highly three dimensional due to the tip clearance vortex and by corner separation induced by secondary flow on the hub. No real satisfactory method has been established to predict the blockage or loss in these regions other than correlation. The normal boundary layer methods are used to model the end wall flows often ignoring the effects of tip clearance flows and assuming the flow to be uniform in the circumferential direction. Cumpsty (1989) highlights the inaccuracy of these methods by arguing that the application of these models which are created for boundary layer flows existing in relatively mild conditions, are unsuited due to the intense pressure gradients and steep variations in end wall flows that exist in blade rows.

1.4.3 Tip Clearance Flow

This phenomenon is generally agreed to be the largest contributor to the end wall losses causing reduction in efficiency and stall margin. It is believed to occur due to the pressure difference across the tip of the blade and the transport of undeflected fluid in the annulus wall boundary layer. This flow is a topic of extensive research and experimental study has been undertaken previously at Cranfield using 3D laser anemometer (Foley, 1995) to take detailed measurements from two different rotor tip clearance builds.

1.4.4 Scraping Vortex

The blade motion relative to the end wall causes this, where the fluid is forced through the gap partly due to the viscous drag of the end wall and also due to the pressure difference across the blade. On the pressure side of the blade tip the boundary layer fluid near the end wall is 'scraped up' and piles up forming a vortex.

1.4.5 Shock Waves

The study of shocks and their effects on the blade passage in a compressor is an area of research in its own right. Michelassi (1997) has recently published a study investigating the interaction of shocks with blade boundary layer transition in turbomachinery flows. The flow within the experimental facility used in this study is primarily subsonic therefore the effects of shocks will not be considered.

1.4.6 Blade Boundary Layers and Wakes

The boundary layer gradually grows, starting from the leading edge, along both the suction and pressure surface of the blade until it is shed as a wake from the trailing edge. In order to keep the profile losses low the width of the wake needs to be kept to a minimum. This requires that the boundary layer remains attached to the blade and as thin as possible. This is particularly difficult in an axial compressor due to the adverse pressure gradient associated with it. Prediction of the boundary layer conditions within compressors is a vital part of turbomachinery design but the 3D flows and unsteadiness make it a very complicated process. The further understanding of the behaviour of

boundary layers especially those subjected to wakes is therefore the objective of this research. Literature on this flow is reviewed further in chapter two.

1.5. This Research: Wakes and Behaviour of Boundary Layers

1.5.1 Motivation

Among the many parameters that affect the performance of gas turbine engines are the boundary layers on the blades of the axial compressor, which contribute to the loss, the blockage and the breakdown into stall. Blockage is used here to describe the effective reduction in the blade passage flow area caused by the slower moving fluid in the blade boundary layer. Until the late eighties boundary layer calculations had not been normally considered as part of the design process because of the poor accuracy of predictions. The design of high-performance turbomachines using the application of computer-aided design procedures has been constrained by the lack of detailed information on boundary layer transition. More information is required on the inception and completion of transition under condition of high free-stream turbulence encountered in turbomachinery. Turbomachinery designers have become reliant on advanced computational methods to predict flows over blading. The ability to predict the state of the boundary layer on the blade surface which is an essential requirement has often encountered difficulties due to lack of experimental transitional data, especially in the adverse (or positive) pressure gradient regimes encountered by compressor blading. Recognising this need for more detailed empirical data and a further fundamental understanding of this complex flow phenomenon undoubtedly makes further research on the topic essential.

This report describes work undertaken in the third phase of the research programme on boundary layer flows in turbomachinery at Cranfield University. The first phase involved experiments using a wind tunnel and flat plate arrangement with varying types of leading edge geometry (e.g. sharp, cylindrical, C4). The study concentrated on the detailed physics of transition and examined the effect of varying

few of the many parameters which affect boundary layer transition such as turbulence intensity and Reynolds number at zero pressure gradient (Kalfas 1994). Intermittency effects were also analysed. The second phase was a continuation of the study using flat plates but with the introduction of pressure gradients representative of the critical "controlled diffusion" type blading by varying the wind tunnel area (Read 1997). Recognising the need for further maturing of this research topic at Cranfield, particularly in relation to the unsteady transitional flows, which occur in real turbomachinery environment, the author has taken a considerable step forward from the wind tunnel studies. This was made possible by taking detailed measurements using Cranfield University's Low Speed Research Compressor (LSRC) facility. The LSRC is a large-scale low-speed compressor with four identical repeating-stages designed to be representative of subsonic middle and rear stages of a medium to highly loaded multistage compressor. The blading used for this study was of a medium load, state of the art 'End-Bend' 3D design provided by Rolls Royce under a contract with Cranfield University for detailed analysis of blade performance. Although the current research programme was not part of the contract, the author was given the opportunity to use this build to carry out tests within a limited time period. This was with the agreement that, due to the commercial sensitivity of the blade design, permission must be obtained from Rolls Royce prior to publication of any experimental results.

1.5.2 Aim of the Project

The aim of this research is to gain further understanding of the behaviour of boundary layers that exist on the suction surface of a medium loaded stator blade within an embedded stage of a multiple stage compressor.

Using constant temperature hot-wire anemometry (CTA), the first part of the study investigates the flow environment, particularly the characteristics of wakes shed by rotor blade rows, by conducting area traverse measurements consisting of a matrix of 16 blade heights and 16 circumferential positions covering approximately two stator blade pitches.

The second part of the investigation examines the interaction of these wakes with, and their effect on, the extent of the boundary layer on the suction surface of the immediately following stator blade row through detailed measurements of the boundary layer at different chord positions of a stator blade. This is achieved by the use of a specially designed traverse mechanism that permitted measurements across the boundary layer at a nominal step increment of 20 μm.

1.6. Outline of Thesis

This chapter introduces the reader to the topic of this research and its relevance to turbomachinery performance, followed by a statement of the objectives. Chapter 2 begins with a brief overview on the concept of the boundary layer then presents the result of the literature review. This mostly focuses on the transitional boundary layer flows within turbomachinery and the unsteadiness induced due to the wake interaction between the blade rows.

Chapter 3 briefly outlines the advantages and disadvantages present in the various experimental arrangements used for investigating fluid phenomena in turbomachinery flows followed by a general description of the main vehicle used for the current investigation. Subsequently, an outline of the criteria used that led to the choice of the principal measurement tool for this study, Constant Temperature Hot-wire Anemometry (CTA), is presented. Finally, descriptions of the experimental methods used during the two parts of this study are given.

Chapter 4 presents the results obtained from the flow field investigations taken place downstream of the rotor row within an embedded stage (Rotor 3). Chapter 5 follows on to present the results from boundary layer surveys carried out on the suction surface of a stator blade at the same stage immediately downstream of the rotor row.

Chapter 6 concludes this investigation by summarising the pertinent findings and makes recommendations for future work. These include suggested modifications to the measurement methods that could significantly improve the quality of the experimental data and therefore enable further detailed understanding of this topic, which over the decades has developed into one of the most crucial yet complex parts of compressor design.

CHAPTER 2

Review of Past Work

2.1. Introduction

This section of the thesis is the result of a literature survey. The fundamental concept of boundary layer flows especially the transition region, which is vital to turbomachinery performance, remains poorly understood. This applies particularly in the flows within turbomachines where many different complex flow mechanisms described in Chapter 1 exist and contribute to transition and losses. This chapter will open with a brief introduction to the concept of the boundary layer then will briefly review the applicability and the effects of its behaviour on the performance and efficiency of gas turbine components especially the axial compressor. Particular attention is given to the boundary layer flows subjected to wakes.

Descriptions of the physics of the boundary layer flows will be given followed by accounts of the different modes of transition that exist with information on the statistical techniques such as intermittency factors. Experimental work on boundary layer flows is subdivided into wind tunnel and rotating machinery investigations. The early studies have preferred the wind tunnel arrangement firstly due to ease of operation, and secondly the larger scale (in both time and space) of the flow phenomena that occur, making it the obvious choice. These studies, whilst not truly representative of the flow in real turbomachines have provided considerable

understanding of the mechanisms involved. The rotating machines (e.g. single stage fans or multiple blade row machines), though providing a more complete modelling of the flow field, introduce more flow interactions resulting in even more complex structures that are harder to measure and interpret. The latter sections of this chapter will provide a brief overview of the different experimental research techniques i.e. both the wind tunnel and rotating machinery. Most of the papers in these sections are not specifically related to turbomachinery flows. However, the models they describe are often adopted in attempts to model the unsteady transition process on gas turbine blades. Due to the scope of this study, potential flow interaction, shock interaction and the statistical analysis will not be considered.

2.2. Brief Introduction to the Concept of the Boundary Layer

When there is flow on a solid surface the effects of the fluid viscosity are greatest in regions close to the solid boundaries. Except in extremely low pressure conditions, it is a characteristic of all real fluids that there is no relative motion between the fluids and the solid surface. No matter how smooth the surface or small the viscosity of the fluid, there is no relative movement between the surface and the particles immediately adjacent to it. This is known as the 'no-slip condition'. If the relative velocity at the boundary is zero, then there must be a region in the flow where the velocity rises gradually from zero to that of the main stream. This region is known as the boundary layer. This layer is usually very thin and the velocity gradient - that is the rate of increase of velocity with increasing distance from the solid surface - is high and therefore it is evident that appreciable shear stresses exist within this region. The velocity within this layer increases continuously and there is no abrupt 'step' in velocity. When Ludwig Prandtl first presented this theory of the boundary layer at the third Congress of Mathematicians at Heidelberg, Germany in 1904 it revolutionised the analysis of viscous flows in the twentieth century (Young, 1989). Although the Navier-Stokes equations were known prior to Prandtl's paper, practical engineering problems could not be resolved by solving these equations. Prandtl's concept of the boundary layer, which permitted some simplifications to the Navier-Stokes equations, brought about more easily solvable equations called the Boundary Layer equations. This

simplified the study of many fluid flows because the flow may be considered in two parts: 1) the boundary layer itself, in which the velocity gradient is large enough to produce appreciable viscous forces, and 2) that beyond the boundary layer where the effect of viscosity is negligible compared with other forces.

2.2.1 Boundary Layer over a Flat Plate

An example of the simplest boundary layer is that formed in the flow along one side of a thin, smooth, flat plate parallel to the direction of the approaching fluid, as shown in Figure 2.1. The pressure of the fluid is assumed uniform. As the fluid moves along the plate downstream of the leading edge, the effects of viscosity slow the fluid near the wall as dictated by the 'no-slip condition.' The flow in the upstream region (i.e. close to the leading edge) is entirely laminar. The boundary layer thickness grows

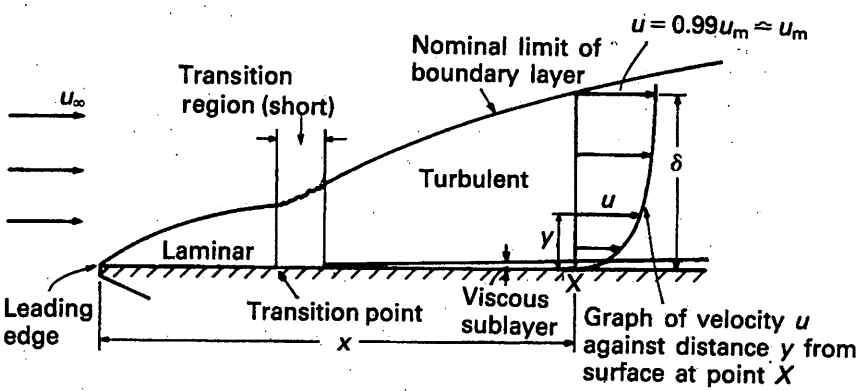

Figure 2.1 Boundary Layer on a Flat Plate (from Massey, 1989)

with distance along the plate as more and more of the fluid is slowed down. With increasing thickness, however, disturbance occurs in the laminar layer and the flow becomes turbulent and consequently the thickness of the layer increases even more rapidly. These changes take place over a small region known as the transition region. Beyond this region, the flow is almost entirely turbulent although a very thin viscous sub-layer remains in the laminar flow mode. This is a very thin layer adjacent to the surface of the order of a hundredth of the thickness of the turbulent layer. It should be noted that the y scale (i.e. perpendicular distance from the surface) in Figure 2.1 is greatly exaggerated for illustration purposes. The boundary layer thickness δ (discussed in the following section) is very small compared with x at any distance x

from the leading edge. In a turbulent layer there is more intermingling of fluid particles and therefore the velocity distribution over much of the layer is nearly constant with distance from the wall, y. As a result the turbulent layer usually has a greater velocity gradient at the surface. Comparison of the velocity distributions in typical laminar and turbulent boundary layers on a flat plate at zero incidence is illustrated in Figure 2.2. Due to the essentially laminar flow immediately adjacent to the surface the turbulent fluctuations tend to be less and the dominant shear stresses there are the viscous ones. This is given by

$$\tau_0 = \mu\left(\frac{\partial u}{\partial y}\right)_{y=0} \tag{2.1}$$

and thus the shear stress associated with a turbulent boundary layer is usually greater than that of a entirely laminar one. It must be noted that due to the higher mixing rate

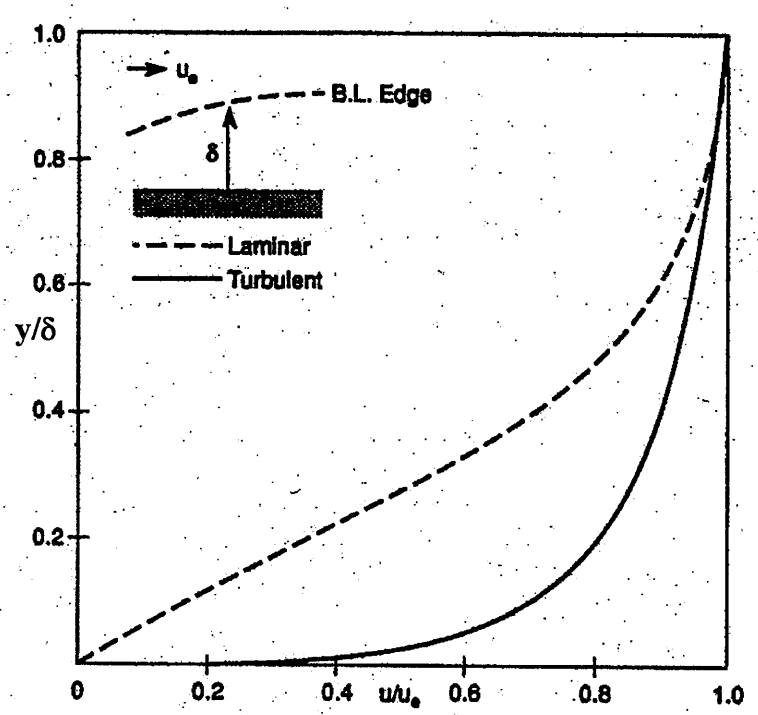

Figure 2.2 Typical Velocity Profiles on a Flat Plate at Zero Incidence for Laminar and Turbulent BoundaryLayers (from Young, 1989).

of the turbulent boundary layer the thickness of the layer grows more rapidly with distance x than with the laminar boundary layer. At a uniform pressure distribution the

thickness of a laminar boundary layer increases as $x^{1/2}$ whilst the turbulent boundary layer grows as $x^{4/5}$.

2.2.2 Transition

The transition process from laminar to turbulent flow in a shear layer has been a topic of active research since over a century ago to this day. In 1883, Osborne Reynolds applied flow visualisation by using a device consisting of a glass tube with water flowing and colour dye being fed into the inlet of the tube, to unravel the problem of viscous flow (Kreider, 1985). He formulated the dimensionless ratio, the Reynolds number, expressed as $U_\infty x/\nu$, where U_∞ is the free stream velocity, ν the kinematic viscosity of the fluid and x is the distance from the leading edge (in the case of pipe flow x would be replaced by d the diameter of the tube). The point at which a laminar boundary layer becomes unstable depends on a number of factors such as surface roughness and turbulence intensity. The predominant factor, however, is the Reynolds number of the flow in the boundary layer. It has been well recognised that the process of transition is not instantaneous and occurs over a finite distance known as the transition region. Detailed studies on the physics of transition have been performed previously at Cranfield University (Kalfas, 1995) using a wind tunnel arrangement incorporating a flat plate with different leading edge geometry at zero pressure gradient conditions. The effect of varying the parameters affecting boundary layer transition such as turbulence intensity and Reynolds number was investigated. The large scale of the experimental facility allowed the intermittency γ, which represents the fraction of time when the boundary layer is laminar or turbulent in the transition region (i.e. 0 for fully laminar to 1 for fully turbulent), to be measured.

2.3. Boundary Layer Properties

2.3.1 Displacement thickness δ^*

Obtaining the boundary layer thickness by measuring the distance from the surface at which the fluid achieves the free-stream value is difficult, particularly in

turbulent flow. Conventionally the boundary layer thickness δ is taken as the distance at which the boundary layer reaches 99% of the free-stream velocity. Even this is very difficult to obtain accurately and a curve fit to the measurements of the velocity profile through a boundary layer is usually used. Because this is susceptible to the accuracy of the curve fit and the fitting function applied, other definitions are also used.

The displacement thickness δ^* is physically the distance through which the external, essentially inviscid, fluid is displaced by the existence of the boundary layer. It can also be interpreted as a measure of blockage (or the mass flow lost) due to the existence of the boundary layer. The deficit in mass flow per unit passage width, due to the presence of the boundary layer is

$$\Delta m = \int_0^{\delta} (\rho U_{\infty} - \rho U_x) dy \tag{2.2}$$

where U_{∞} is the free-stream velocity and U_x is the velocity in the boundary layer parallel to the surface, which varies with distance y from the surface. If we define a distance δ^* as being proportional to the lost mass flow rate, such that

$$\rho u \delta^* = \text{mass flow lost}$$

then in order to have the same mass flow rate it is necessary to imagine the boundary displaced by distance δ^* to compensate as illustrated in Figure 2.3.

$$\rho U_{\infty} \delta^* = \Delta m \tag{2.3}$$

and therefore

$$\delta^* = \int_0^{\delta} \left(1 - \frac{U_x}{U_\infty}\right) dy \tag{2.4}$$

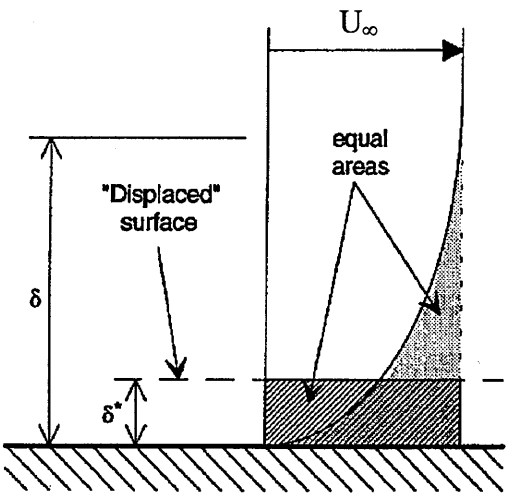

Figure 2.3 Boundary Layer Displacement Thickness

2.3.2 Momentum thickness θ

The momentum thickness θ is defined in terms of the deficit in streamwise momentum flux of the boundary layer fluid due to the velocity deficit (U_∞-U_x). This momentum deficit is due to drag force acting on the fluid by the wall. By applying the force-momentum equation to a control volume between the stagnation point, where there is a uniform velocity $\mathbf{U}_\infty$, and some point distance x along the wall, where velocity $\mathbf{U}_x$ varies as a function of distance y from the wall, the drag force can be calculated by:

$$D(x) = \rho \int_0^{\delta} U_x (U_\infty - U_x) dy = \rho U_\infty^2 \theta \tag{2.5}$$

where

$$\theta = \int_0^{\delta} \frac{U_x}{U_\infty} \left(1 - \frac{U_x}{U_\infty}\right) dy \tag{2.6}$$

θ is known as the momentum thickness. Note that for the definition of both the displacement thickness and the momentum thickness, the fluid was considered incompressible and therefore the density terms have been cancelled out.

2.4. The Role of Laminar Turbulent transition in Gas Turbines

The necessity for the flow in inviscid turbomachines to be unsteady in order to do work or that work can be done on it has been shown by Dean (1959). This inherent unsteadiness gives rise to a variety of interactions that were previously ignored in the design practice. Unsteady flows within turbomachinery are increasingly becoming the centre of attention and in order to achieve a higher level of sophistication in the design of turbomachines these have to be accounted for.

Flow phenomena such as instability in the free stream, background homogenous and isotropic turbulence and coherent flow structures of vorticity can actually influence the conditions under which the boundary layer 'transitions' from laminar to turbulent. Mechanical vibrations, acoustic noise as well as surface roughness and dimensional accuracy of the solid wall of the flow passage are also significant factors that affect the behaviour of the boundary layer flow. The effects of these are more apparent in multi-stage components where the interaction between consecutive stages contributes to creating an unsteady and highly turbulent flow environment. Even in these conditions the flow next to the solid surfaces may be either laminar or turbulent. The Reynolds number variation through a medium sized gas turbine engine is illustrated in Figure 2.4. A widely accepted rule-of-thumb is that transition from laminar to turbulent occurs when the Reynolds number based on the streamwise distance along the surface is about $3.5*10^5$. Thus, it may be presumed that transitional flows are very likely to occur in a gas turbine.

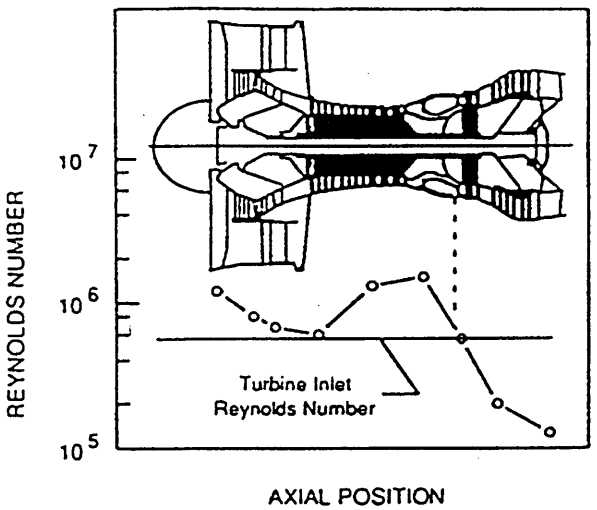

Figure 2.4 Reynolds Number Variation through a Medium-Sized Gas Turbine Engine (Hourmouziadis, 1989)

This exceedingly complex process of transition from laminar to turbulent in the boundary layer flows in turbomachinery still remains an active area of research since its behaviour determines the heat transfer and the drag. Due to the very rapid changes in both space and time the simulation of transition is, arguably, the most challenging problem in computational fluid dynamics. It is interesting to note that transition modelling, to predict the transition from laminar to turbulent flow, has received less attention for turbomachinery applications until the late 80's. Presently, the solution of the full unsteady 3-dimensional Reynolds-averaged Navier-Stokes equations in the design process is limited to only certain boundary conditions and turbulence modelling still remains one of the weakest parts of CFD. Therefore experimental work will remain a necessary and vital part to validate a design or to improve the understanding of the effects of certain flow features on compressor performance.

Mayle (1991) provided an extensive and critical review of the state of knowledge in this field by summarising the available well-documented experimental results. Among Mayle's conclusions were that transition in gas turbines is largely influenced by free-stream turbulence, pressure gradient, and the periodic, unsteady passing of wakes. In contrast, surface roughness, surface curvature, compressibility and heat transfer have only a secondary effect on transition (i.e. one in five). Walker

(1992) followed by providing a discussion and offered an additional viewpoint on Mayle's work. While focusing on transition in decelerating flows and the implementation of the concept of intermittency in the theoretical studies of transition, Walker (1992) raised a few questions regarding the appropriate interpretation of published results and offered alternative approaches for the explanation of transitional phenomena to the ones proposed by Mayle (1991). The differences in philosophy presented in the papers by Mayle and Walker largely reflect their different backgrounds. Mayle's is the field of turbines and Walker is from the area of compressor design and thus the physics of transition in decelerating flow. The primary conclusion that may be drawn from these papers is that the field is not yet mature enough to provide a tested and consistently reliable model for transition in turbomachinery flows. This is especially the case when transition on a compressor blade's suction surface is caused in an unsteady manner by the transport of wakes from upstream blade rows.

2.5. Transition Processes

A physical understanding of transition is vital for many engineering applications of turbomachinery aerodynamics and therefore it is useful to be aware of the types and causes of transition that exist in real flow. There are generally three substantially different ways in which laminar to turbulent transition occurs, more commonly referred as "modes of transition." The modes of transition that occur in steady flow conditions are also relevant for the unsteady flows in turbomachinery.

2.5.1 Natural Transition

This mode occurs where the laminar boundary layer is susceptible to small disturbances arising from a variety of different sources such as free stream turbulence, acoustic noise, surface roughness, and vibration. If the free stream turbulence level is low, that is TI is less than 1.0 percent, the laminar boundary layer develops linear oscillations of well defined frequency when the Reynolds number exceeds a critical value. Transition occurs in the form of two-dimensional Tollmien-Schlichting (T-S) instability waves that are much akin to sinusoidal waves and these convect at a typical

speed of 0.30-0.35 U_∞. The instability is amplified where three dimensional waves and vortices form with large fluctuations. In the final stages, turbulent spots develop in the regions of high fluctuations where the boundary layer alternates between laminar and turbulent states. These spots eventually grow and convect downstream within the boundary layer to coalesce into a fully developed turbulent boundary layer. A modern description of the natural transition process can be found from Schlichting (1979), along with a description of the theory of instability. Figure 2.5 illustrates schematically the various stages involved in the transition zone of the boundary layer of a flat plate at zero incidence.

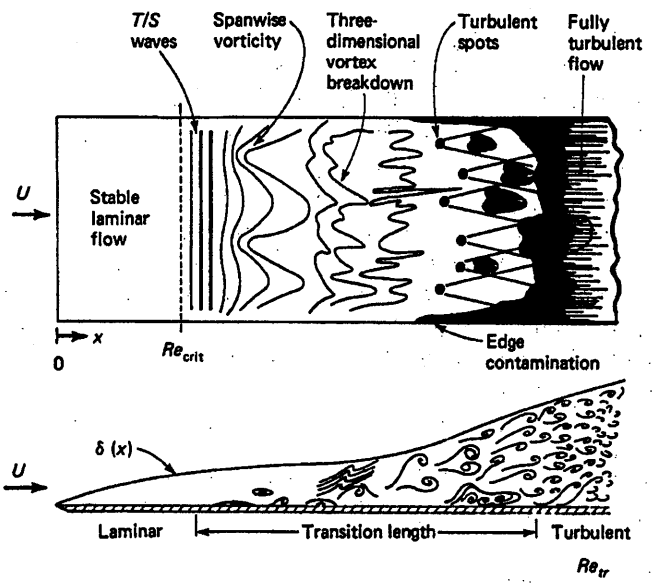

Figure 2.5 Idealised Sketch of Tollmien-Schlichting and Bypass Transition (from White, 1974)

2.5.2 Bypass Transition

This mode of transition exists in high free-stream turbulence levels as found in a real turbomachine environment and, as the name indicates, the first and possibly second stages of the natural transition process previously described are "bypassed". Turbulent spots are directly produced within the boundary layer by the influence of disturbances such as free-stream turbulence and surface roughness. Hence the length of unstable laminar flow is significantly reduced and transition occurs earlier. No Tollmien-Schlichting waves are found and according to Mayle (1991), the theory for

this mode is only concerned with the process of the production, growth and convection of turbulent spots. Emmons (1951) provides this theory and will be discussed later. A recent work by Mayle & Schulz (1996) presents a theory for calculating the fluctuations in a laminar boundary layer at turbulent free-stream conditions. A laminar-kinetic-energy equation that is obtained similarly to the turbulent-kinetic-energy (see Bradshaw, 1971) is modelled to help in predicting the onset of transition. While the idea presented is novel, Mayle & Schulz (1996) states that considerable experimental and computational work must be done before the onset can reliably be predicted.

2.5.3 Separated-Flow Transition

This mode of transition is common in gas turbines. When a laminar boundary layer separates, transition can occur in the free-shear-layer-like flow near the surface. In this case, the flow may re-attach as turbulent forming a laminar-separation/turbulent-reattachment "bubble" on the surface (see Figure 2.6). This type of transition occurs under the influence of strong adverse pressure gradients, typically encountered in compressors, which result in laminar separation. The length of the bubbles depends on the transition process within the free shear layer and may possibly involve all of the stages described above for natural transition. Gaster (1969) observed

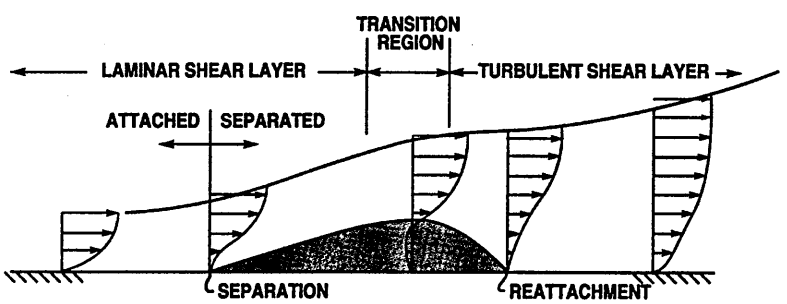

Figure 2.6 Separated Flow Transition with Separation Bubble shaded (after Walker 1975)

that in longer bubbles at low free-stream turbulence levels much of the flow is laminar and Tollmien-Schlichting waves are apparent. Long bubbles cause large losses as well as large deviations in exit angles and therefore should be avoided.

2.5.4 Turbulent Spot Theory

Emmons (1951) first discovered the turbulent spots, now named after him (see Figure 2.8), and developed a statistical theory for transitional flow in terms of the so-called intermittency factor. The intermittency is the probability that a point *P(x,y,t)* in space and time is covered by turbulent flow (Figure 2.7). Emmons showed this to be

$$\gamma(x,y,t) = 1 - \exp\left[- \iiint_{R(x,y,t)} g(x_0, y_0, t_0) dx_0 dy_0 dt_0 \right] \tag{2.7}$$

which makes intermittency a function of the so-called dependence volume *R(x,y,t)* and the production rate of turbulent spots $g(x_0,y_0,t_0)$ within the volume of dependence (i.e. number of spots formed per unit time per unit surface area). *R(x,y,t)* is defined as a function of the spot geometry and its propagation, containing all points that could have been the source of turbulent spot that turned the point *P(x,y,t)* turbulent. The spot production rate can be considered as a probability itself.

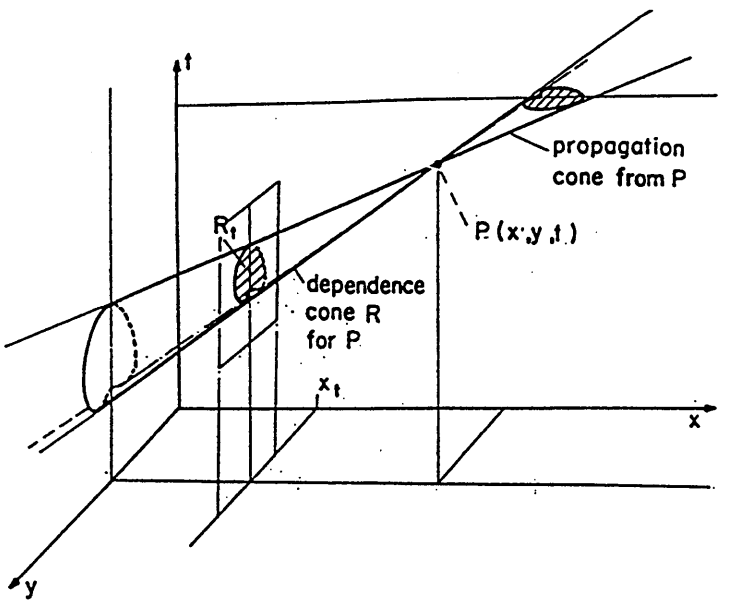

Figure 2.7 Schematic of 'Dependence' and 'Propagation' Cone of a point P in Time and Space (Emmons 1951)

Emmons (1951) suggested that the probability of the spot production rate assumes a constant value downstream of the position of turbulent breakdown (i.e. the first

occurrence of turbulent spots). This assumption proved to be not very successful and further extension has recently been shown by Schulte (1995).

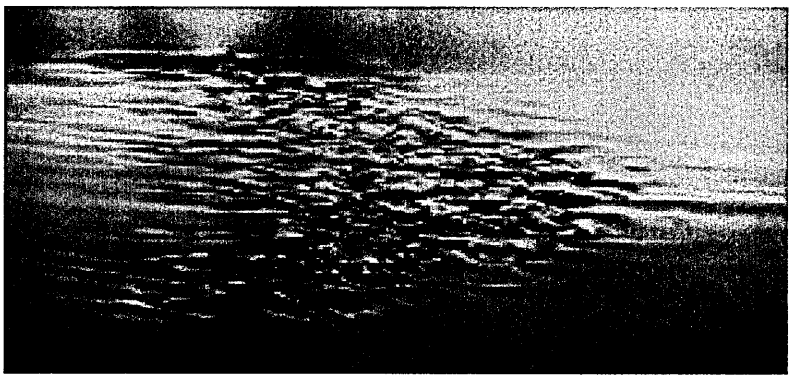

Figure 2.8 Emmons' Turbulent Spot (After Milton Van Dyke)

By generating electric sparks and artificially generating turbulent spots, Schubauer and Klebanoff (1955) measured their propagation velocities. The spots subsequently developed into roughly triangular regions where the forward apex and the rear edge moved downstream at approximately 88% and 50% respectively of the free stream velocity. Chen and Thyson (1971) introduced an approximate turbulent spot geometry illustrated in Figure 2.9 together with the spot shape as measured by Schubauer and Klebanoff.

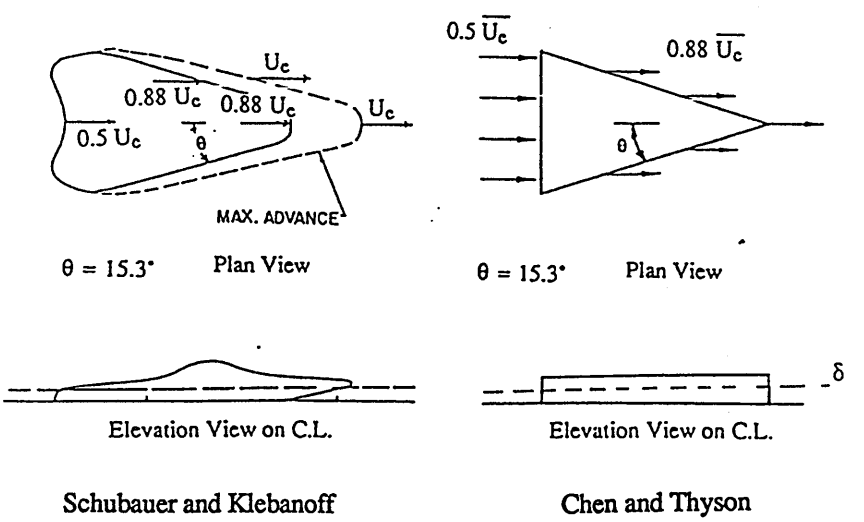

Figure 2.9 Geometry of a Turbulent Spot as Measured by Schubauer and Klebanoff (1955) and Simplified by Chen and Thyson (1971)

Narasimha (1957, 1985) also put forward a hypothesis that assumes the formation of turbulent spots to occur in the vicinity of one particular stream-wise position. This so called Concentrated Breakdown Hypothesis, which is still accepted today leads in conjunction with Emmons' formula (equation 2.7) to Narasimha's universal intermittency distribution

$$\gamma(x) = 1 - \exp\left[\frac{g(x_{tr})\sigma}{U}(x - x_{tr})^2\right] \tag{2.8}$$

Other researchers, for example Abu-Ghannam and Shaw (1980) developed similar expressions that yield generally the same result. They based their correlation predicting the onset of transition from measurements in strong adverse and favourable pressure gradients at different levels of isotropic free-stream turbulence levels provided by grids. The onset of transition cannot be predicted by analyses but correlations, which contain the main parameters that influence the behaviour of transition (e.g. free-stream turbulence and stream-wise pressure gradient), such as those of Abu-Ghannam and Shaw (1980) are still being used today. Mayle (1991) also put forward a correlation but does not consider the influence of pressure gradient.

2.6. Wakes and Transition

2.6.1 Turbulence and Unsteadiness

The flow in axial flow turbomachines is inevitably turbulent and unsteady. This is due to the blade wakes, end-wall boundary layers, secondary flows, tip clearance flows and blade row interactions. High turbulence is evident in the end-wall regions because of the end-wall boundary layer, secondary flow and tip clearance flow. Evans (1975) was one of the earlier studies that published extensive measurements of the turbulence and unsteadiness levels downstream of an axial flow compressor rotor at different values of flow coefficient at mid span. Hot-wire measurements by Wisler et al. (1987) show turbulence intensities as high as approximately 20% (rms values non-dimensionalised by the local flow velocity) near the hub and casing across the third

stator of the GE four-stage research compressor. The reason for this high turbulence has not been well understood.

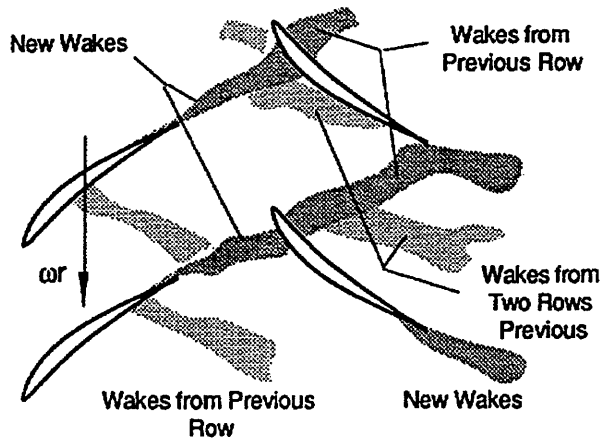

Figure 2.10 The Choppping of Wakes by Downstream Blade Rows.

Early works investigating the effect on a blade-row of wakes (Figure 2.10) shed by an upstream blade-row include Smith (1966) and Horlock (1968). Smith examined the effect of a succeeding rotor blade-row on the dispersion of the wake from a stationary blade. Questions were raised whether this wake would have a detrimental effect on the performance of the rotor blade-row. Evidence was presented in the form of hot-wire anemometer traces for a process in which the wake from an upstream row was chopped into segments by a following blade-row. The contribution this makes to dispersing the wakes was discussed but the question of the effect on rotor performance was left unanswered.

Pfeil et al (1983) studied the effects of unsteadiness that occurs in the stages of turbomachines by employing a squirrel cage type cylinder cascade which rotated upstream of the measurement plate. Measurements of transition were taken at zero and favourable pressure gradients and a model for the transition process was developed from the time-space distributions of the turbulent spots during transition. Hansen and Okiishi (1987) verified their transition model by taking hot film measurements on a single stage low-speed axial-flow compressor. Their measured influence of rotor-wake segments on the boundary layer development was consistent with modeling the influence of wake segments as turbulent spots. Camp and Shin (1995) have described the measurement and processing of turbulence data from three low-speed, multi-stage

compressor rigs, one of which was Cranfield University's LSRC facility. Their results show how the values of turbulence intensity and length scale at the midspan, change with position in the blade passage with flow coefficient and with the value of the design stage loading coefficient.

As a wake passes over a blade surface, it may trigger transition, so that there are regions of the boundary layer that are sometimes laminar and sometimes turbulent. Using the same arrangement as that of Pfeil et al (1983), Orth (1993) took detailed velocity measurements within the boundary layer of a flat plate using hot-wire probes. The results were compared with the boundary-layer development in undisturbed flow. It was found that the wake disturbances enters the boundary layer leading to a formation of a turbulent patch. Laminar becalmed regions were also observed behind the turbulent patches where brief periods of laminar flow exist far beyond the location at which the boundary layer would have been fully turbulent in the undisturbed flow case. Funazaki (1996b) also observed turbulent patches immediately behind a wake where the velocity profile is characteristic of a turbulent boundary layer.

2.6.2 The Concept of the Becalmed Region

Schubauer and Klebanoff (1955) were the first to observe the so-called becalmed region trailing a turbulent spot. They described the flow behind the turbulent spot as stable and resistant to further disturbances. The explanation given for this was that the propagation speed of T-S waves (approximately 1/3 of the free-stream velocity), is smaller than that of the rear of the turbulent spot and hence the region following the spot must be free of disturbances. The becalmed region received little attention for several years until Cumpsty et al (1995) performed tests on two different types of blades (C4 and Controlled Diffusion). It was found that a turbulent patch initiated by a wake is followed by a calmed region, which is resistant to the initiation of transition. Just after the turbulent patch the calmed region has very high shear stress and resembles the viscous sub-layer in the turbulent region. The calmed region not only resists transition, but it can also over come adverse pressure gradients that would cause separation in a normal laminar boundary layer. Using a wind tunnel, Gostelow et

al (1996) performed extensive investigations by taking detailed measurements of the calmed region behind a triggered turbulent spot under a strong adverse pressure gradient at different streamwise locations. These were done to gain a more detailed understanding of turbulent spot behaviour and to provide more accurate information in order to aid in the computational modelling of turbomachinery flows. Gostelow et al (1996) confirm Cumpsty's (1995) findings by stating that the calmed region exhibits a significantly more stable velocity profile than the natural boundary layer.

Recent experiments of Halstead et al. (1995), Solomon and Walker (1995 a,b), and Solomon (1996) have indicated that transitional flow may cover as much as 70 percent of compressor airfoil suction surfaces and 50 percent of turbine airfoil suction surfaces in the presence of periodic wake disturbances. The periodic transitional or turbulent flow strips generated by wake disturbances are followed by regions of relaxing laminar flow with a shear stress higher than steady laminar flow levels. Independent studies of the latter phenomena in a compressor rotor (Cumpsty et al., 1995), turbine cascade (Schulte and Hodson, 1998) and triggered turbulent spot and compressor experiments (Gostelow et al., 1996) have shown these "calmed" regions to be more stable and resistant to separation than a steady laminar boundary layer flow. Extensive surveys of periodic transition effects and their importance in relation to blading design for axial turbomachines can be found in discussions by Hourmouziadis (1989), Mayle (1991, 1992), and Walker (1993).

2.7. The Effect of Stator/Rotor Indexing

Among his conclusions, Read (1997) states that wakes from previous stator row are clearly visible at the leading edge of a downstream stator row. Therefore, it cannot be assumed that wakes have completely "mixed out" prior to entering the next stage. A suggestion was made that "clocking" or "indexing" the rotor or stator rows could improve the compressor performance. Barankiewicz and Hathaway (1997) have studied the impact of stator row indexing on a multistage axial compressor. The study found that stator indexing produced a 0.2% change in overall efficiency at both peak pressure and peak efficiency conditions and a 5% and 10% change in stator 3 total

pressure loss coefficients respectively. The study concludes by stating that this potential for performance gains due to stator indexing can be expected only in multiple stages with equal number of blades.

2.8. Summary

The reader has been given a brief overview on the concept of the boundary layer, definitions of related properties, and the relevance of its behaviour to the stability and performance of gas turbines. Descriptions of the different types of boundary layer transition have been given followed by a review of past work.

The literature survey has shown that various researchers have undertaken many fundamental investigations by isolating the various components that contribute to the transition of the boundary layer (i.e. free-stream turbulence, pressure gradient etc.) using flat-plates or cascade arrangements in wind tunnel systems. The physics of transition has been well documented but detailed study on transition applied to turbomachinery has not occurred until the early seventies. Studies related to wake affected boundary layers have been performed using either flat plates or cascade arrangements with rotating bars to simulate the wakes. A number of experiments have been conducted in real turbomachinery environment using a single stage compressor arrangement where the inlet flow is usually clean and does not take into account the wake disturbances representative of an embedded stage of a multi-stage axial compressor. Most of the above experiments have been performed using multi gauge hot film anemometry to give a time scale of the influence of the wakes on the surface. The most recent study in the literature with regards to boundary layer flow phenomena in multi-stage turbomachinery is the extensive work by Halstead et al (1995). More detailed tests are needed to confirm and to develop a solid foundation on transitional flows in turbomachinery, which will help more accurate computational models to be created.

CHAPTER 3

Experimental Arrangement and Measurement Techniques

3.1. Introduction

This chapter opens by justifying the use of a real low-speed compressor facility for this investigation. This is done by discussing the applicability, the advantages and disadvantages of the different arrangements used for the study of fluid phenomena that occur in turbomachinery blades particularly the behaviour of boundary layers. This is followed by a general description of the vehicle used for this investigation, Cranfield University's unique large-scale low speed multistage research compressor (LSRC) facility. Descriptions of the instrumentation and measurement techniques as well as the data acquisition system used in both the flow field and boundary layer survey experiments are given. The blading used for this study comprised of a 'state of the art' 3D, modern control diffusion design, providing the desired non-dimensional velocity distribution typical of a high-speed design. Rolls Royce supplied the blades to Cranfield University under a contract entirely non-related to the present research programme.

3.2. Comparisons of Different Testing Arrangements

As occur in all experimental research techniques there are technical advantages and disadvantages associated with the different testing arrangements used for studying flow phenomena such as the boundary layer flows. The following sections discuss these and identify the reason for the choice of the present experimental rig.

3.2.1 Wind tunnel Arrangement with Flat Plate/Cascades

The difficulties involved in conducting studies in realistic turbomachinery environment such as high cost of operation, small physical size of blades and therefore the short time scales of flow phenomena led early researchers to isolate individual aspects of the flow and conduct experiments using simpler arrangements. There are comprehensive reports of boundary layer studies using flat plates (e.g. Abu Ghannam and Shaw, 1980), with rotating rods to simulate wakes (e.g. Pfeil et al, 1983, Orth, 1993, Funazaki, 1996 a & b).

Pfeil et al (1983) state that problems can arise when taking measurement along stationary blades in a real turbomachine environment because of the small dimensions and the impossibility to change only one of the various parameters alone which may influence transition in unsteady flow. For example, a variation of the circumferential velocity of the machine alters both disturbance frequency and Reynolds number simultaneously, while changing the through-flow coefficient alters both the disturbance amplitude and the mean stream-wise pressure gradient over the transition region. They justify the use of a flat plate (which was 700 mm long in their case), because of the ease of accurate measurements due to its large dimensions and the possibility of independent variation of the parameters influencing transition.

During the period when compressor design was performed about the blade mean height, cascades have been a popular arrangement for deriving empirical correlations from the parametric studies of blade shapes, stagger angles, camber and space/chord ratios. Gostelow (1984) summarises the concept of testing linear cascades of compressor aerofoils, which was extensively used by early workers in turbomachinery. The availability of extensive data bases of experimental cascade results have allowed the development of numerical codes, which reflect much of the flow physics and have now superseded the use of cascades for testing blade profiles. The role of cascades has advanced from producing design data to more fundamental investigations such as transition and separation behaviour. Detailed studies using cascades have been described in the previous chapter (e.g. Hodson, 1985, Dong & Cumpsty, 1989 a & b). A novel method of investigation has been reported by Steinert

and Starken (1996) who studied transition, local separation and complete separation on subsonic controlled diffusion aerofoil (CDA) cascades using a new visualisation technique based on Liquid Crystals (LC).

The major limitation to flat plates and cascades is that, being 2 D in nature, they cannot fundamentally give a true representation of the flow phenomena that occur in rotating machines. Examples of these are secondary flows, which are functions of the radial gradients of the primary flow and the coriolis forces that are present in a rotating environment.

3.2.2 Single and Multi-Stage Compressor Facilities

Evans (1978) was one of the first to investigate the boundary layer development on real axial-flow compressor blades using a low speed single stage compressor facility. Both the time-mean and instantaneous velocity profiles on the suction surface of a stator blade were measured. This was compared with boundary-layer measurements on a cascade blade and it was found that the time-mean measurements showed a very much larger rate of boundary-layer growth on the stator blade than the cascade blade. As the three-dimensional flow in the boundary layer appeared to be small, the most likely explanation of the large growth rate is the unsteady nature of the boundary-layer development.

The main technical weakness of a single-stage testing facility is the absence of the detail of the flow structure that exists within an embedded stage, depicting the history of its passage through previous blade rows. As the performance of an embedded stage is strongly influenced by those around it, it is essential to simulate the likely stage entry and exit conditions. In the case of a single stage machine this can be partially improvised by the use of inlet guide vanes or spoilers for thickening the annulus wall boundary layers and the use of an outlet guide vane.

In an extensive study using a multiple stage compressor facility, Halstead et al (1995) have found that the level of turbulence intensity of the incoming wakes, rather

than the level of the wake velocity defect, is the dominant factor, not only in producing the wake-induced strips found in turbomachinery but also in determining their strength and the effectiveness of calmed regions they produce. Upon these findings, they state that selecting a rod size and location based solely upon the criterion of duplicating the velocity defect of the incoming wake, as some papers have reported, can easily result in turbulence intensities from the rods being too high relative to those from aerofoils in high efficiency turbomachines. This difference can alter the transitional characteristic significantly and can draw a misleading picture on the nature of transition in multistage turbomachinery. They therefore conclude that the use of rods to simulate airfoil wakes should be approached with great care.

3.2.3 High-Speed Compressor Rigs

The use of high-speed compressors allows the experimentalist to capture all the flow phenomena that occur in real machines including compressibility effects. However, there are significant difficulties associated with this type of testing, the first and of primary importance being cost. Robinson (1991) has obtained figures representing the inflation-adjusted average of research and engine development projects at the time and quotes the cost of a new high-speed test rig as approximately £4,000K. Subsequent re-blading costs range between £50K and £75K per stage with an addition £250K for fitting and testing. The combination of the initial costs and the high running costs due to vast power requirements imply that such rig arrangements are normally used by commercial engine companies. And such tests are for performance demonstration towards the very late stages of engine development and not for investigative purposes.

Another significant difficulty associated with this type of testing is the small physical size of the blades that make access for instrumentation (e.g. Hot-wire probes, pneumatic probes) and the intrusive effects associated with it a serious problem. For instance the large size of the measurement probes compared to the characteristic dimensions, such as blade thickness and pitch, will inevitably render the spatial resolution and time response insufficient to measure satisfactorily the very phenomena of interest.

3.2.4 Low-Speed Compressor Rigs

Having briefly reviewed the different testing arrangements, the benefits of using low-speed compressors for investigative purposes are quite straightforward. A large-scale compressor running at low-speed can reproduce the aerodynamic flow physics found in today's high speed core compressors at a comparatively low set up and running cost. The larger annulus diameter makes access to the compressor a simpler task and the phenomena of interest are correspondingly bigger enabling conventional instrumentation to measure them successfully with improved spatial resolution and time response. The power required to attain the necessary Reynolds number is inversely proportional to the linear scale of the machine, which correspondingly reduces the running costs. More significantly, the lower stress levels associated with lower operating speed make rig and blade manufacture simpler resulting in reduced manufacturing costs (Robinson, 1991).

The only significant limitation to low-speed compressor rigs is the restriction to simulate subsonic high-speed blading found in the rear stages of the HP compressor. However, by careful profile design the non-dimensional aerodynamic parameters of a high-speed machine can be replicated in the low-speed compressor, with the exception of Mach number. A discussion of the techniques for obtaining this aerodynamic similarity can be found in Foley (1995).

In summary, the three principal advantages to low-speed testing are lower cost, lower risk and greater accuracy. These make detailed investigation of various fundamental loss mechanisms in different high-speed blade designs economically practicable. The large scale of the facility permits accurate probing with blockage effects virtually eliminated. The principal disadvantage of this type of testing is the inability to evaluate the shock wave effects, but this is not a major consideration in middle and rear stages of core compressors (Wisler, 1985). Subsequent to the early popularity and success of the wind tunnel cascades, low-speed test results are the next step to introducing further sophistication in numerical modelling of turbomachinery flows. The following introduces the reader to Cranfield University's four-stage Low Speed Research Compressor (LSRC) facility and the accompanying instrumentation

used in this study.

3.3. The Low Speed Research Compressor (LSRC)

Cranfield University's four-stage Low Speed Research Compressor (LSRC) facility was the main vehicle used for this investigation. This large-scale low-speed compressor with repeating-stage blading has been designed to duplicate many of the essential flow features of subsonic middle and rear stages of a medium to highly loaded multistage compressor. The LSRC facility, which has a constant casing diameter of 1.22 meters, is described in more detail in Robinson (1991). A basic schematic diagram and photograph of the LSRC are shown in Figures 3.1a & b.

The large physical size of the Low Speed Research Compressor facility offers investigators the opportunity of very detailed investigations of the flow. The outer diameter of the compressor makes it possible to carry out traverse measurements in between blade rows and very close to the annulus walls. The mechanical arrangement of the facility allows rotation of the rotor casing rings relative to the stator rings, thus enabling circumferential traversing of measurement probes without any disturbance of the flow near the annulus walls (i.e. no circumferential probe slot is needed). This 120 kW, 1100-rpm multistage compressor has identical rotor and stator blading on each stage. The third stage was used as the study stage with the first and second stages setting up the inlet conditions for it. A window cut out for optical access for the application of LDA system in a previous study has been modified to accommodate the traverse mechanism for the boundary layer survey. The inlet flow was from ambient air and the flow through the facility was essentially incompressible. The LSRC was fitted with a filter at the inlet to minimise the amount of dust particles, which could contaminate and/or damage the measurement instrumentation.

3.4. Blading

Typical of modern designs, the compressor had a hub/tip ratio of 0.85, low aspect ratio, and high-solidity blading with stators shrouded both at the hub and the tip with a nominal chord of 70mm. The blading used, series VRB 3 & 3.5, designed by Cranfield and Rolls Royce, were a low-speed aerodynamic model of 3 D "*End Bend*"

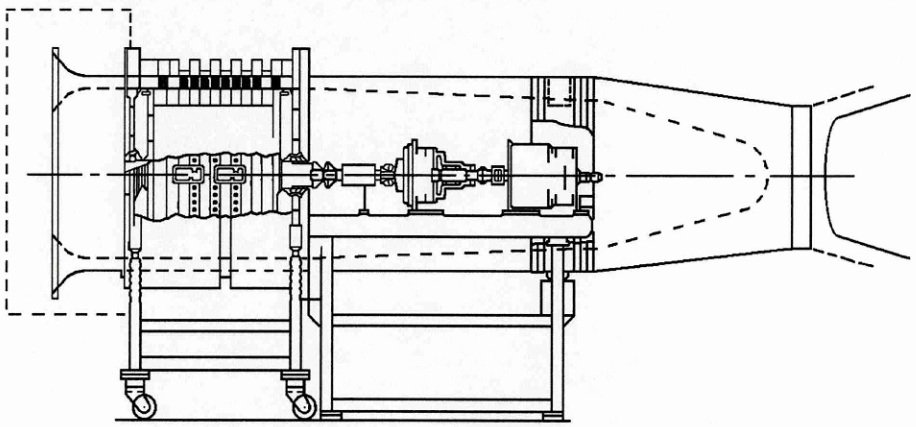

Figure 3.1a Schematic Diagram of the Four-Stage Low Speed Compressor

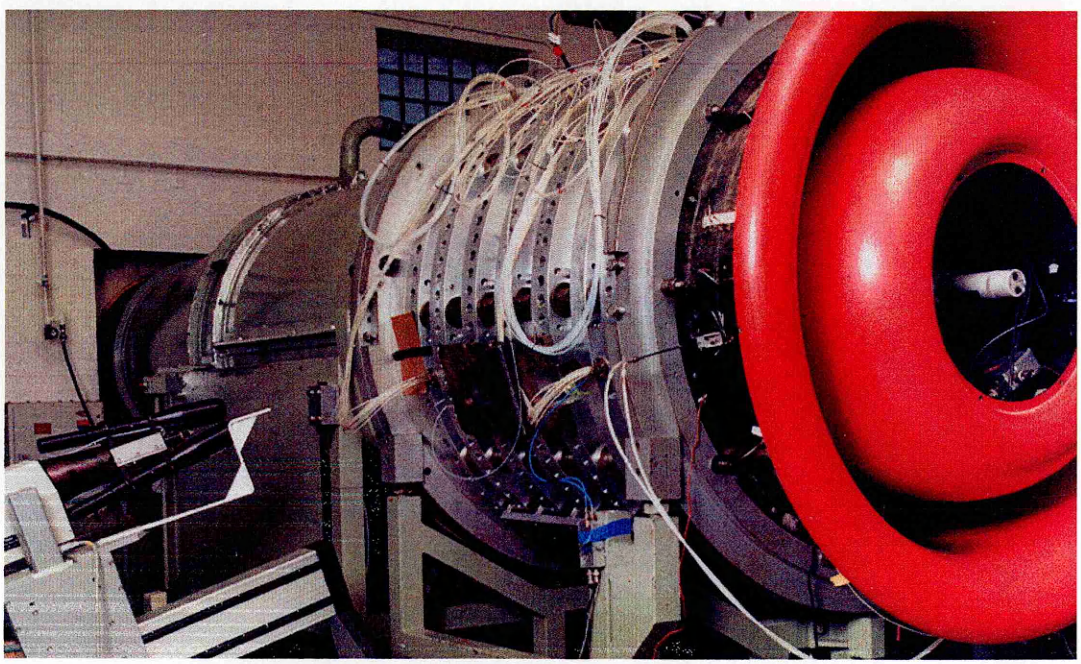

Figure 3.1b Photograph of the LSRC Facility

design to control the diffusion and give the desired surface velocity distribution (Robinson, 1991). Both the flow-field measurement and the investigation of the boundary layer characteristics were performed using this build. Table 3.1 below summarises the general specifications of the LSRC facility, the general blade geometry and the aerodynamic test conditions for the compressor during the build used for this investigation.

Figure 3.2 illustrates a typical performance map of the LSRC with the VRB 3.5 build. Data were acquired at two flow conditions, Design and Near Stall. These flow coefficients were based on the area average axial velocity $\mathbf{V_a}$ and the rotor blade speed at midspan $\mathbf{U_m}$ of the first stage.

Casing radius	609.6mm
Inner wall (hub) radius	518.16mm
Number of Rotor blades	74
Number of Stator blades	96
Rotor Tip radius	607.86mm
Stator Blade height	91.44mm
Mid Height stagger Angles:	Stator = 27.542° Rotor = 46.145°
Design flow condition ∅ (Va/U)	0.485.
Near stall flow condition ∅ (Va/U)	0.410

Table 3.1 General Specifications and Operating Conditions of the LSRC

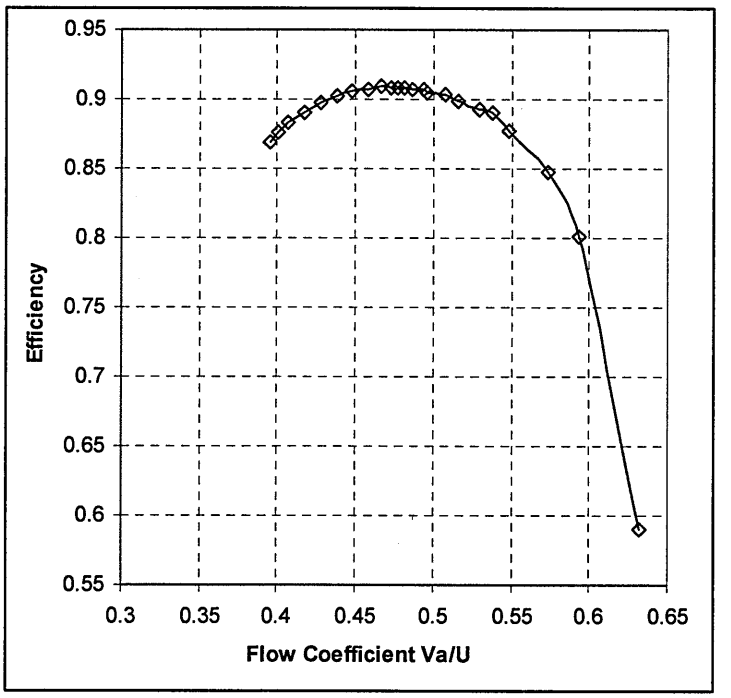

Figure 3.2 Typical Performance Map of the VRB3.5 Build

The measurement plane chosen for the flow field study was downstream of the third rotor stage, shown in Figure 3.3, where both radial and circumferential traverse measurements were carried out using a dual sensor X array CTA probe (see section 4.3) to capture two velocity components (i.e. axial and circumferential) at each of the measurement points.

Physical measurements have shown that the minimum and maximum axial gap between the rotor row and the following stator row of the measurement stage ranged from 24mm to 32mm respectively. This was due to the 3D design characteristics of the blading used where the profile at different heights varied in position relative to the centreline of the blade. This variation of the axial gap between the rotor and stator stage can have a significant effect in terms of the level of rotor wake mixing out prior to impinging on the leading edge of the downstream stator blade.

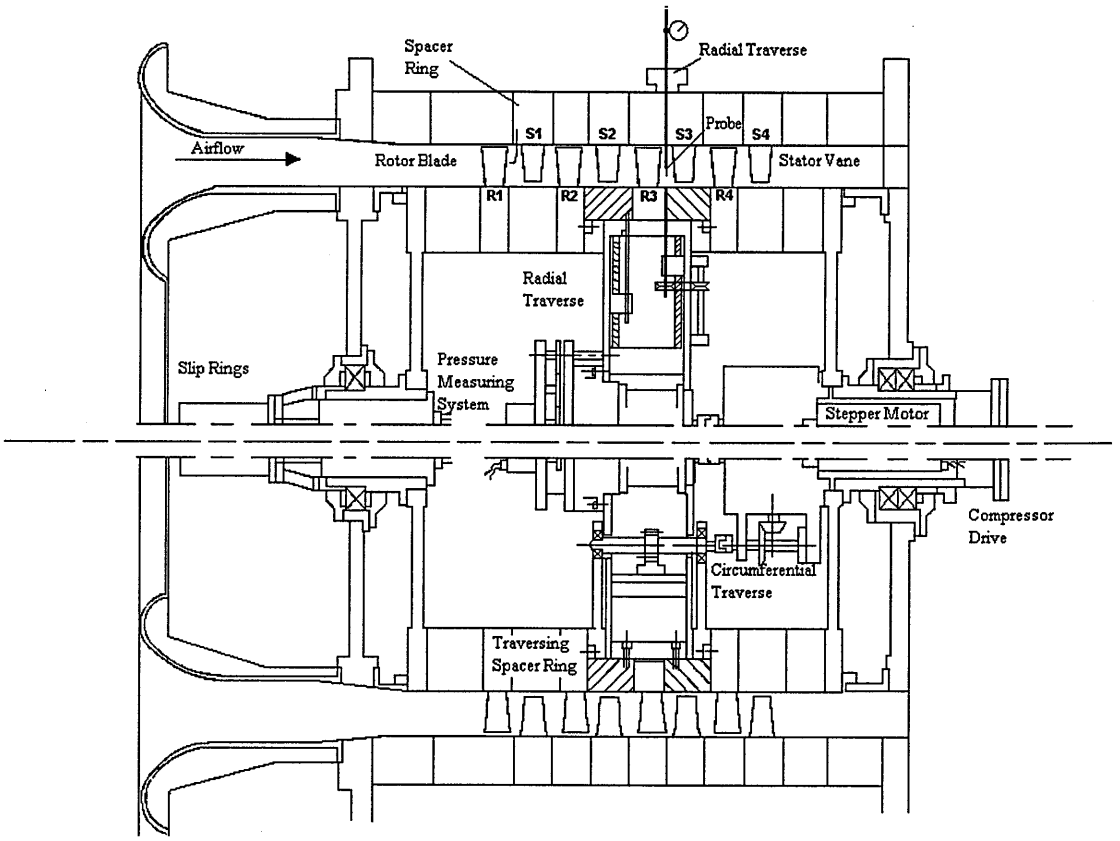

Figure 3.3 Traverse Location for the Flow Field Measurements (from Ivey & Swoboda, 1998)

3.5. Instrumentation

The following sections provide an outline of the criteria used for the selection process of the appropriate principal measurement system. Then general descriptions of the hardware of the measurement tools and the calibration techniques are given.

3.5.1 Thermal Anemometry

Constant Temperature Hot-Wire Anemometry (CTA) has been chosen as the principal tool of measurement in this investigation. This measurement technique has been proven to a be a very robust method to obtain data concerning the random motion involved in turbulent flows because it employs a fast response sensor with a small physical size. The absence of a complicated seeding arrangement such as required in an LDA system is a significant convenience and consequently there are no problems measuring regions of recirculation near surfaces. The principles of hot-wire

measurements are well established and can be found in the literature on fluid measurement techniques such as Lomas (1986), Bradshaw (1971) and more recently Bruun (1995). A summary of the fundamentals of CTA accompanied by examples of the calibration techniques used in this investigation can be found in Appendix A.

Briefly, the hot wire anemometer is an instrument designed for detailed investigation of flow and turbulence. The basic principle is that a small heated sensor is placed in the flow and is cooled by the passage of fluid over it. If one can measure the cooling effect on this probe then one can relate this to fluid velocity by calibration. Such a technique will involve the use of a probe and electronics, which will satisfy certain basic requirements. These are:

1. The sensor must be very small so as to approach the ideal situation of a point measurement.

2. The physical size of the probe must be small so as to create the minimum possible flow disturbance.

3. To define the fluid velocity one must know both the magnitude and direction of the flow and so the probe must have a directional characteristic, which facilitates the determination of flow direction.

4. The probe and electronics should form a system, which has a response fast enough to enable it to respond to the most rapid velocity fluctuations that may be encountered. And the frequency response curve should be flat up to the required upper frequency limit.

5. The relationship between the output voltage and velocity should ideally be linear.

In summary, the major advantages of the hot-wire instrumentation are the low cost of installation, small size of the measuring probe and the fast frequency that makes

measurement up to several hundred kilohertz easy to obtain. Despite the advantages outlined above, hot wire anemometry is still an intrusive method of flow measurement, but considering the large scale of the measurement vehicle, the effect of flow disturbances could be minimised by carefully positioning the probes at optimum locations.

3.5.2 The Hot-Wire Flow Measurement Probes

Mainly two types of hot-wire probes were used to fulfil the requirements of this investigation. DANTEC's 55P52 X array Dual sensor probe was used for the flow field measurement to assess both the magnitude and the direction of the flow downstream of an embedded rotor stage (i.e. rotor 3). DANTEC's 55P01 General-purpose and 55P05 Boundary layer single sensor probes were used for the detailed boundary layer survey on the suction surface of a stator blade downstream of the third rotor row. Probes used for both the flow field measurement and the stator's suction surface boundary layer survey are shown in Figures 3.4 a and b below.

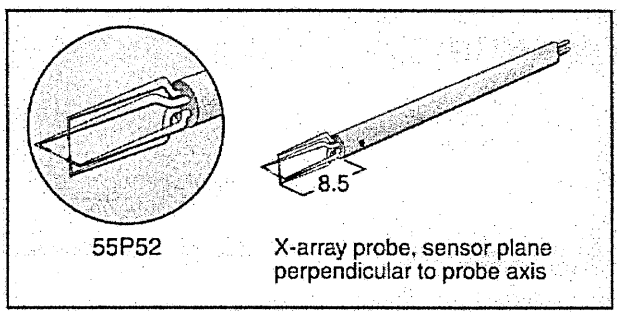

Figure 3.4a Dual X array Probe used in Flow Field Investigation (DANTEC)

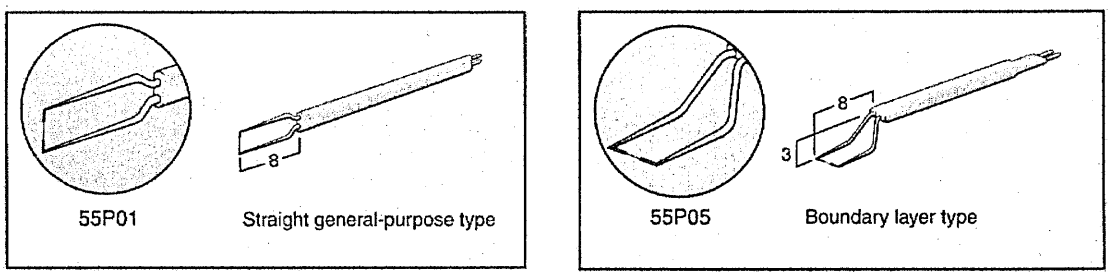

Figure 3.4b Single Sensor Probes used for BL Surveys (DANTEC)

The sensing wires of all the probes used in this study were made of Platinum-plated Tungsten, 5 μm in diameter with a sensitive length of 1.25 mm. The ends of the wires were Copper and Gold-plated to a diameter of approximately 15 μm. Including these Copper and Gold-plating features, which made the overall length of the wire to become 3 mm, proved to be aerodynamically vital for collecting accurate instantaneous 2 D velocity data. This was particularly the case during flow field measurements, where the sensor measurement plane was orientated perpendicular to the probe axis. The longer wire, which kept the supporting prongs sufficiently apart plus the coating at the edges, significantly reduced the effect of the prong wakes on the sensing length of the wire. Another useful purpose of the edge coating was an accurate definition of the sensing length and a uniform distribution of operating temperature. Bradshaw (1971) and Bruun (1995) recommend the use of gold-plated sensors for measurement in highly turbulent flows of one, two and three dimensions. The separation distance of the sensor wires of the 55P52 X array dual sensor probe was specified to be 1mm to eliminate any heat transfer errors from neighbouring sensors.

3.5.3 Calibration of Hot-Wires

The following provide brief descriptions of the hardware and the methods used for the calibration of the two types of hot-wire probes used in this study. Further details of the calibration techniques employed for each type of sensor probe can be found in the following chapters. Example calibration data sets with the corresponding characteristic curve fitting procedures can be found in Appendix A.

Calibrations of both of probe types were performed using an existing DANTEC's 55D90 calibration kit with a variable laminar flow output. Compressed air first passes through a filter and an integrated valve system regulates the mass flow. The flow then enters the nozzle unit of varying diameters and emerges as a free laminar jet. A differential pressure micro-manometer measured the pressure drop (Δp) across the nozzle permitting the exit velocity to be calculated. The temperature of the air exiting the nozzle was periodically measured using an analogue thermometer. As the temperature at calibration could vary from the temperature during testing, a correction

for effects of ambient temperature drift (Bearman, 1971) was implemented during the processing of the results. Detailed discussion on the correction method used in this study can be found in Appendix A.

A computer code was developed as a module to the data acquisition system allowing the calibration of the hot-wires to be a speedy, semi-automated procedure. This was necessary because firstly, although recognised as a robust and accurate measurement system, the relation between the voltage output from the hot-wire anemometer and velocity is not linear. Secondly, due to the high sensitivity to drifts in temperature and resistance (e.g. sensor wire, cable etc.), the hot-wire requires calibration prior to and after testing to ensure consistency of measurement data. The overall duration of a typical calibration session ranged between 30 to 45 minutes.

Prior to exposing the hot-wire probe to the flow from the calibration unit, the anemometer bridge unit was balanced. The variable resistor in the Wheatstone bridge (see Figure 3.5) was adjusted to maintain the sensor's operating temperature at a desired value (280 °C in this case). This was done via the selection of an overheat ratio **a**, defined as the ratio of the wire resistance at operating temperature to the wire resistance at ambient temperature. This ranged between 0.8 and 1 for the type of sensor used in this study.

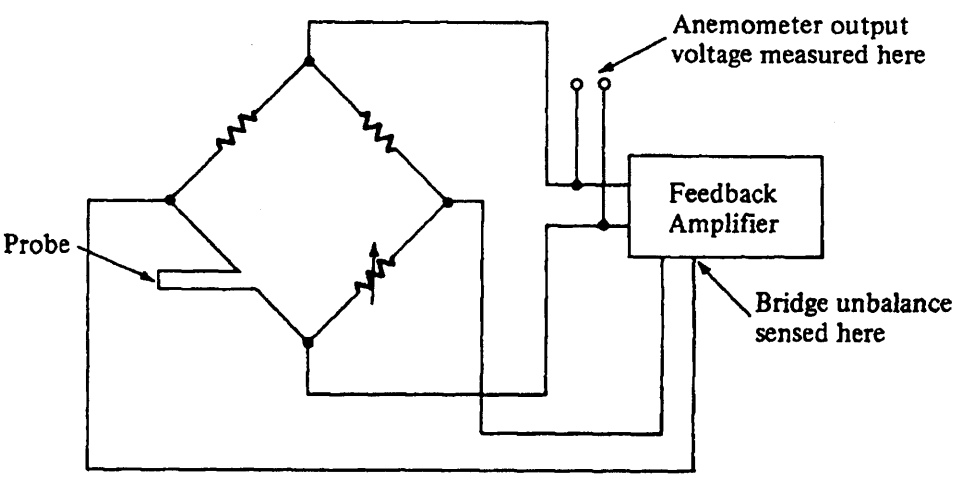

Figure 3.5 Block diagram of a Constant Temperature Anemometer (Lomas, 1986)

3.5.4 Single Sensor

Calibration of both the 55P01 General purpose and 55P05 Boundary layer single sensor probes was performed using the general form of the King's Law formulation (Lomas, 1986),

$$E^2 = A + B * U^n \tag{3.1}$$

where B and n are calibration constants and A is the anemometer output voltage at zero flow conditions.

3.5.5 X array Dual Sensor

The 55P52 X array dual sensor probe makes it possible to obtain the direction as well as the magnitude of the flow of interest. Due to the orientation of the probe relative to the flow in the present application, a slightly modified method of calibration curve fitting procedure consisting of a fourth order polynomial equation using the effective cooling velocity was adopted to represent the characteristic of each sensor. This is discussed in more detail in Chapter 4.

3.6. Area Traverse Measurement

The radial traverse of the flow-field measurement was performed manually through the use of a vernier gauge traverse gear onto which was mounted a support for a dual sensor probe. The dial gauge of the traverse gear had an accuracy of up to 0.05mm allowing the radial position to be varied to 0.05 % of the blade height. Circumferential locations were performed via the LSRC facility's main control deck computer, which controlled the stepper motor driving the rotor casing rings. In this study, the total circumferential traverse angle was set to 7.375 degrees covering nearly two stator blade pitches. The driving software allowed the option of varying the resolution of the circumferential traverse increments. The software was modified to provide 16 equal steps within the total circumferential displacement i.e. 0.46-degree increments. This resulted in the full area traverse measurement plane becoming a

matrix of 16 × 16-measurement points i.e. 16 blade heights and 16 circumferential positions. Figure 3.6 below shows a photograph of the general layout of the testing arrangement.

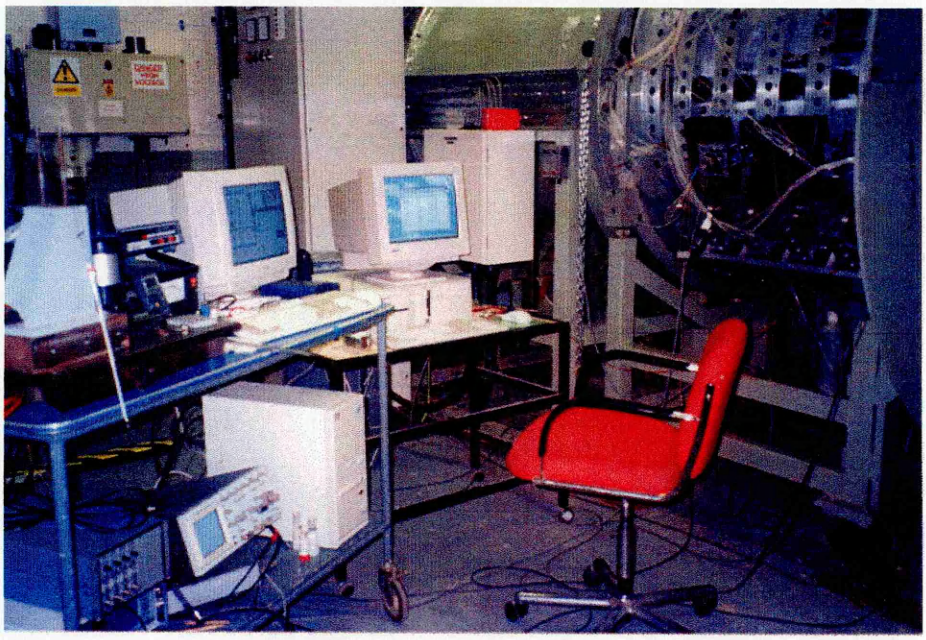

Figure 3.6 General Layout of the Experimental Facility

3.7. Stator Blade Suction Surface Boundary Layer Survey

A specially designed traverse mechanism enabling precise positioning of the measurement probe formed the crucial component of this part of the investigation. The design made it possible to collect velocity data at desired locations on the stator blade's suction surface (i.e. height and chord). A stepper motor, in combination with a micro-stepping electronic gear ratio integrated in the driver/interface card allowed the probe to move at very small increments (e.g. 20-25μm depending on position) in a virtually perpendicular direction from the blade surface. Detailed descriptions of this traverse mechanism from initial design concept to manufacture with outlines of the methodology used for this part of the investigation are given in Chapter 5. Figures 3.7 & 3.8 show the traverse gear assembly in isolation and as mounted on the LSRC facility respectively. In this study it was intended to perform boundary layer surveys at

four chord positions and at three blade heights. However, the 3D '*End-Bend*' design characteristics of the blade made measurements at some positions difficult. This will be described in further detail in Chapter 5.

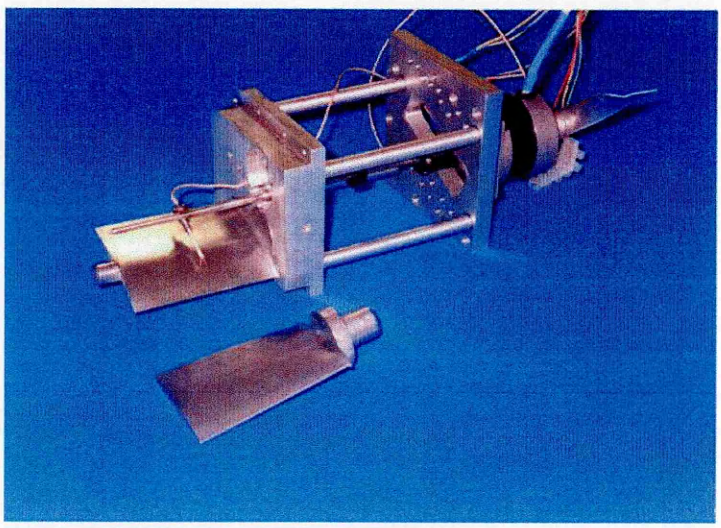

Figure 3.7 Traverse Gear with DANTEC 55P05 BL Probe

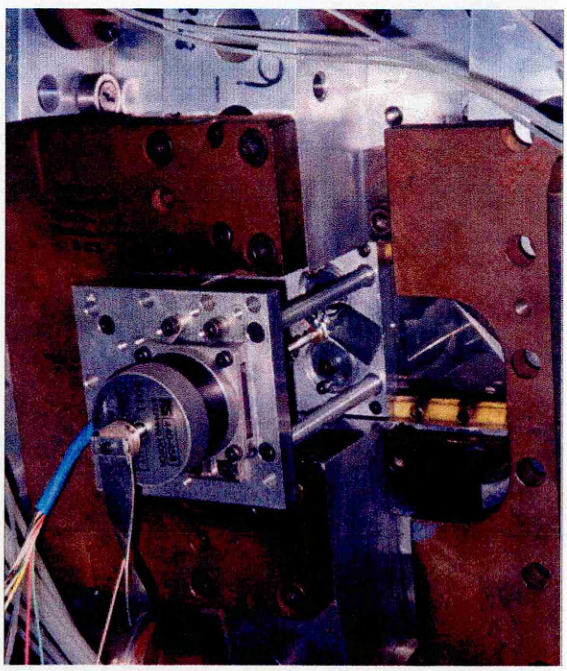

Figure 3.8 Traverse Assembly Mounted on the LSRC Facility

3.8. Data acquisition, Stepper Motor Control & Processing System

The data acquisition and stepper motor control was fully automated. A high-speed PC-based data acquisition hardware and software system had been developed with sufficient computing power to cope with all the data collected. This PC-based data acquisition system was developed with the unsteady flow operation in mind. Figure 3.9 below illustrates the layout of the data acquisition scheme used in the calibration of the hot-wires and testing. During measurement the probes were mounted onto the appropriate traverse gear.

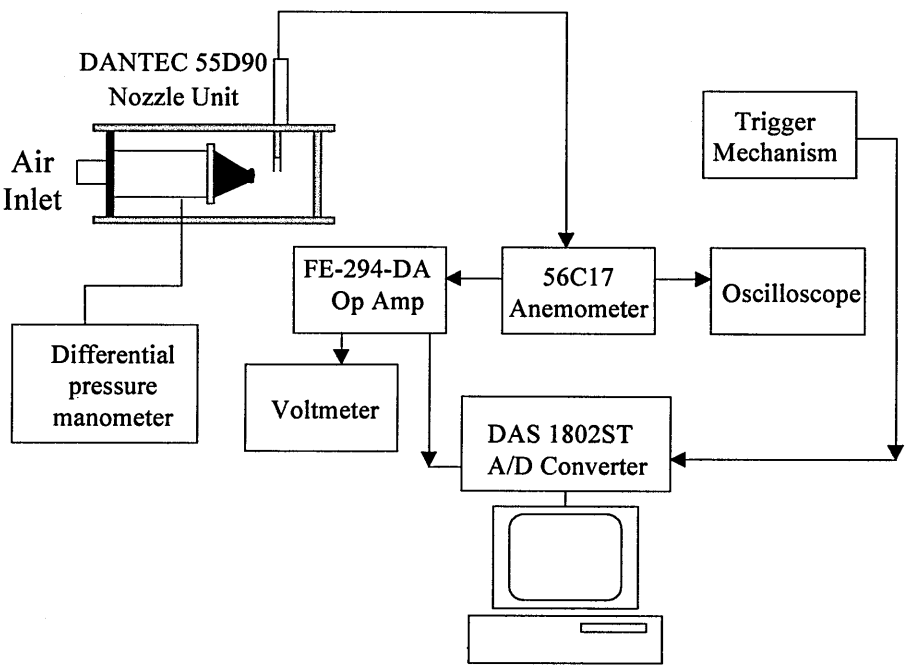

Figure 3.9 Data Acquisition Scheme Used During Calibration and Testing

The hardware of the hot-wire data logging system consisted of a general-purpose high precision 56C17 multi-channel anemometer with modules mounted in a 56B12 Mainframe. The 56C01 main unit contains all the circuits required for establishing an anemometer (except the bridge itself). It contains a servo amplifier, filters, protection circuits, and a square wave generator for dynamic balancing of the bridge. The 56C17 CTA Bridge is a universal bridge for all standard measurements

with maximum frequency of 150 kHz. An FE-294-DA (C13742) operational amplifier designed to back off an input voltage and apply gain to the residual was connected to the output of the 56C17 anemometer unit to increase the resolution of the output voltage.

A Keithley Metrabyte DAS-1802ST Series high performance IBM PC compatible computer A/D converter card was installed in a 486X computer and configured for the appropriate applications. The DAS-1802ST card features continuous, high speed, gap-free data acquisition under Windows or DOS. An on-board FIFO (first in first out) buffer and dual channel DMA (Direct Memory Access) allows the acquisition of large amounts of data without loss. The DAS-1802ST has 16 single-ended or 8 differential inputs with the ability to externally expand to 256 differential inputs at 333 Ksamples/sec.

The hardware system for the stepper motor control was based on an interface card that was installed externally of a Pentium II PC. Communication from the control software was achieved through a RS232 connection. The interface card served the purpose of both as an interface and driver of the stepper motor allowing desired movement of the traverse gear from ASCII text command inputs. An electronic micro-stepping facility allowed the user to vary the gear ratio thus enhancing the resolution of the step angles.

Data acquisition/post-processing and stepper motor control software were developed in Visual Basic (Version 3 & 5). These software modules could be run individually or in combination and allowed the user to read in the raw data files then compile the final processed data to a nominated file/directory for easy access in the future.

3.9. Hot film Anemometry

The use of multi-gauge hot film anemometry had been considered during the early stages of this study but this method of measurement was not used mainly due to the time constraints and the difficulties associated with its application. There were two

primary factors that contributed to the difficulties. The first was of a mechanical nature: the complex geometry of the measurement blade surface, which was curved along both the chord and the span of the blade. This made sticking the sensors on the blade surface a complex matter requiring precision machining of the blade to accommodate the thickness of the polyamide film. Secondly, obtaining accurate records of the flow field using multiple sensors simultaneously required an appropriate data acquisition system, which could accommodate multiple channels (there were a maximum of four available during the present study). Another requirement would be the development of a sophisticated electronic system that would enable rapid switching between alternate sensor elements.

3.10. Other Instrumentation

Throughout the whole testing period, which lasted several days, the ambient conditions such as temperature and atmospheric pressure were carefully recorded in order to ensure consistency. A laboratory standard analogue thermometer and a temperature sensor located at the inlet bellmouth of the LSRC facility were used to record the ambient temperature. The barometric pressure reference was taken from the output of a Druck Digital Pressure Indicator (DPI 140) that was regularly read via a PC connected to the instrument. The 'Furness' differential pressure manometer used to evaluate the air velocity from the calibration nozzle was periodically calibrated against a Druck DPI (1800) pressure gauge. Finally, the operational speed of the LSRC experimental rig was constantly maintained at optimum from the control room.

CHAPTER 4

Hot wire Investigation of the Flow Field

4.1. Introduction

It is well known that turbulent flow within a turbomachine has a significant effect on the blading characteristics primarily through its influence on the boundary layer (Mayle, 1991). Higher turbulence levels can help in suppressing separation as described earlier, which can be useful at operating conditions where the blades are more highly-loaded. On the other hand, higher turbulence levels bring on earlier boundary layer transition from laminar to turbulent contributing to higher values of skin friction and heat transfer (the latter is more applicable to turbines and not considered in this study).

The flow within multi-stage compressors is periodic and unsteady and further development of blade design requires improved understanding of the flow field. Its impact on blade loading and boundary layer transition is of particular importance. This chapter describes in detail the methodology applied for investigating the unsteady flow field that exist within an embedded stage of Cranfield's Low Speed Four-Stage Research Compressor and presents the results. It should be noted that the author had limited access to the LSRC rig facility, which at the time was commissioned under a separate contract with Rolls Royce. Therefore, the data is not as extensive as would have been wished. A unique feature of this part of the investigation is that the reader may observe the dynamic nature of the flow field that has been captured and compiled in the form of AVI movie clip files. The executable files are stored in the Compact disc accompanying this thesis and can be accessed via a CD-ROM drive. These can be played with 'Microsoft Media player' software available on most PC's or 'Real Player' software (Demonstration Version), which can be downloaded free of charge from the Internet.

4.2. Experimental Test Programme

In order to gain an understanding of the nature of the flow within the repeating stages of an axial compressor, DANTEC's 55P52 dual sensor X array probe was used to carry out area traverse measurements downstream of the third rotor stage. This stage has been used extensively by previous investigators (Robinson, 1991, Howard et al, 1994, Foley, 1995, Read, 1997) as it is very representative of an embedded stage, with the first two stages setting up the repeating flow conditions while the fourth stage provides the appropriate downstream pressure field. The space limitations imposed by the small axial gap between the rotor and stator blade rows made measurement possible only with the orientation of the probe set up with its axis perpendicular to the flow. Figure 3.3 in Chapter 3 shows this orientation of the probe when mounted on a radial traverse mechanism. The measurement plane is illustrated in Figure 4.1 below. This orientation of the measurement probe introduced certain effects that required particular attention during calibration and is discussed in detail in Section 4.3.

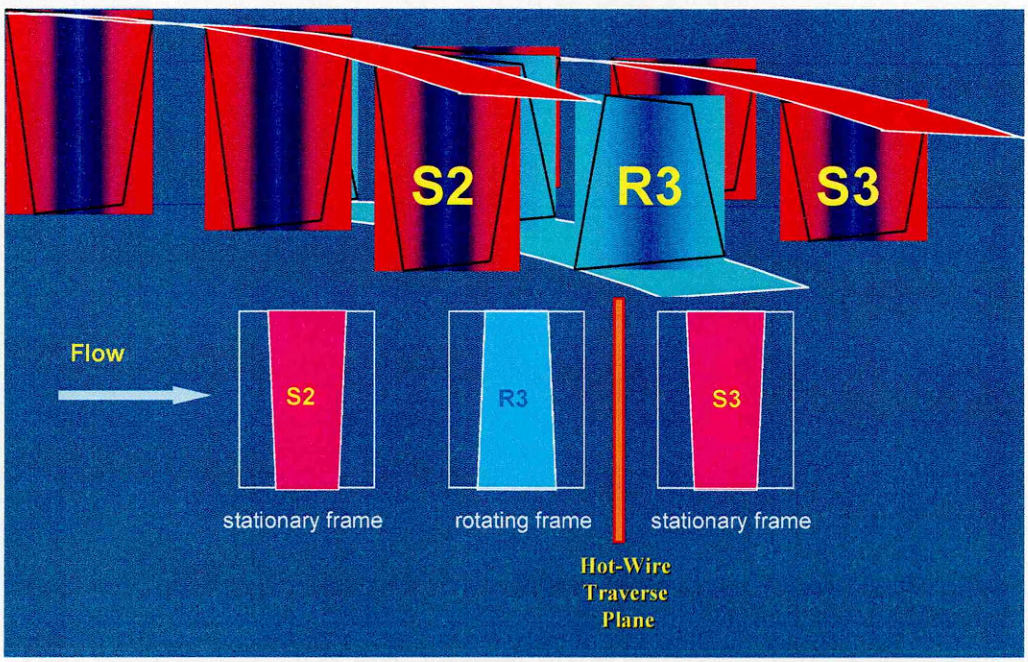

Figure 4.1 *X Array Hot Wire Traverse Plane Downstream of Rotor Three (after Lockwood, 1999)*

The unsteady flow field measurements were carried out with the radial positions covering from 2% to 98% blade height and the circumferential traverse spanning a total of 7.375 degrees, which was equivalent to approximately two stator blade pitches. This area traverse resulted in a measurement matrix of 16 heights and 16 circumferential positions. Figures 4.2 and 4.3 show a schematic representation of the circumferential traverse and the measurement matrix respectively. It should be noted that the small radial distance (i.e. 1mm) that separates each sensor wire of the X array probe made it physically impossible to start the radial traverse measurement from either absolute 0 percent height or finish at absolute 100 percent height.

The angle of the flow leaving the rotor immediately at the trailing edge and approaching the probe varies at each radial height. It was therefore necessary to yaw the hot wire probe accordingly to avoid errors caused by wakes from the hot wire support prongs impinging on the sensors. Mean flow angle data obtained from measurements taken previously with pneumatic probes (Bennett, 1999) was used to optimise the probe orientation. Flow angle data at the corresponding blade height at two operating conditions of the LSRC compressor are outlined in Table 4.1 below.

Height %	2	5	10	15	25	35	45	50	55	65	75	80	86	92	96	98
Design (Degrees)	57	48	48	48	48	48	48	48	48	48	48	48	48	54	54	58
Near Stall (Degrees)	60	54	54	54	54	54	54	54	54	54	54	54	54	62	62	64

Table 4.1 Mean Exit Flow Angles Downstream of Rotor 3

DANTEC's C type 57C17 multi channel anemometer was set at constant temperature mode and data was acquired at a sampling frequency of 100 kHz for each channel. The high-speed data acquisition program allowed the user the flexibility of logging different number of samples and cycles during the experiment. The triggering mechanism was a once per revolution pulse via an optical sensor, which picked up a signal from the same point on each rotor blade revolution. This made it possible to observe the wakes of the same rotor blades. Partial post processing of the data was

carried out during the acquisition and though limited to the memory capacity of the computer, it was of sufficient quality to ensure that the system was functioning correctly and could detect any anomalies during testing.

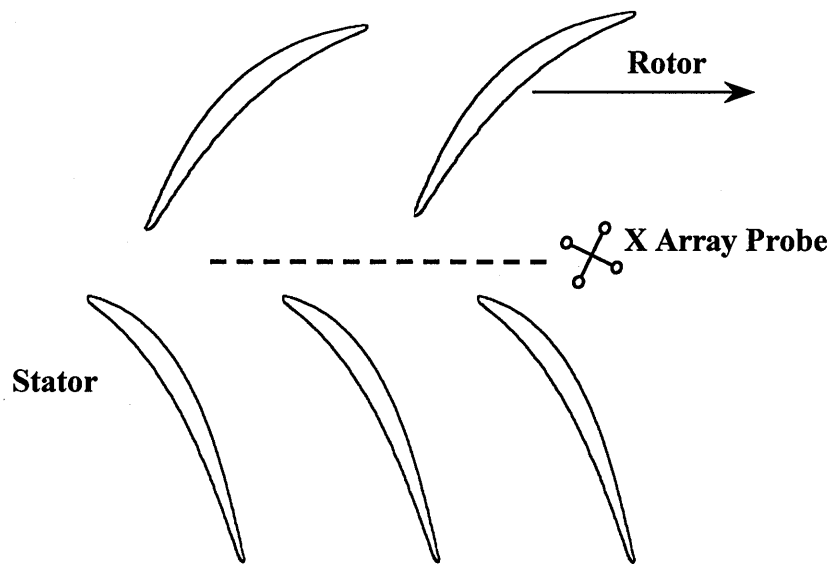

Figure 4.2 *Dual Sensor Probe Circumferential Traverse Location in the Axial Gap (Not to Scale)*

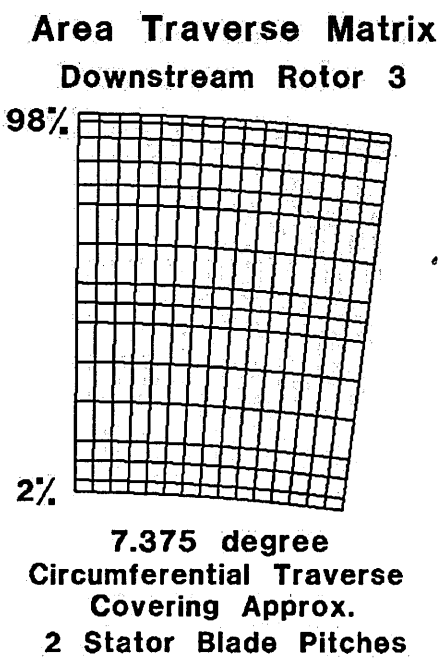

Figure 4.3 *Measurement Matrix of Hot-Wire Area Traverse*

4.3. Hot Wire Measurement Techniques

4.3.1 X Array Probe Calibration

DANTEC's 55D90 low turbulence open-jet calibration facility was used to calibrate the dual sensor probe for both velocity magnitude and angular sensitivity. Calibration data was collected by recording 15 laminar air jet velocities from 0 m/s to 70 m/s while varying the angle of approach from 0 degrees to 90 degrees at 5 degree increments (see Figure 4.4). Previous investigators at Cranfield have used an existing calibration program (Hodson 1985), to perform a least-squares fit of the King's Law formulation and Champagne's Law (Equation 4.2). It was found that this curve-fitting program used the calibration data to treat each sensor separately without taking into consideration the wake effects from the prongs of the outer wire. This method merely 'forced' the calibration constants of each sensor to a certain value in order to establish the full 'quadrant' (see Figure 4.4), as the measurement zone. This resulted in the program producing inaccurate characteristic curves for each sensor of the probe.

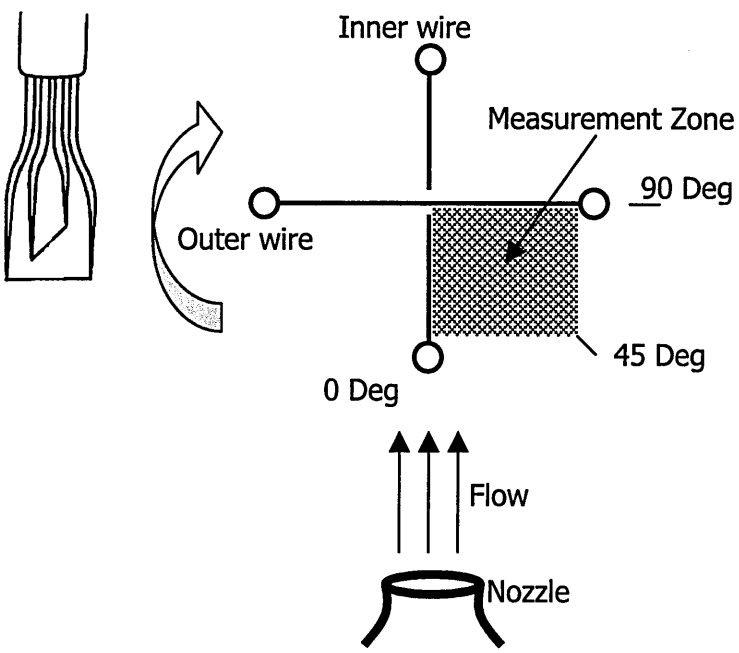

Figure 4.4 Datum Position of X Array Probe during Calibration.

Different calibration techniques for dual sensor application can be found in the literature and a recent general compilation of thermal anemometry techniques can be found in Bruun (1995). For the present study, the author has chosen a method that used the effective cooling velocity $\mathbf{U_{eff}}$ (velocity vector normal to the sensor) to establish a fourth power polynomial characteristic for each sensor. The wake effects of the prongs reduced the measurement quadrant/area, which is termed the 'Confidence Zone' shown in Figure 4.5 below. This method proved to be very practical in terms of time spent collecting calibration data and more importantly accuracy. A sample of this calibration technique can be found in Appendix A, along with comparison of resolution between the 'Standard' and 'Gold-Plated' sensors. The X array dual sensor probe coupled with DANTEC's 56C17 multi-channel anemometer bridge system allowed two-dimensional components of velocity to be captured simultaneously. Three-dimensional investigations were considered during the course of this research but due to major time constraints and limited mechanical modifications allowed on the LSRC facility, this work had not been pursued further.

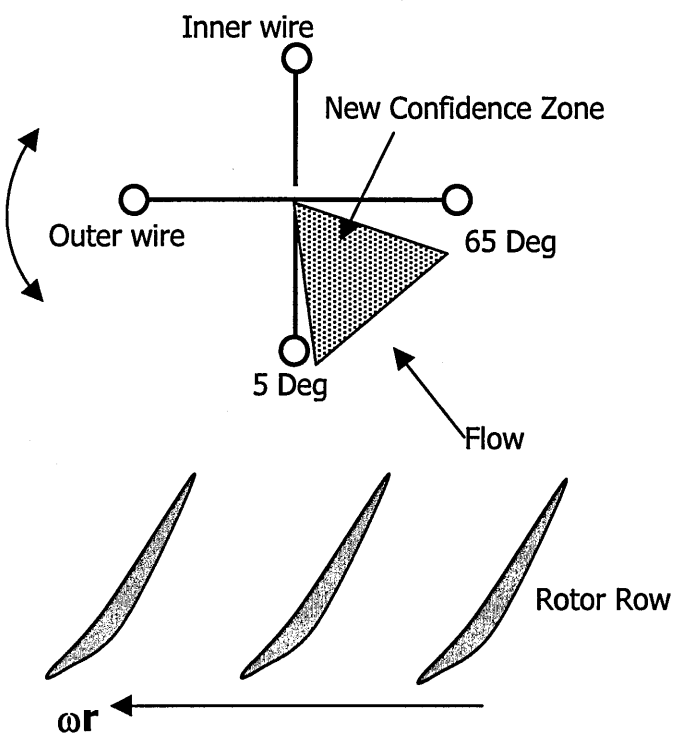

Figure 4.5 New 'Confidence Zone' Due to Prong Effects

As mentioned earlier, the mean flow angle leaving the rotor row varied along the blade span from the hub toward the casing. The unsteady rotor exit flow angle was anticipated to fluctuate up to ±10 degrees from the mean angle (Bennett, 1999). To ensure that accurate values of unsteady velocities and flow angles were obtained, the probe was yawed along its axis so that the mean flow approached the centre region of the 'Confidence Zone' (i.e. 35 degrees from the Normal to the Outer sensor). This permitted flows that deviated no more than ±30 degrees from the mean and therefore remained within the 'Confidence Zone' to be measured accurately by the probe. The consequence of this different alignment of the probe at various radial heights was that the local sensor co-ordinate differed from the absolute reference co-ordinate of the experimental rig. This was not a problem as the offset values were recorded during testing and automatically input into the data acquisition program to ensure correct data processing.

Another factor that had to be taken into account was the fluctuations of ambient conditions. The inlet to the LSRC compressor facility was from ambient air from outside and as mentioned in Chapter 3 calibration of hot-wires was required before each experimental session. Every effort was made to stabilise the temperature by opening the test house doors prior to each test session to ensure that the air temperature during calibration was equal to that during testing. Despite those measures taken, a full flow-field measurement session at each flow condition lasted a whole day and therefore fluctuations in ambient conditions were inevitable. The ambient temperature and pressure were periodically recorded both manually and via the computer in the control room. These values were used to take into account any fluctuations that occurred and applied in the corrections during post processing of data.

It was later discovered that the trigger sensor that picked up a signal from a once per rotor revolution was not fixed in a stationary point as was expected but rotated with the circumferential traverse ring. This resulted in the relative distance between the trigger sensor and each pitch-wise measurement point to remain constant. Introducing an artificial time delay in the data analysis program rectified this minor problem.

4.3.2 Application

The yaw-angle relationship from Hinze (1959), gives:

$$U_{eff}^2 = U_x^2 + k^2 U_y^2 \tag{4.1}$$

where U_{eff} is the effective cooling velocity and k is the yaw factor, which takes into account the additional cooling by the tangential component of velocity (Champagne et al, 1967). The above equation can be rewritten as:

$$U_{eff}^2 = U^2(\cos^2\theta + k^2 \sin^2\theta) \tag{4.2}$$

This expression is also known as the 'Champagne's Law' where the angle θ is taken as the angle between the normal of each wire to the mean flow. So from the above:

$$\begin{aligned} U_{normal} &= U\cos\theta \\ U_{parallel} &= U\sin\theta \end{aligned} \tag{4.3 a, b}$$

Since each sensor wire of the probe is oriented perpendicular to the other, ignoring the third dimension, it can be deduced that velocity normal to one wire is parallel to the other. From this assumption the following derivation was previously applied by Read (1997), who also used dual sensor probes of similar specifications to take circumferential traverse measurements at a fixed height only.

$$U_{normal\ 1} = U_{parallel\ 2}$$

or (4.4 a, b)

$$U_{parallel\ 1} = U_{normal\ 2}$$

and

$$\begin{aligned} U_{eff\,1}^2 &= U^2{}_{normal\,1} + k_1{}^2 U^2{}_{parallel\ 1} \\ U_{eff\,2}^2 &= U^2{}_{normal\ 2} + k_2{}^2 U^2{}_{parallel\ 2} \end{aligned} \tag{4.5 a, b}$$

Then, substituting the parallel components of one wire with the normal components of the other we obtain:

$$U^2_{eff\,1} = U^2{}_{normal\,1} + k_1{}^2 U^2{}_{normal\,2}$$
$$U^2_{eff\,2} = U^2{}_{normal\,2} + k_2{}^2 U^2{}_{normal\,1} \qquad (4.6\text{ a, b})$$

the above gives a linear relation of the squared values of velocities which can be represented in a matrix form. This gives,

$$\begin{bmatrix} U_{eff\,1}{}^2 \\ U_{eff\,2}{}^2 \end{bmatrix} = \begin{bmatrix} 1 & k_1^2 \\ -k_2^2 & 1 \end{bmatrix} \begin{bmatrix} U^2_{normal\,1} \\ U^2_{normal\,2} \end{bmatrix} \qquad (4.7)$$

Therefore:

$$\begin{bmatrix} U^2{}_{normal\ 1} \\ U^2{}_{normal\ 2} \end{bmatrix} = \frac{1}{1 - k_1{}^2 k_2{}^2} \begin{bmatrix} 1 & -k_1{}^2 \\ -k_2{}^2 & 1 \end{bmatrix} \begin{bmatrix} U_{eff1}{}^2 \\ U_{eff2}{}^2 \end{bmatrix} \qquad (4.8)$$

Although this gives the squares of the velocity components, by ensuring that the probe was oriented so that the mean flow approached the probe within the 'Confidence Zone' the same sign could be assigned to all the instantaneous measurements. As stated previously, the deviation of the flow measured did not exceed ±10 degrees from the mean so it was reasonably certain that there were no velocities beyond this direction. Any velocities that were very close to the axial or circumferential direction would have caused errors due to the wakes from the probe supports and directional ambiguities. Thus from the above derivation, the true velocities normal to each hot wire sensor could be obtained from the apparent effective cooling velocities. The reader is referred to Appendix A where a sample calibration of velocity and angular sensitivity of an X array dual sensor probe can be found.

4.4. Data Reduction

The main method of data reduction used throughout this study was the well-established ensemble average technique. Data set compilation ranged between 500-700 ensembles each consisting of approximately five wake passing periods.

The ensemble average of a time-dependent quantity ***b*** is given by:

$$\tilde{b}(t) = \frac{1}{N} * \sum_{j=1}^{N} b_j(t) \tag{4.9}$$

where N is the number of ensembles and the ensemble RMS is given by:

$$\sqrt{\tilde{b}'^2(t)} = \sqrt{\frac{1}{N} * \sum_{j=1}^{N} \left(b_j(t) - \tilde{b}(t)\right)^2} \tag{4.10}$$

The above data reduction formulae were introduced to form part of the data acquisition/post-processing software. Figure 4.6 below gives an example of the noise and turbulence present in the measured axial velocity.

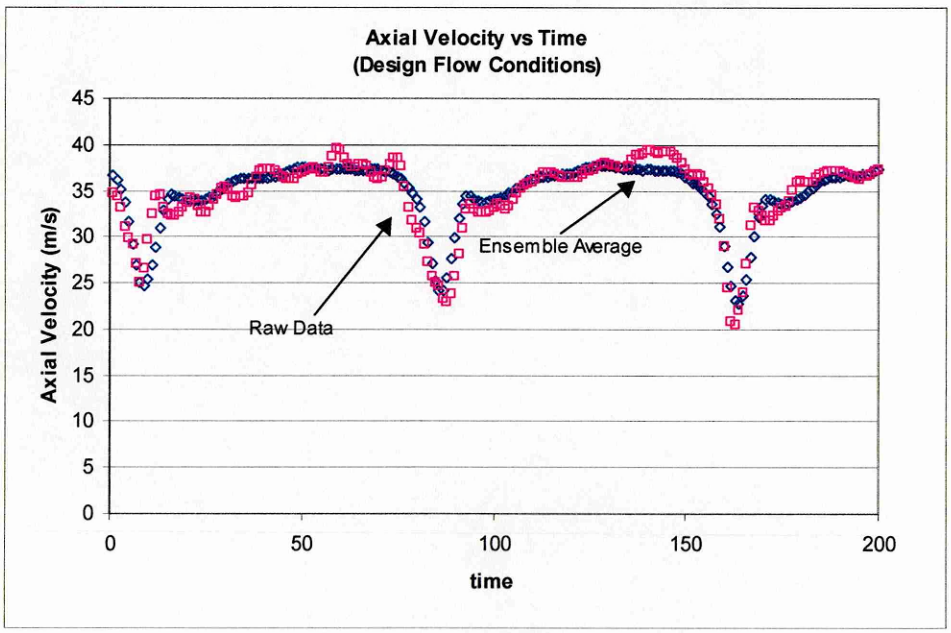

Figure 4.6 Axial Velocity at Peak Efficiency Design Flow Conditions

4.5. Results and Discussion

4.5.1 Circumferentially Averaged Data

During the initial stage of post-processing of data, preliminary plots of the circumferentially averaged values of the absolute and relative flow angles (α & β) at Peak Efficiency Design and Near Stall conditions were compared with those obtained with pneumatic probe measurements (see Figure 4.7). These pneumatic measurement data, taken from the same LSRC facility by a previous investigator (Bennett, 1999), were obtained using cobra probes having an accuracy of ±0.25 degrees. Detailed error analysis of cobra probes can be found in Robinson (1991). The bands shown on the pneumatic measurement plot do not represent errors but maxima and minima values at each measurement point. Hot-wire measurement of the absolute flow angle are in good agreement with those of the pneumatic measurements starting from the hub region until toward the mid span region where the flow can be

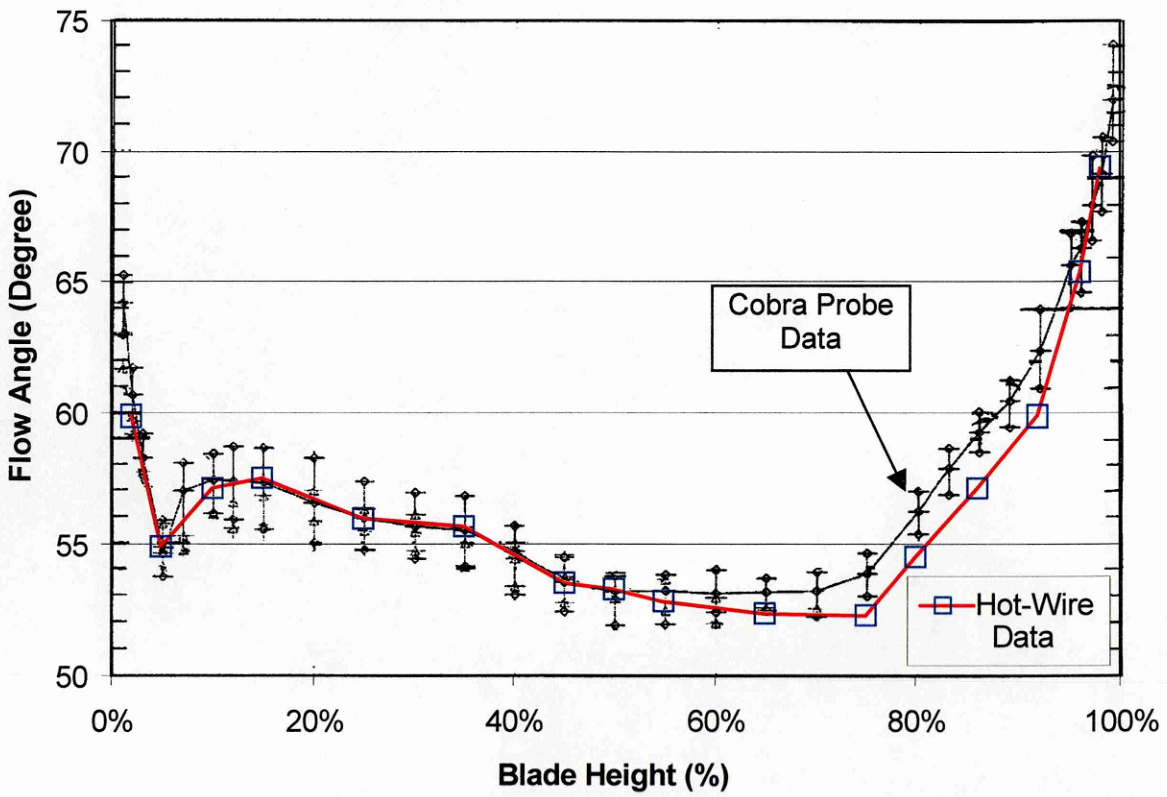

Figure 4.7 Comparison of Circumferentially Averaged Absolute Flow Angles at Near Stall Condition Downstream of Rotor 3

considered to be mainly two-dimensional. Maximum disagreement of approximately two degrees occurs between the two types of measurements in the region of 55% to 96% heights near the casing end-wall region. This can be attributed to the high level of secondary and end wall flows that might have been captured by the hot-wire probes, particularly in the region where tip clearance flows exist and contribute to highly disturbed flows. It must be noted that pneumatic probe measurements were taken in a rotating frame of reference while the hot-wire measurements were taken in a stationary frame. The rotating frame technique was used to minimise the unsteadiness caused by the passing of rotor wakes (Bennett, 1999). There are two significant factors that must be considered. First, neither of the two measurement techniques took into account any radial component of velocity. Second, the axial distances of the different measurement probes, relative to the trailing edge of the rotor, were not the same. This difference in the measurement location may be one of the contributing factors in the disagreement in relative flow angle distribution along the height at Design conditions as shown in Figure 4.8. The trends of the curves are similar but considerable

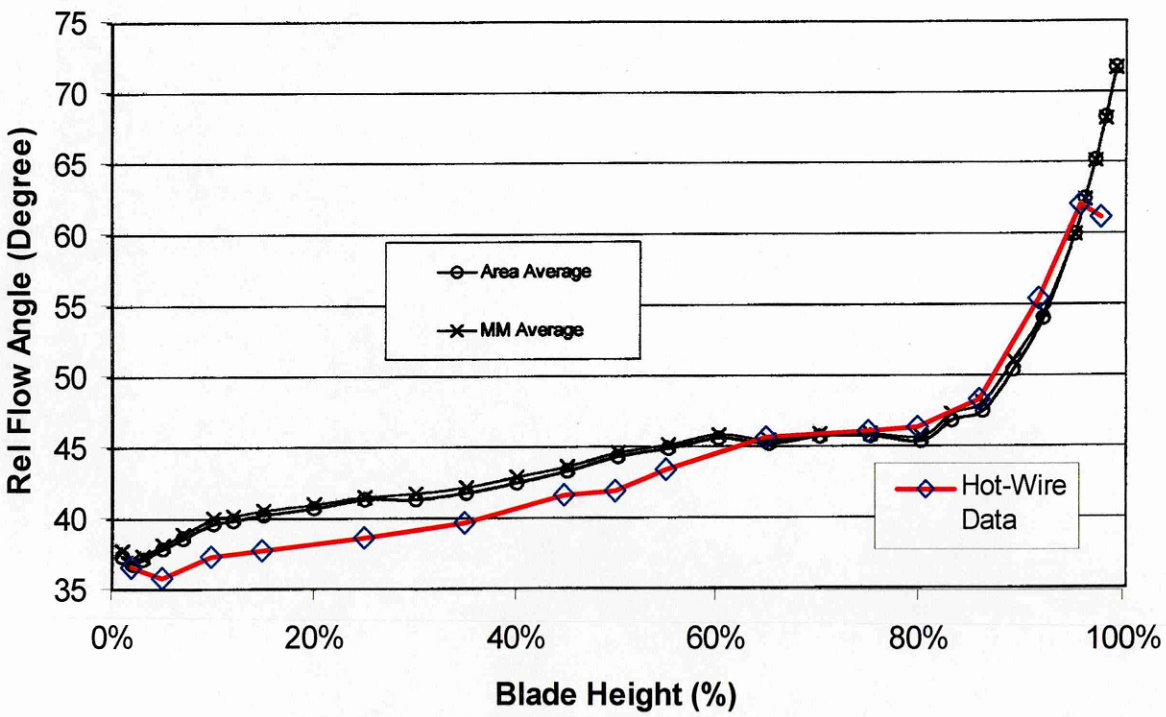

Figure 4.8 *Comparison of Circumferentially Averaged Relative Flow Angle at Design Condition Downstream of Rotor 3*

differences in flow angle values are present from 5% to 65% blade span. The primary cause of this disagreement between the two types of measurement is believed to be the effects of the rotor wakes, the extent of which vary with distance downstream of the blade trailing edge. A discussion on the effect of wake mixing on compressor performance can be found in Adamczyk (1996), who describes the relation between the wake recovery and the change in kinetic energy of the unsteady velocity field across a blade row.

Figures 4.9 to 4.12 show the collection of the spanwise distributions of absolute and relative flow angles (α & β) respectively and the absolute and axial velocities ($\mathbf{V_3}$ & $\mathbf{V_a}$) at the two operating conditions. The high values of absolute flow angles are present at both end-wall regions where in the hub region the effect of hub corner vortices and corner stall affect the flow. Higher flow angles are present toward the casing due to the various complex phenomena that exist, such as the end-wall boundary layer flows, tip clearance flows and scraping vortices. The blade motion relative to the end wall causes this, where the fluid is forced through the gap partly due to the viscous drag of the end wall and due to the pressure difference across the blade. The consequence of this is shown by the plots of axial velocities illustrating the significant drop in velocity in the outermost 20% span. These indicate the level of loss and blockage caused by the tip clearance flows and corner vortices. The percentage drop from the span average axial velocity at Design condition is higher (i.e. 40%) than that at Near Stall (35%). A comparison between the flow angle results and blade metal angle at the rotor exit and the stator inlet would have been useful but this could not be carried out since no blade metal angle data was made available.

The plot of circumferentially averaged absolute velocity show similar features from 30% to 90% span at both flow conditions. This is not the case at the end-wall regions of the hub and the casing where higher values are present at Near Stall. The reason for this trend could not be identified. Plots of the relative angles downstream of rotor 3 show very similar trends for both flow conditions all but for a nominal 5-degree shift in the measured values. This is most likely due to the wider blade wake avenues

that occur at Near Stall conditions caused by the thicker boundary layer leaving the suction side of the blade.

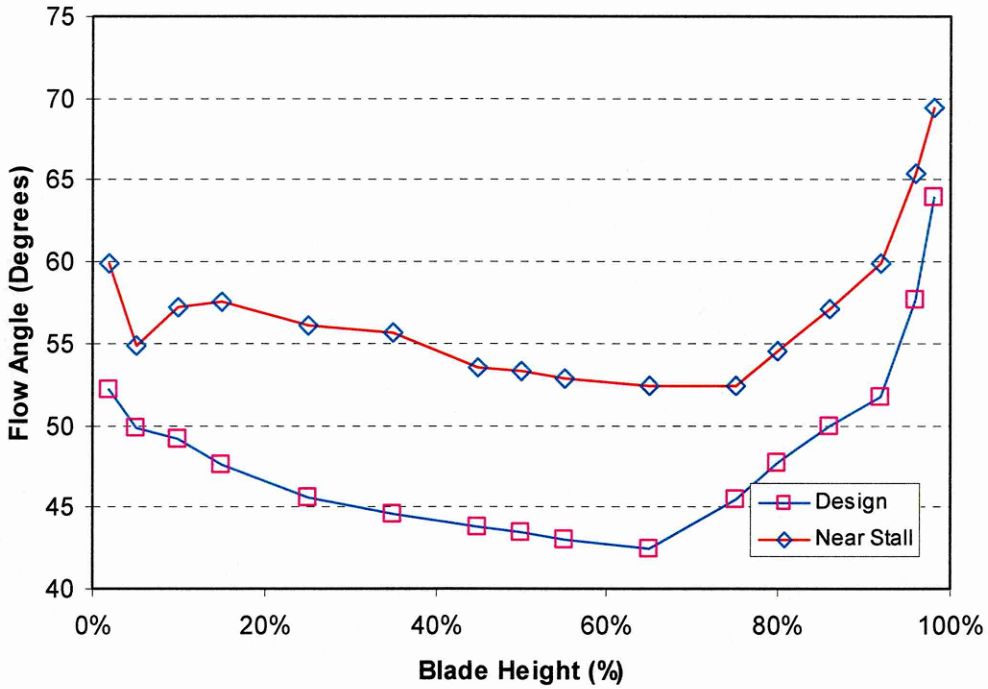

Figure 4.9 Spanwise Distributions of Absolute Flow Angle Downstream of Rotor 3

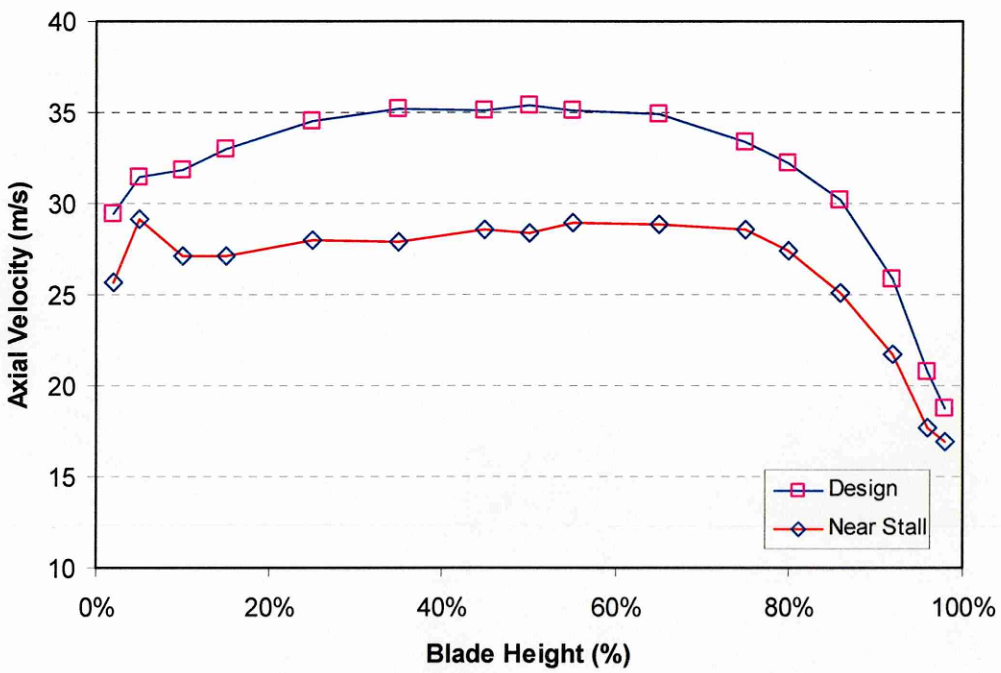

Figure 4.10 Spanwise Distributions of Axial Velocity Downstream of Rotor 3

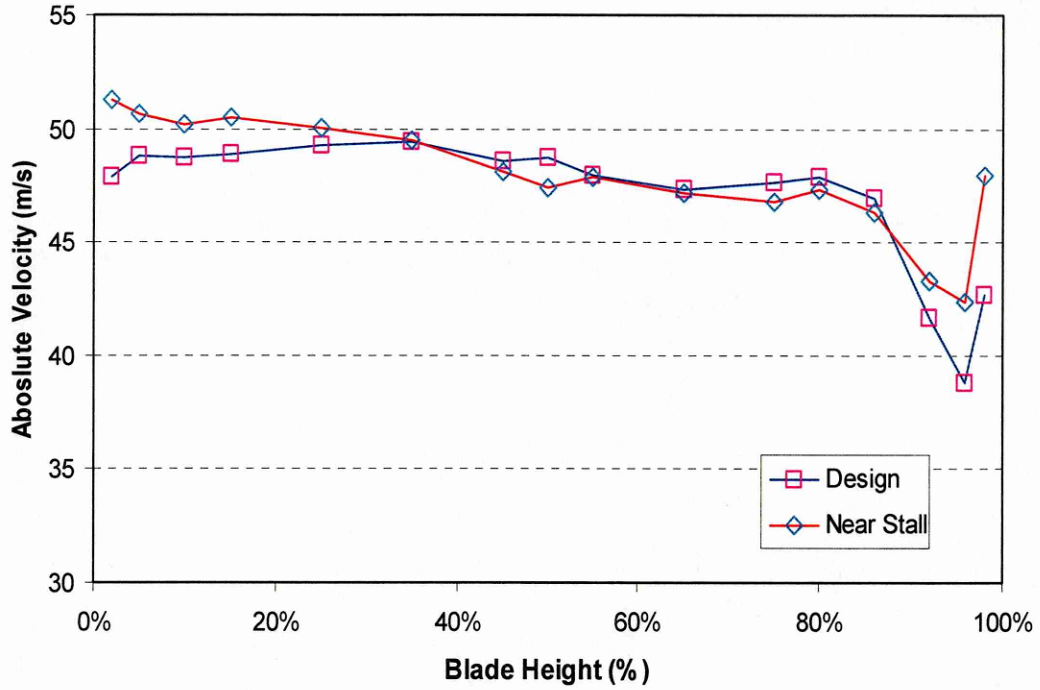

Figure 4.11 Spanwise Distributions of Absolute Velocity Downstream of Rotor 3

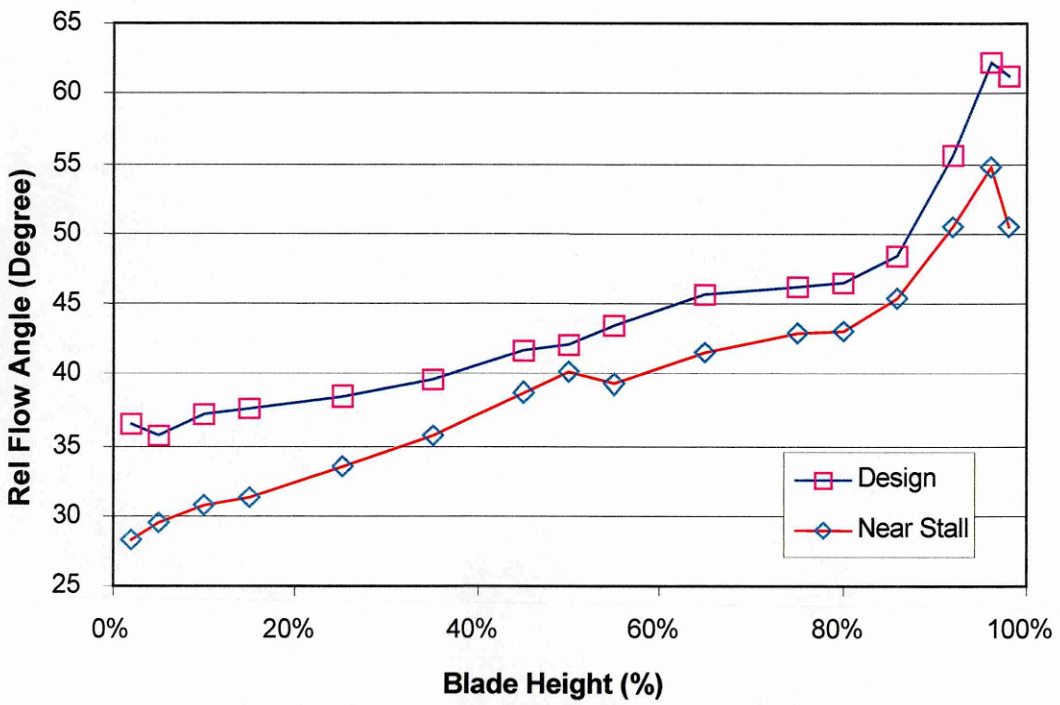

Figure 4.12 Spanwise Distributions of Relative Flow Angle Downstream of Rotor 3

4.5.2 Unsteady Area Traverse Data

So far, only the circumferentially averaged values of velocity and flow angles have been discussed without observing the unsteady periodic flow phenomena that exist within a multi-stage compressor. Nevertheless, as mentioned earlier, the circumferentially averaged features, especially the flow angles, are useful for comparison with the blade metal angles to investigate the effects of flow coefficient on these parameters (Joslyn & Dring, 1985).

Part of this investigation was to observe the fluctuating behaviour of velocity and flow angles with time. The circumferential traverse consisted of 16 equally spaced steps of 0.461 degrees effectively covering two stator blade pitches. Therefore the relative locations of the measurement points with respect to each other are known, and the location of the points as a group with respect to the upstream and downstream stator blades was measured. Figure 4.13 illustrates the locations of the measurement points. These were subsequently confirmed from the measurements themselves. Selected raw hot-wire measurement traces taken downstream of rotor 3 at mid blade height and Design flow conditions are shown in Figure 4.14. In this case, the sharp downward spikes represent the rotor wakes. Since time increases from left to right, the left side of the spikes corresponds to the pressure side of the rotor blade and the right side to the suction side. The wakes from the previous stator row can be easily identified at locations ***C*** and ***G*** from the turbulence. This is an indication that those two measurement locations are within the avenue along which the upstream wakes proceed. Because these wakes impinge on the probe at the same frequency as the rotor blades, they appear at the same location on the traces. This is an important fact to be aware of as one could easily and erroneously conclude that the wake turbulence is caused by the rotor blades. The potential effects of the downstream stator row will also play a role in this situation, which may explain the distinct peculiar traces such as those of positions ***B*** and ***F***. Each different location across a stator pitch produces a distinct hot-wire trace which indicates that probe location is an important consideration when drawing conclusions regarding the rotor blade performance.

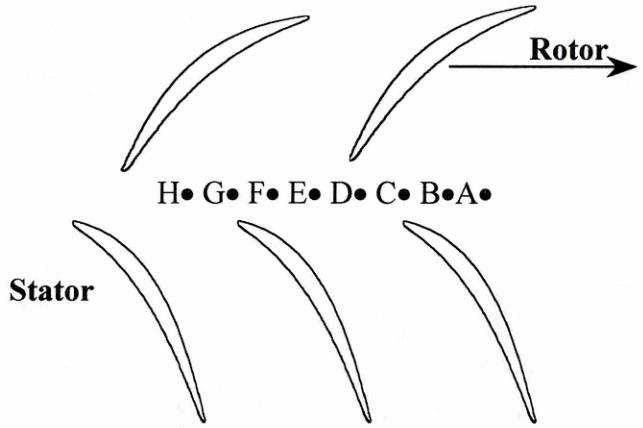

Figure 4.13 Selected Hot-Wire Measurement Locations Downstream of Rotor 3

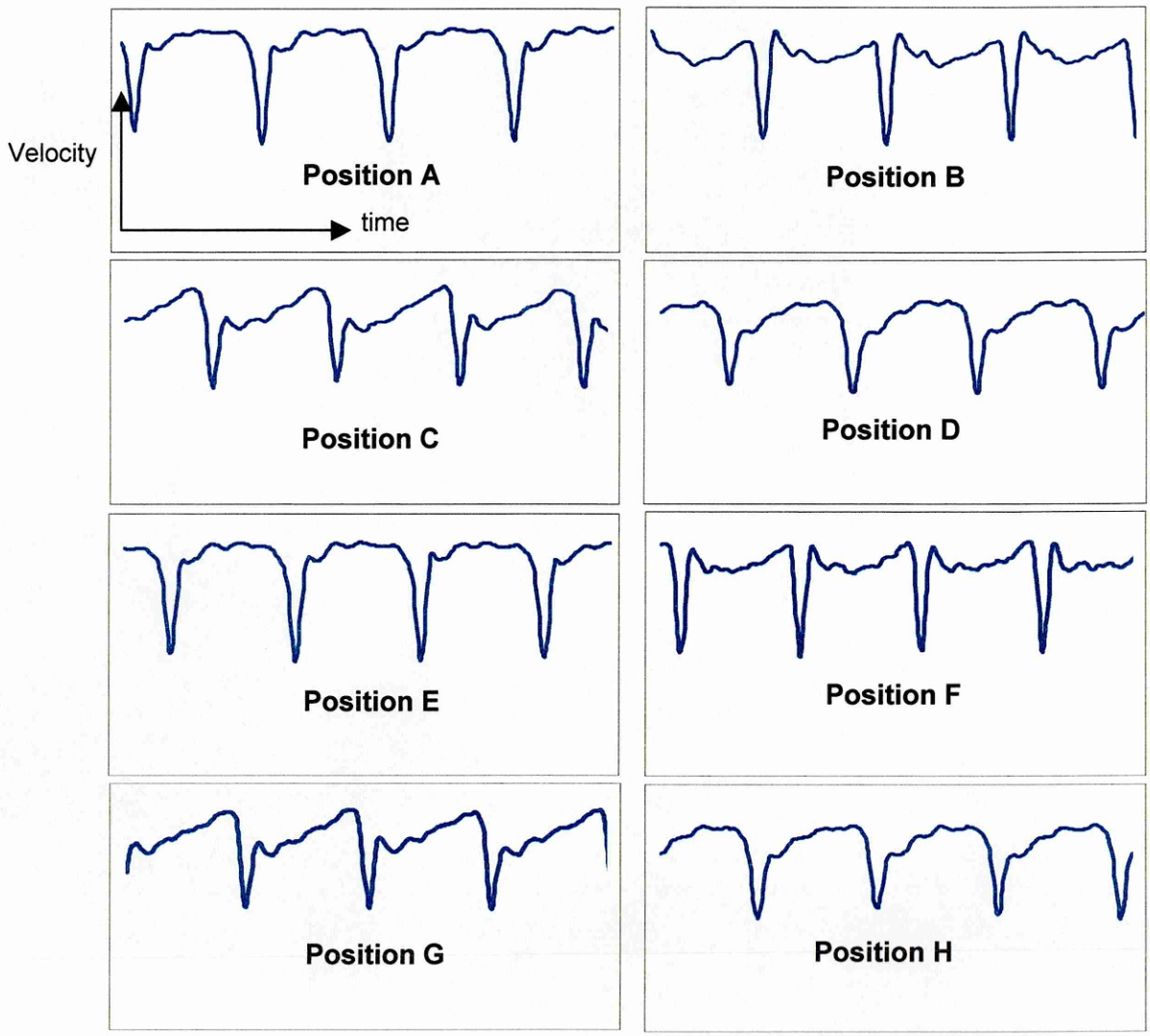

Figure 4.14 Hot-Wire Measurement Traces at Design Mass Flow at Locations Shown in Figure 4.13

Although the position of each stator row relative to the other was not measured, very different flow patterns could occur by setting the stator rows at different circumferential positions with respect to each other. Smith (1966) states that moving the inlet guide vanes (IGV's) alone altered the flow pattern behind the third rotor. A modern form of this technique, more commonly known as stator 'clocking' or 'indexing', has been the subject of recent study by Walker et al (1998) who investigated the effects of incidence and clocking. They found these effects to significantly influence the strength of the periodic wake-induced transition phenomena and also alter the nature and extent of transition by other modes (i.e. natural, bypass and separated flow transition).

The wakes from the second stator row are weaker than the wakes from the third rotor row, which gives an approximate indication of the extent of wake decay that occurs when passing through a blade row. This however cannot be an exact comparison since the geometry of the rotor blades and stator blades are different. The influence of wakes from an upstream stator row on the downstream stator row could be used to different effects at different compressor operating conditions. Small though significant reduction in loss could be obtained by 'steering' the upstream stator wakes so that they impinge on the pressure surface of the downstream stator row. On the other hand, when nearing stall, wake-blade interaction could be used to purposefully induce turbulence in the blade boundary layers to help resist separation. However, this technique must be used with careful consideration due to the complex flow phenomena that contribute to the initiation of stall, particularly near the end wall region where the flow is inevitably three-dimensional. The 'steering' of the wake only apply when there are equal numbers of blades in adjacent stator and/or rotor rows. Different number of blades from one row to the other would inevitably cause the wakes to always impinge on the downstream blades resulting in wake-induced transition.

4.5.3 Contour Plots of Flow Field

A small Fortran 90 code was developed to compile all of the area traverse measurement data with the aim of creating a slide show of the time varying contour plots of velocity and flow angles. A Computational Fluid Dynamics Graphics tool, *FieldView (Version 6),* was used to make this method of presentation possible. Viewing these plots as real time movie clips enables one to appreciate the dynamic features of the flow that are present within the current embedded study stage. These executable files (.AVI) can be played using a Microsoft Windows Media Player software (available in most current PC's) or 'Real Player' (demonstration version) software which can be downloaded free of charge from the Internet.

The selected sequential frames in Figures 4.15 to 4.22 show one rotor blade passing cycle at increments of approximately 6.33 time steps. All contour plots are viewed in the upstream direction and show the behaviour of the wakes in terms of flow angles and velocities at both operating conditions of the compressor. The difference in the wake characteristics at the two flow conditions is very distinct with much thicker wakes at near stall and substantial range of flow angle variations more toward the casing than the hub. The end-wall effects at the casing are more pronounced at near stall indicating more losses due to tip clearance flows from the rotor and secondary flows. The high variation of flow within the wake near the hub and the casing are visible due to the turning of the flow. Another contribution to this deflection could be the eddies shed by the blade trailing edge.

It can be seen from the plots of both absolute flow angle and axial velocity that toward the centre of the passage and at approximately 75 percent pitch from the suction surface, the diffused effects of an upstream stator wake are apparent with a velocity increase at the exit from the rotor. Smith (1966) discusses the mechanism by which such wakes are attenuated through a rotating blade row. The rotor wakes in the axial velocity plots (Figures 4.19 & 4.20) are shown as velocity deficits along the height of the rotor blade and eventually merge with the slower moving fluid near the casing region. Another interesting feature that can be observed from these sequential plots is that the rotor wakes exhibit periodic variations in thickness, which indicate

blade loss fluctuations. This is more prominent at Near Stall conditions with separation occurring at the casing regions.

As expected, the effects of the end wall boundary layer and the tip leakage flow from the rotor dominate near the end walls. The turbulent nature of the suction side boundary layer accounts for the thicker wake and higher unsteadiness region at the suction side, which is significantly more extended at the hub and tip than at the mainstream flow. At near stall conditions the rotor blade wake is considerably thicker along the span and in the casing region. This is not the case in the hub region although it was expected that there would be a significant increase in the wake flow and fluctuation in the hub region due to the existence of corner stall.

Although the flow-field measurements were taken with the objective of investigating the two-dimensional characteristics of the flow environment downstream of the third rotor stage, radial migration of flow deviation can be detected with each passage of a rotor wake. Although this must not be confused with radial components of flow activities, it clearly indicates that there exist significant radial asymmetries in velocity profiles. These asymmetries will certainly be affected with different flow coefficient and would be of interest for gaining a more in depth insight of the imbalance between the centrifugal and pressure forces in the wake area.

4.5.4 Accuracy of Results

Locating the probe at its desired height during the radial traverse was achieved with a vernier gauge traverse gear onto which was mounted the probe support. The accuracy of this instrument was within ±0.05 mm, which translates to ±0.05 % of the blade height. Prior to each traverse experiment, the datum position was established with a 'dummy' probe made with a tolerance of ±0.01 mm. Angular orientation (i.e. yawing) of the probe during testing was performed using the same protractor as that used for calibration. This protractor formed an integral part of the radial traverse assembly and had an accuracy of ± 0.25 degrees.

The hot-wire measurements were taken from a stationary frame throughout the whole height of the blade and because the measurement probe had only two sensing elements, only two-dimensional components of velocity were captured. Any radial component that existed would appear as distortions in the two-dimensional flow-field. The hot-wire sensors were oriented to measure both the U and V component of velocity simultaneously and any radial component of velocity (i.e. component W) would be normal to both sensors and would be captured by each as a component in the flow. In this part of the investigation measurements were taken with the assumption that the radial component of velocity would be small in comparison to the other components. This may be accepted for measurements in the region of 50 % blade height (Read, 1997) but does not apply in the endwall regions where highly disturbed flows exist.

4.6. Conclusions

A dual sensor X array probe was implemented to take area traverse measurements of the two-dimensional unsteady flow field downstream of the third embedded rotor stage. The area traverse covered the rotor blade span from 2% to 98% height and a circumferential pitch of approximately two shrouded stators. Hot wire measurements and pneumatic probe measurements have shown positively good agreement when the circumferentially averaged values of absolute and relative flow angles were initially compared.

The unsteady features captured by the hot-wire measurements distinctly show the strong wake features of the rotor row and that of the previous stator row. It can be seen quite clearly that the inlet conditions to the downstream stator blade-row vary considerably along the span, which is a significant consideration in blade design toward the hub and casing region. Strong variations are present in the end-wall regions where corner stall and corner vortex and tip clearance flows dominate.

Hot-wire circumferential traverse measurements have also shown that the flow regimes are different across the stator pitch. This indicates that great care should be taken when drawing conclusions about rotor blade performance.

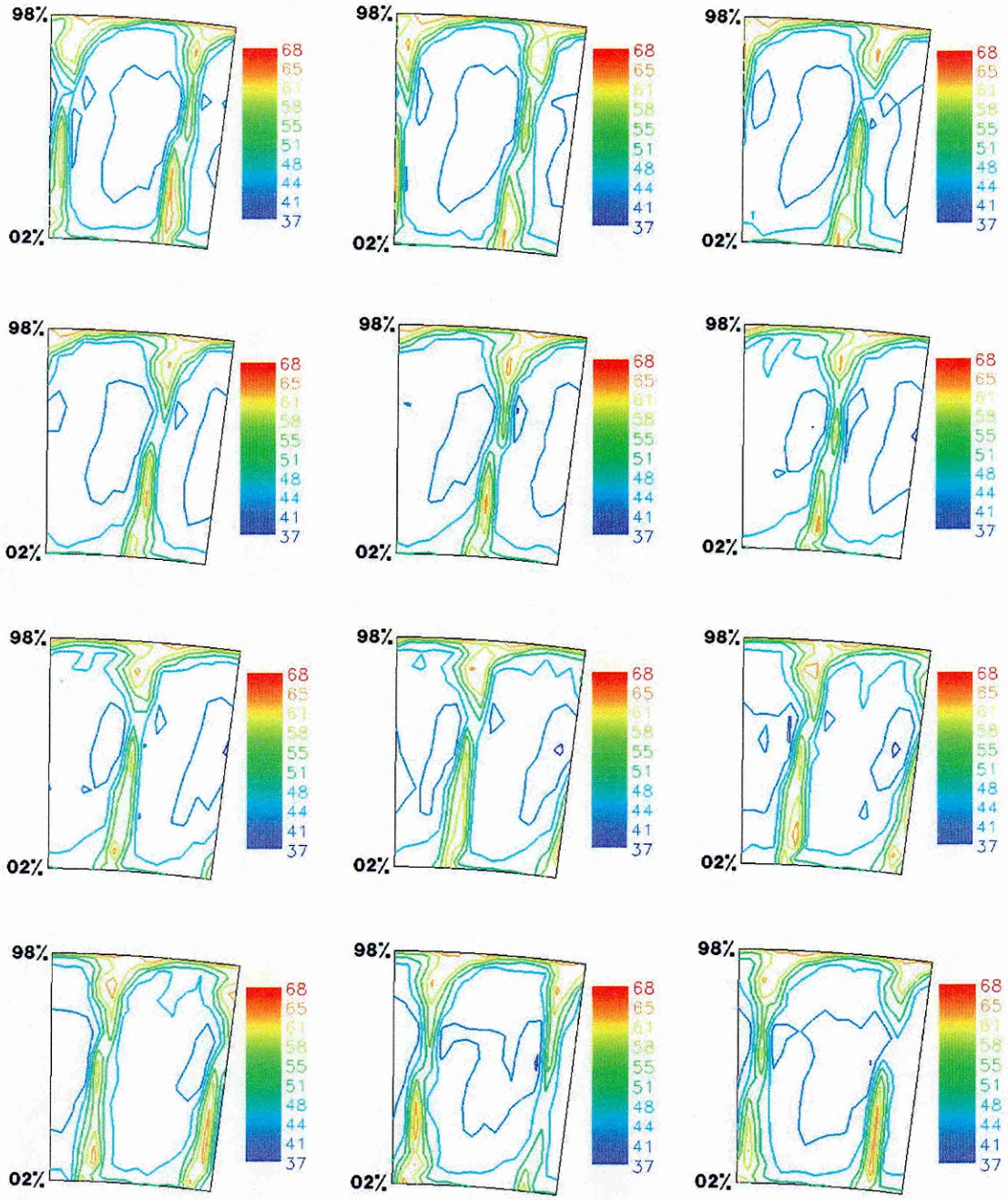

Figure 4.15 Contour Plots of Absolute Flow Angles Downstream of Rotor three at Design Flow Conditions

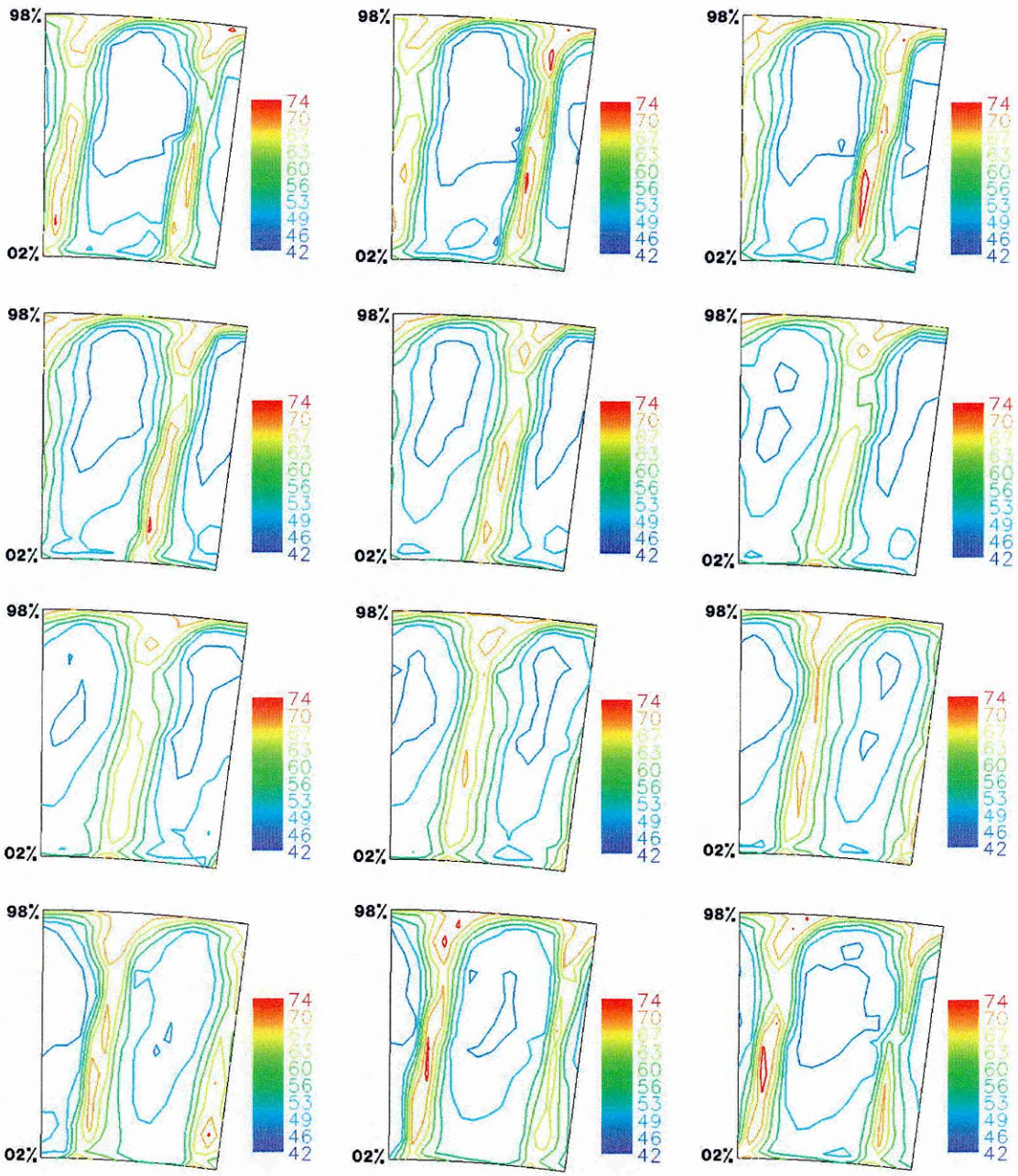

Figure 4.16 Contour Plots of Absolute Flow Angles Downstream of Rotor three at Near Stall Flow Conditions

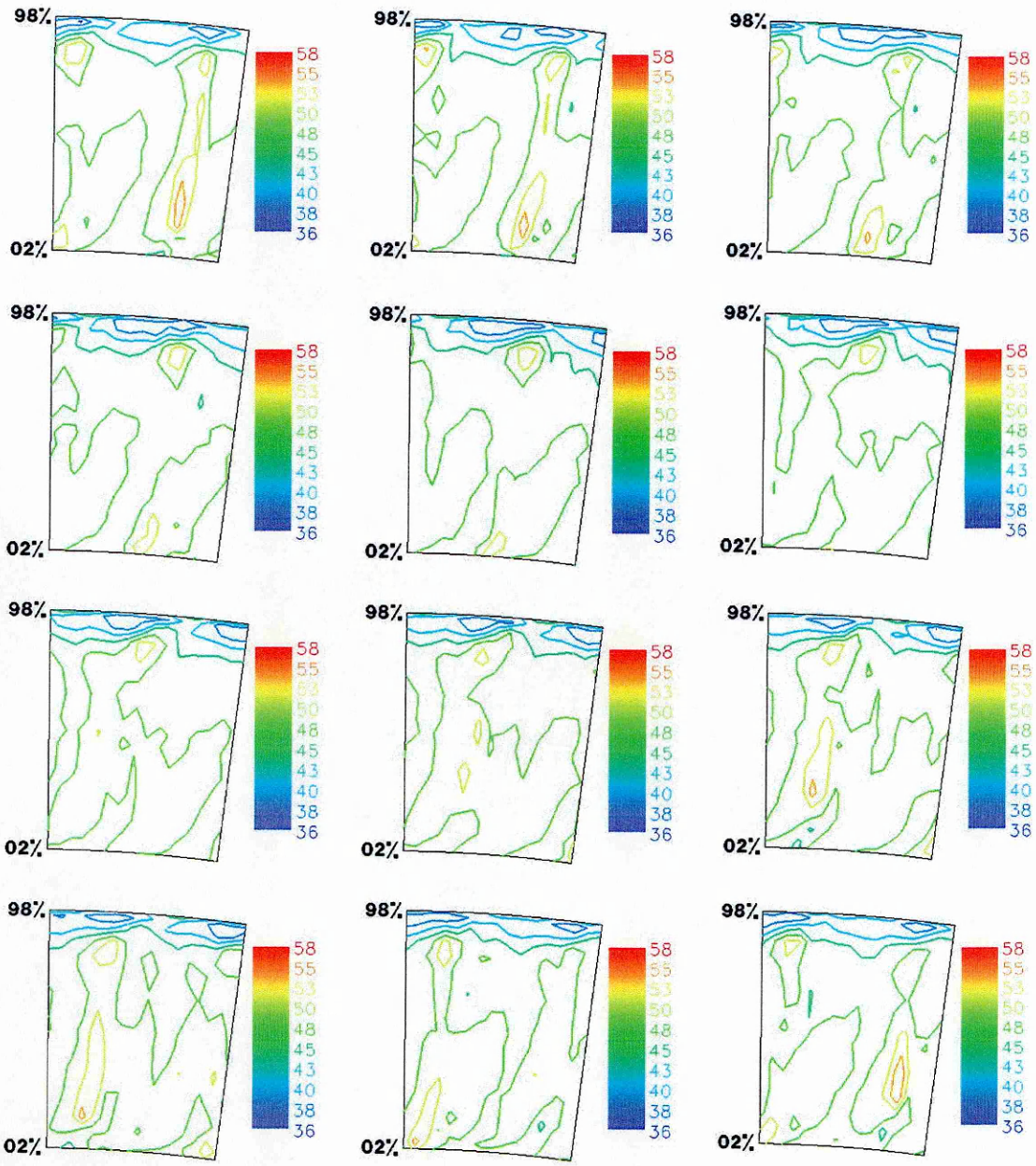

Figure 4.17 Contour Plots of Absolute Velocity Downstream of Rotor three at Design Flow Conditions

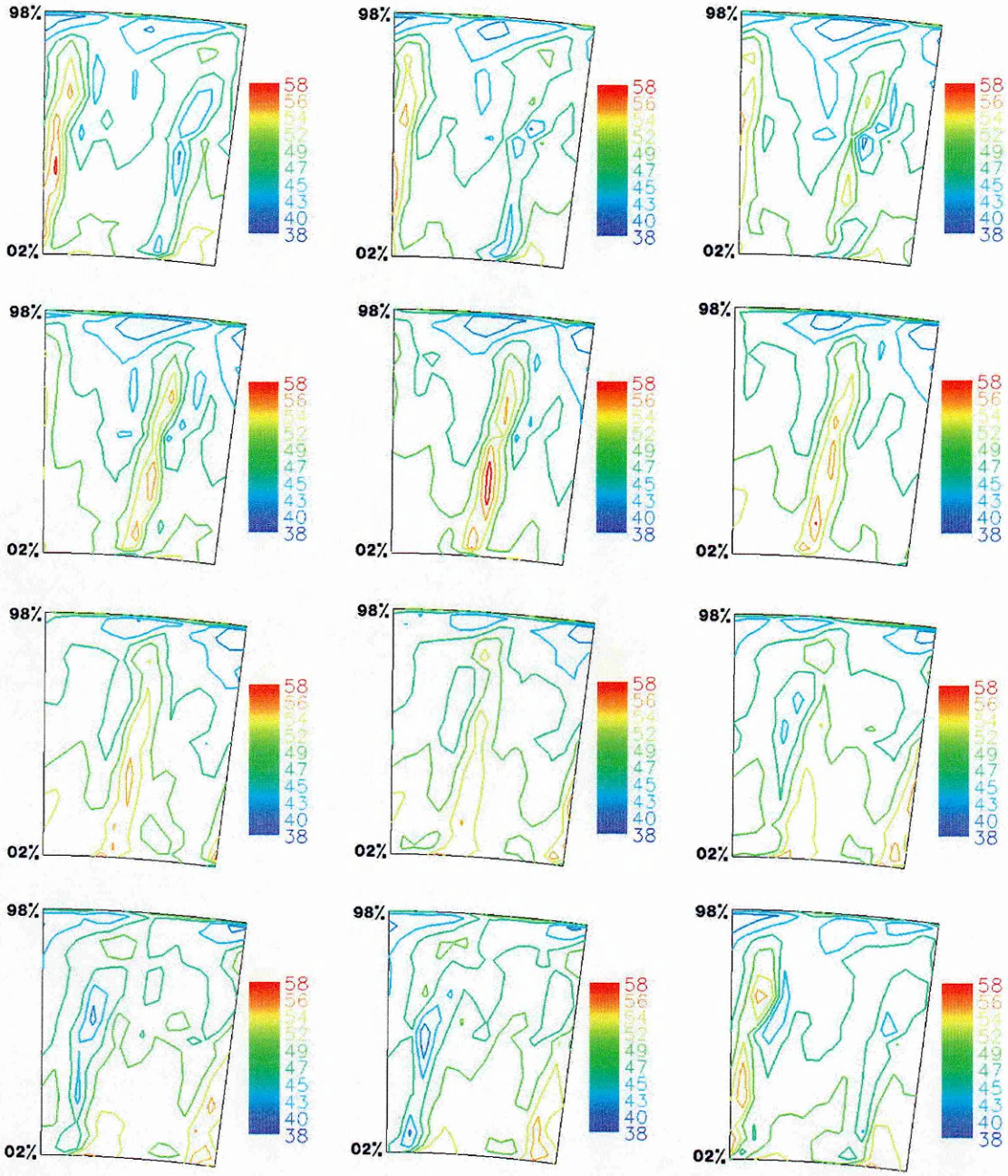

Figure 4.18 Contour Plots of Absolute Velocity Downstream of Rotor three at Near Stall Flow Conditions

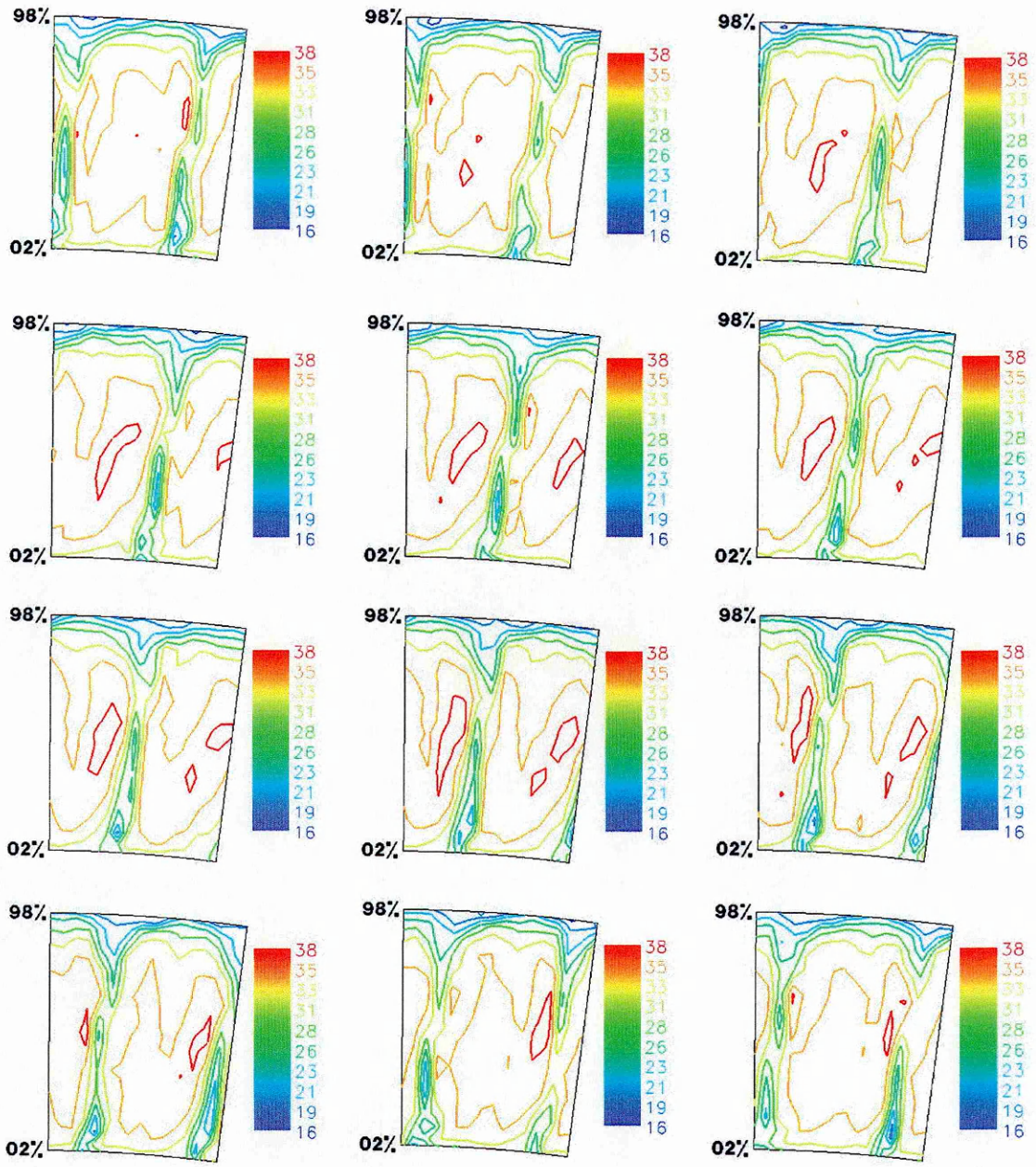

Figure 4.19 Contour Plots of Axial Velocity Downstream of Rotor three at Design Flow Conditions

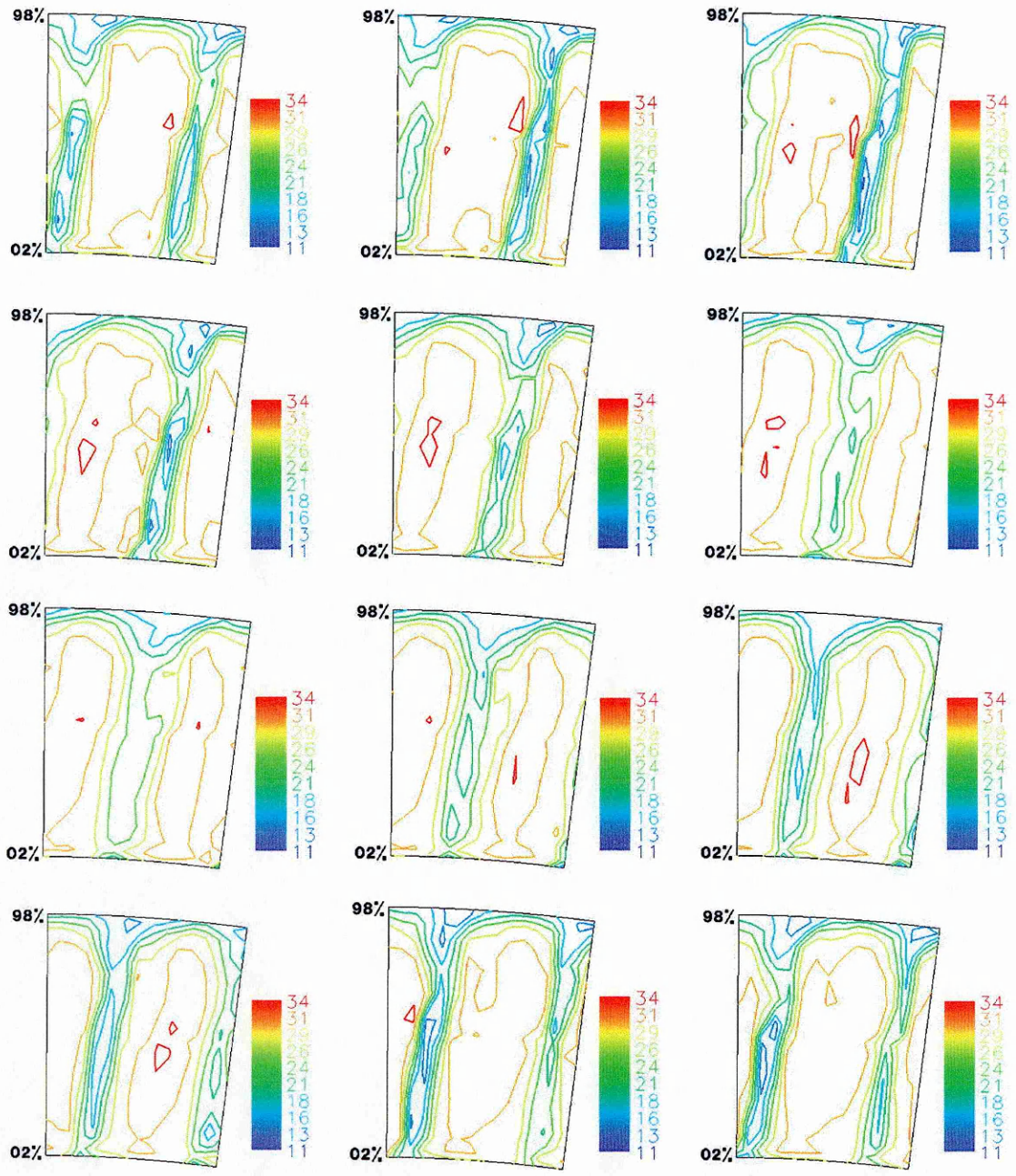

Figure 4.20 Contour Plots of Axial Velocity Downstream of Rotor three at Near Stall Flow Conditions

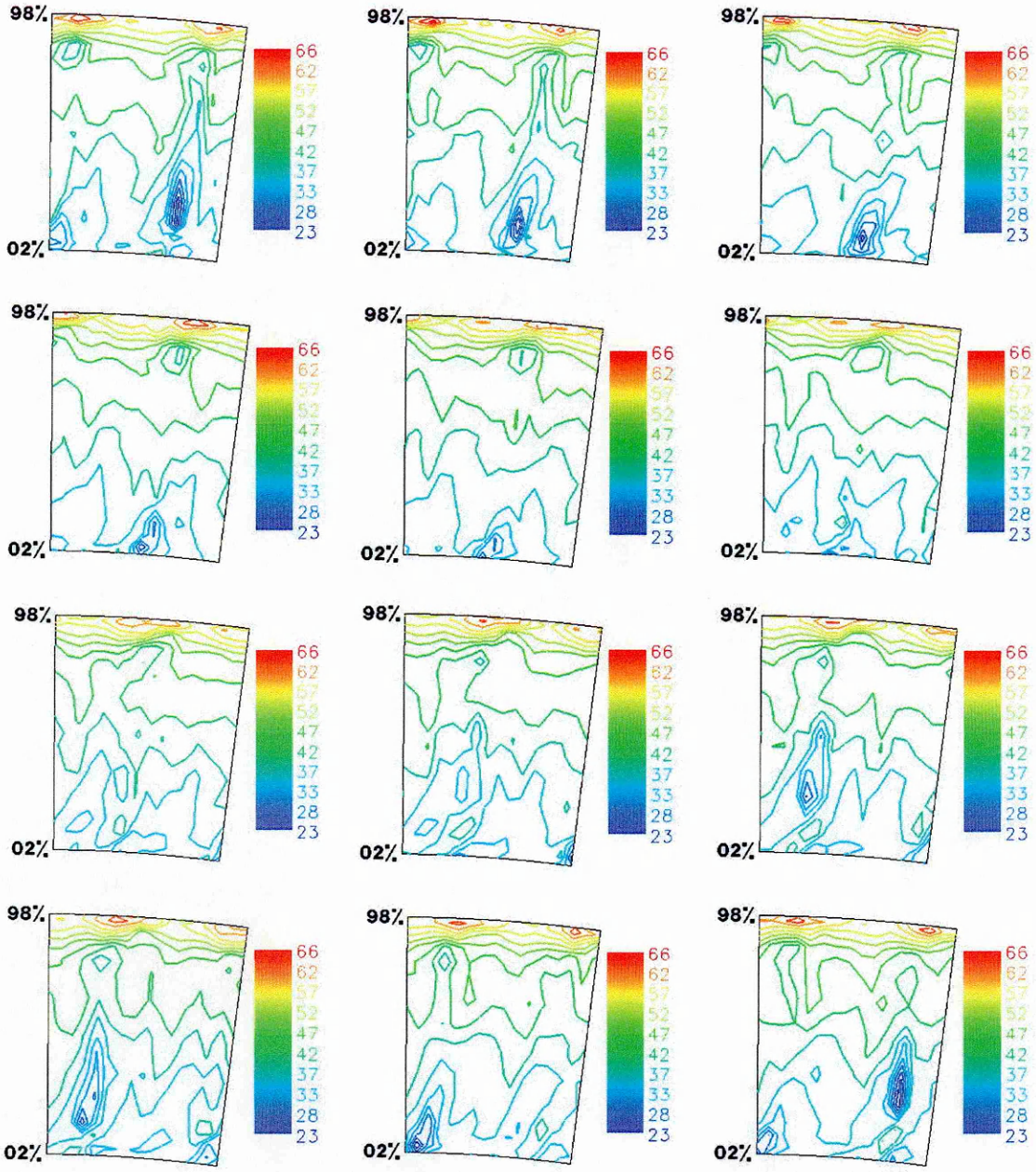

Figure 4.21 Contour Plots of Relative Flow Angle Downstream of Rotor three at Design Flow Conditions

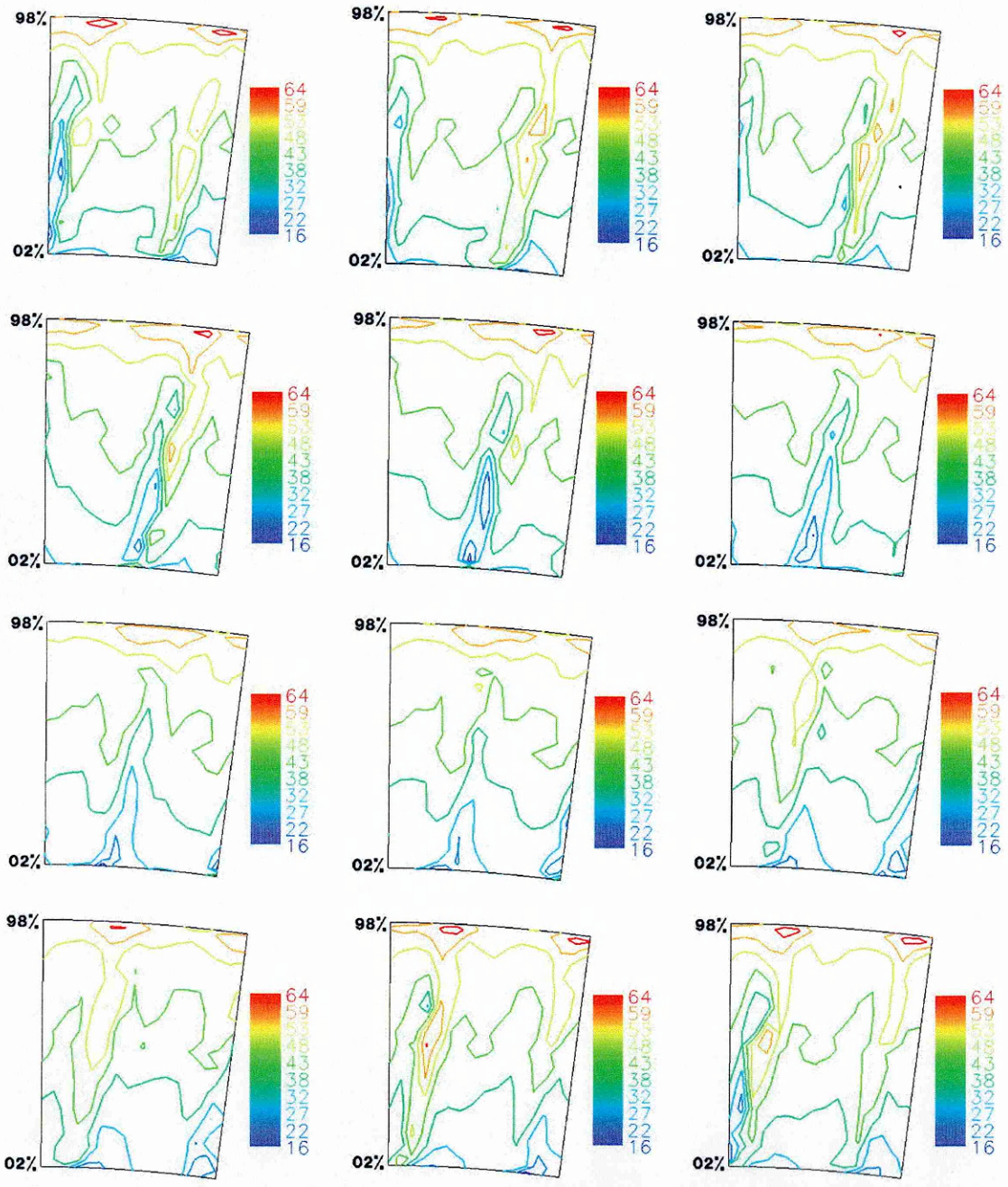

Figure 4.22 Contour Plots of Relative Flow Angle Downstream of Rotor three at Near Stall Flow Conditions

CHAPTER 5

Boundary Layer Survey on the Suction Surface of Stator

5.1. Introduction

There is considerable amount of work documented in the literature on boundary layer studies using hot-film anemometry (Cumpsty et al 1995, Solomon & Walker, 1995). Recently Halstead et al (1995) instrumented real airfoil blades with densely packed hot-film sensors to describe the time history of the boundary layer development with space-time (s-t) diagrams by using ensemble averaged random unsteadiness and skew. These are useful in analysing the effects of transition on the surfaces in question and particularly the statistical analysis of the intermittency of transition. However, hot-film measurements show only what is occurring on the blade surface, and understanding the state of the boundary layer can only be achieved by studying the boundary layer profiles.

This chapter describes the methodology adopted for carrying out detailed surveys of the boundary layer on the suction surface of a stator blade within an embedded stage of Cranfield University's Low-Speed Research Compressor (LSRC) facility and presents qualitatively the results. The core component that made this first ever attempt to measure boundary layer flow within a real turbomachine environment at Cranfield successful was a specially designed boundary layer traverse mechanism driven by a high precision stepper motor. A single sensor hot-wire probe could be located at different chordwise position of the measurement blade at a predetermined height. The probe then traversed the blade surface at small increments capturing the unsteady velocity profile within the boundary layer. Similarly to the flow-field measurements described in the previous chapter, the fluctuating profiles of velocity with time have been compiled into AVI files in the form of movie clips.

5.2. Design of the Traverse

5.2.1 The Concept

From the initial concept design, manufacture and through to the actual measurement sessions, the operational costs and time constraints imposed by the contractual commitments of Cranfield's LSRC rig to its major client (not related to this study) played a significant part in the level of sophistication achieved in the measurement techniques. Furthermore, the most important concern during the design stage was that measurements were to be taken in a real turbomachinery environment. Restrictions in both time scale and space are introduced when considering the flow phenomena that occur on real compressor blades due to their small physical size and the limited access through the axial gaps. It was apparent that the difficulties associated with using compressor rigs are notably different to those encountered when using the large wind tunnel and flat plate arrangement.

The steps taken during the initial stages of the BL traverse design primarily involved the author's familiarisation with the inner and outer mechanical layouts of the LSRC rig facility plus its physical dimensions. The concept stage of the design mainly consisted of making preliminary drawings, both 2D and 3D (examples shown in Figures 5.1a & b) of the proposed measurement probe orientation within the experimental facility. These drawings were used to help guide the author to explore and assess the possibilities as well as the inevitable restrictions in space associated with instrumenting a real turbomachinery facility for measurement purposes.

During the 'brainstorming' stage of the traverse design, the concept of a three-probe rake system, shown in Figure 5.2, was considered with the aims of obtaining simultaneous measurement data at three different blade heights and also reducing testing time. However, this was converted back to a single sensor system due to two main considerations. The first was the significant blockage effects that could introduce errors in measurements. Secondly, the author believed it crucial to minimise if not eliminate any dimensional errors that might occur in manufacture by avoiding extreme complexities of the traverse construction. The option of using custom-made shortened

boundary layer probe was also investigated due to the unusual trait of the pitch accompanied by the three dimensional characteristics of the blades. Unfortunately, this idea was eventually dismissed, as the equipment's lead-time would have not made it available in time for the author's scheduled experimental session on the LSRC facility.

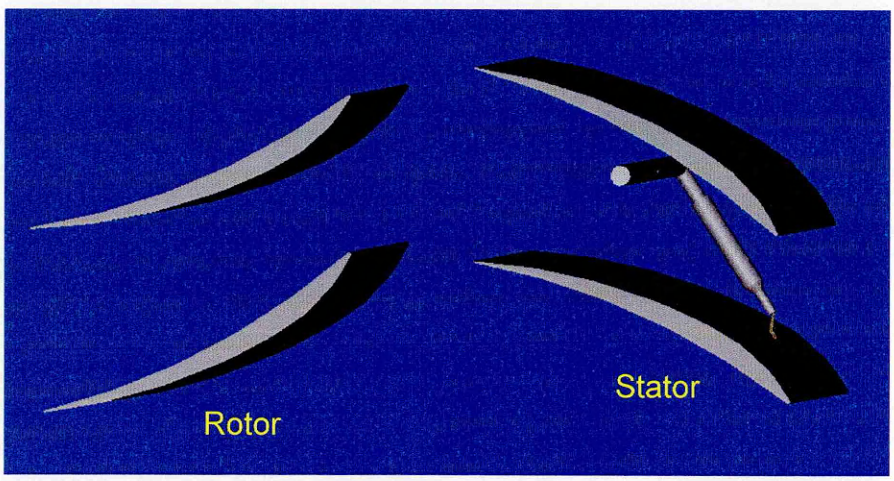

Figure 5.1a Initial Traverse Concept Drawing (Leading Edge)

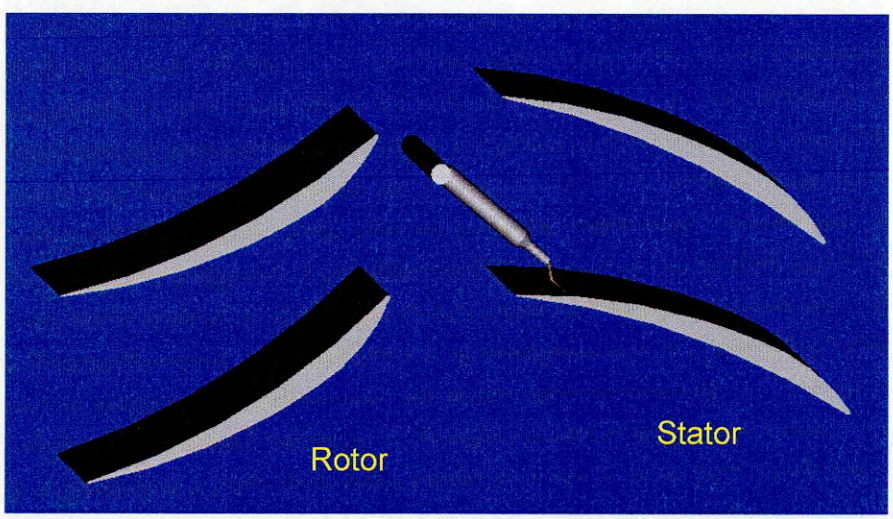

Figure 5.1b Initial Traverse Concept Drawing (Trailing Edge)

The whole traverse mechanism was designed so that when assembled together with the measurement blades, it formed an integral unit of the LSRC rig facility. This allowed the assembly to be mounted precisely and rigidly onto the experimental rig with ease. Figure 5.3 shows the traverse assembly fitted with VRB 3.5 blades used in this study.

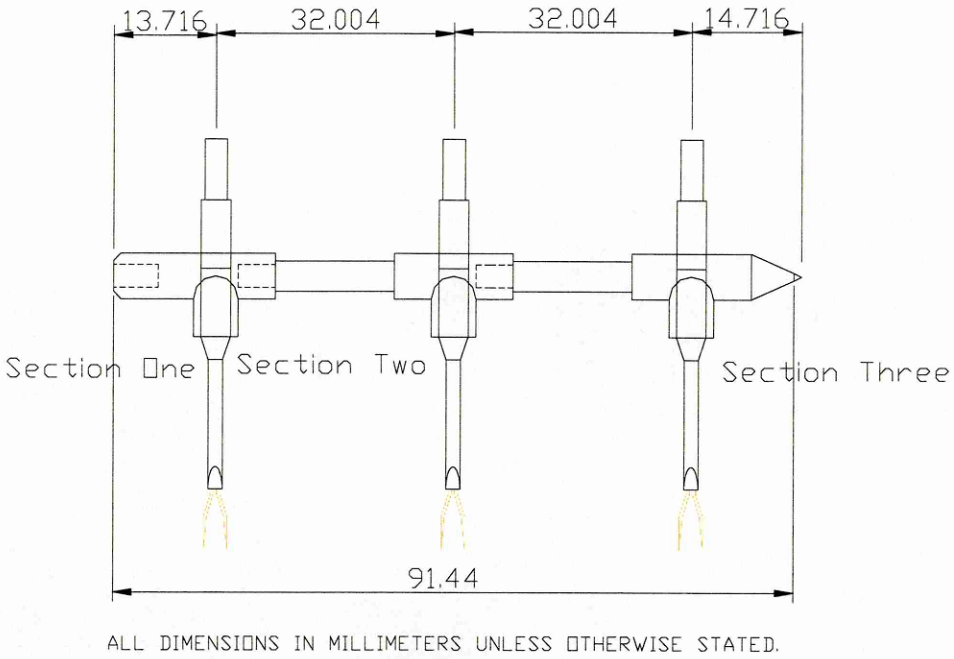

Figure 5.2 Three Probe 'Rake' Arrangement

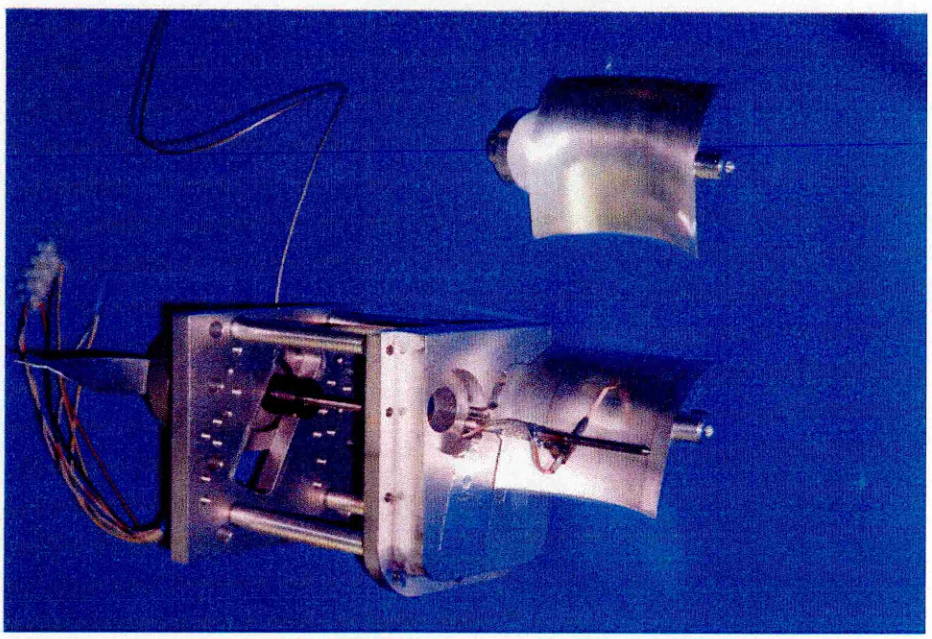

Figure 5.3 Traverse Assembly Fitted with VRB 3.5 Blades

The entire duration of the design process of the BL traverse assembly from concept to manufacture was approximately two and a half months (i.e. six man working weeks). This was deemed to be reasonable considering the Manufacturing Job Request Queuing System at Cranfield University's engineering workshops. Higher priority was given to Job Requests from Staff and/or industrially sponsored projects, causing minor delays.

The final set of the engineering drawings (i.e. one probe system) of each individual element that make up the entire traverse assembly can be found in Appendix C. The drawings are the result of four iterative processes that involved consulting with the technical staff in assessing and modifying the mechanical feasibility of the system (e.g. material compatibility, dimensional tolerances) while minimising any compromises that could affect the accuracy of measurement data.

5.2.2 Traverse Control System

The key objective of this part of the investigation was to collect as much data as possible within the boundary layer developing on the measurement blade. It was therefore necessary to develop a control system that would allow the boundary layer to be traversed at very small and precise increments. Furthermore it must be robust and reliable providing consistent resolution while allowing the user the flexibility to vary the step parameters during measurement.

The virtually microscopic nature of the required movement of the measurement probe led to the logical choice of a high-precision stepper motor system as the driving element. **RS Components Ltd's** precision stepper motor with half-step capabilities (i.e. 1.8 degrees/2) was connected with the main traverse shaft via a bellows coupling to form a direct drive system as illustrated in Figure 5.4. Prior to this set up, the holding torque and the detent torque of the motor were assessed to ensure that the torque requirement was met for driving the traverse shaft assembly during measurement. This procedure involved estimating the anticipated Strouhal number of the probe assembly when exposed to the aerodynamic forces generated by the flow

within the experimental rig. Any mechanical friction forces that might occur between the traverse shaft and the casing part of the cassette assembly, although minimal, were also taken into account.

A self-contained single axis control board and drive card also from **RS Components Ltd** that included an electronic micro-stepping function was selected for driving the motor. This "electronic gears" feature allowed the user to select gear ratios in the range of 200 to 12800-steps per revolution. This was of considerable convenience as it eliminated the need for a mechanical reduction gearbox system, which in addition to its bulkiness would introduce accuracy problems due to the significant backlash usually present in such a system. Despite the benefits of a direct-drive arrangement, a small initial backlash was found to be present in the stepper motor system affecting the positional accuracy by ±5% (RS Components Ltd, 1999). This minor problem was resolved during measurement by initially moving the measurement probe five to ten steps beyond the 'Datum' position in the opposite direction then returning to the 'Datum' point in the intended traverse direction. An ASTEC type LPT 22 power supply unit provided 12 and 5 Volts (DC) to the motor and control board drive/interface card respectively.

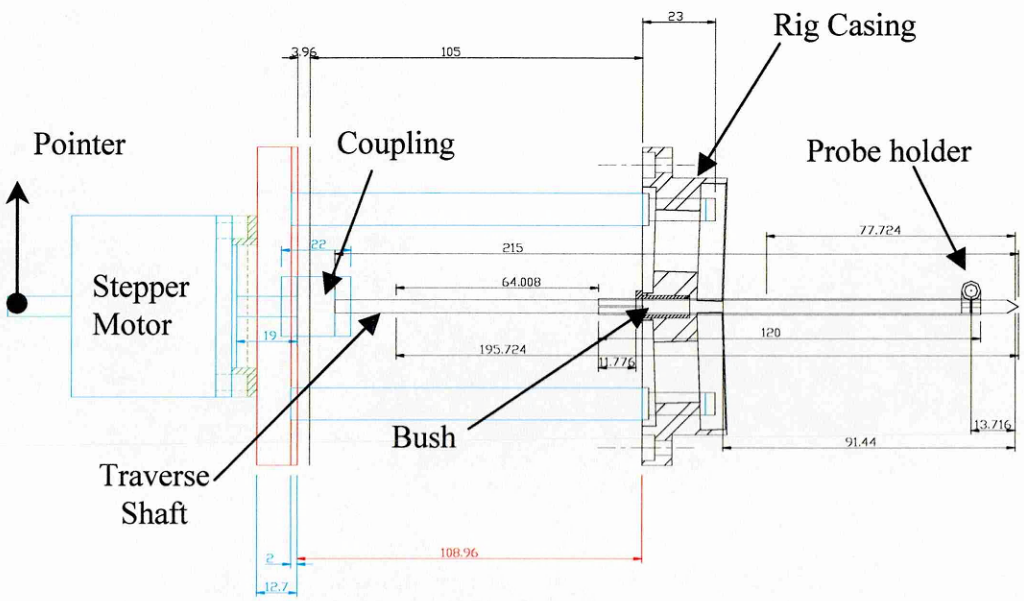

Figure 5.4 Traverse Cassette Assembly Without Stator Blades

Communication was achieved via a RS232 link through which the control board interface card received commands in the form of ASCII characters from the computer. The commands were sent via interactive control software developed in Visual Basic (Version 5) that provided full control and flexibility to alter various parameters (e.g. current, motor speed, gear ratio etc.) during testing. The monitor display provided continuous 'real time' feedback with information on the selected motor parameters and the status of the measurement probe. The limited visual access inside the experimental rig made this a vital feature during the measurement session, as the user was informed of the probe's exact position relative to the blade surface and thus avoiding any accidental damages to the measurement probe. A pointer was mounted on the rear shaft of the motor to provide a visual indication of the stepper motor movement and to ensure that the traverse system was functioning properly. Although the application of an optical encoder was the author's preference for monitoring the stepper motor movement while testing, such a system was not developed due to constraints in time and costs. An alternative method using an existing laser displacement meter was applied to assess the micro-step resolution of the motor before and after testing.

5.3. Measurement Method

A probe holder was precision welded at 90 degrees onto a sliding sleeve, which travelled along the traverse shaft, permitting the hot wire probe to be positioned at a desired blade height. The probe holder itself was a miniature 'bracket' that extended upstream into the stator passage, making it possible to vary the length of the probe support as well as rotate it along its axis. This was a crucial feature in accommodating the three-dimensional characteristic of the measurement stator blade. Holes in the rig casing part of the cassette assembly that accommodated the main traverse-drive shaft were precision drilled to enable accurate location of the measurement probe at the designated chordwise positions (i.e. 15%, 26%, 37% and 65% chord). These holes were fitted with a brass bush instead of a bulky roller bearing system. In addition to its simplicity, it was a vital element in minimising friction between the rotating traverse shaft and the casing section of the cassette assembly while providing stability to the

system. A small groove was centre punched on the hub of the experimental rig to accommodate the hub end of the traverse shaft, which was machined to a point to minimise friction (see Figures 5.3 & 5.4). This ensured that the traverse shaft was positioned accurately and secured firmly upon mounting the traverse assembly onto the rig. Furthermore, this method of mounting prevented vibration that may occur due to the aerodynamic forces in a cantilevered traverse system.

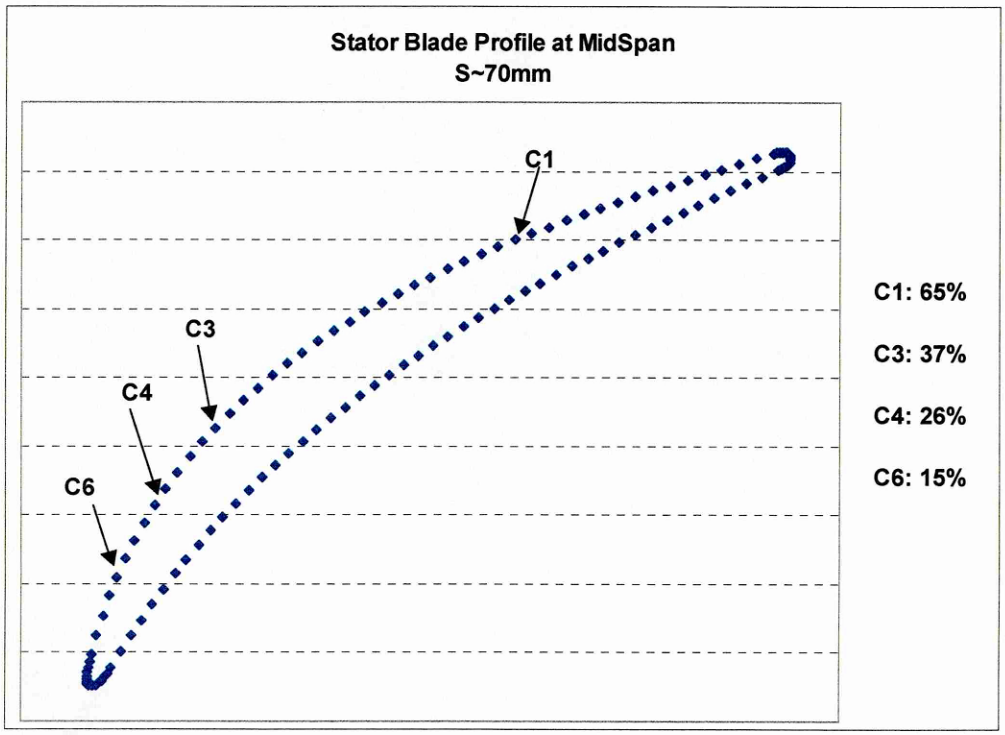

Figure 5.5 Designated Chord Positions for Boundary Layer Survey Measurements

Figure 5.5 shows schematically the four chordwise positions at which boundary layer surveys have been carried out and Figure 5.6 illustrates the orientation of DANTEC's 55P05 boundary layer probe during measurement at those positions at mid-height. As the stepper motor rotated the traverse shaft in small precision increments, the hot-wire probe moved very nearly perpendicular to the stator blade surface and thus surveyed the boundary layer. At each chordwise position, an average of 18 velocity measurements was taken across the boundary layer (normal to the surface) as well as additional measurements of the free stream. The traverse at each location started from the free stream, i.e. away from the surface. Near the surface the

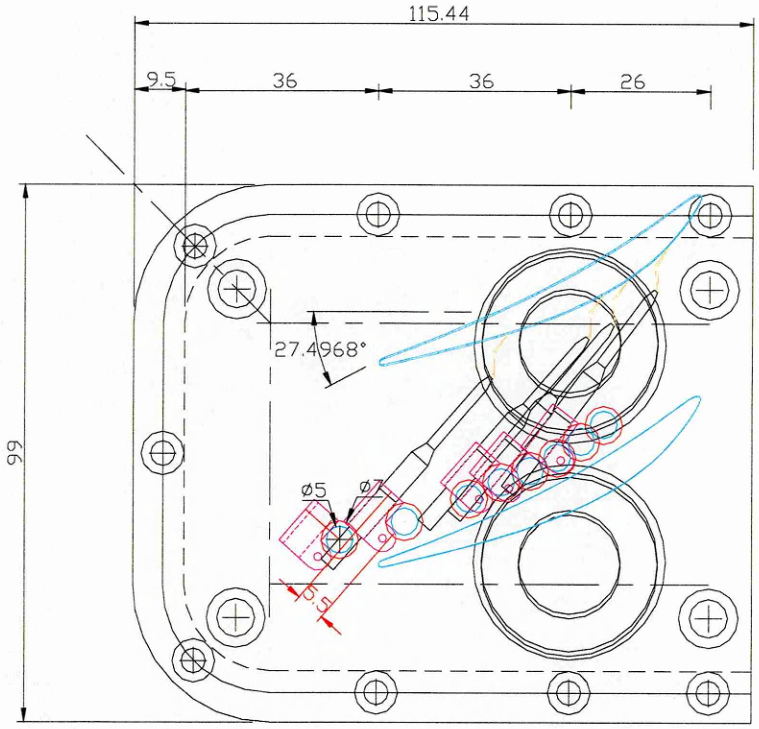

Figure 5.6 Technical Drawing Illustrating Probe Orientation

probe was moved in software controlled step increments of 0.019 to 0.025 mm (depending on the length of the probe) towards the blade surface. The last measurement (i.e. when the probe touched the blade) was ignored. The same trigger system as used in the flow field measurement initiated the data acquisition system at a maximum sampling frequency of 100 kHz. In order to apply the ensemble-averaging technique, 500 ensembles each consisting of 500 samples that covered approximately two wake-passing periods, were logged after each trigger signal

5.4. Difficulties Encountered

This part of the investigation was the lengthiest in terms of preparation prior to testing (i.e. calibration, probe location). As stated earlier, the LSRC facility's contractual commitments to its client allowed the author only limited access to the rig in terms of both time and mechanical modifications. The consequences of these are the certain compromises made in the measurement methods and the data set not being as extensive as it was hoped. Despite those obstacles, unsteady periodic velocity profiles of the boundary layer on a stator blade's suction surface were successfully captured at

different blade heights and various chordwise positions. This is the first time such measurements were performed on the LSRC facility. Comparable measurements have been carried out at mid blade height on the G.E. compressor facility in Cincinnati, Ohio (Halstead et al, 1995).

In the present study, a total of five working days were dedicated to collecting boundary layer traverse data. Day to day testing conditions varied and these were not limited to the ambient fluid temperature and pressure, which were periodically recorded during measurement. The vibrational frequency characteristics of the LSRC compressor facility also varied from day to day. This was determined not to be a major problem as the traverse instrumentation was attached rigidly to the rig as to form part of it. Any vibration occurring from the rig would be in phase with that of the cassette assembly.

The considerable difficulties encountered during boundary layer measurements were mostly due to modifying an existing layout for mechanical access in between the embedded rotor stages of the LSRC facility, prepared for previous research (Foley, 1995). The limited access has highlighted the challenges associated with instrumenting real turbomachines for measurement purposes. These and their resulting effects on accuracy of data are described below.

5.4.1 Positioning of Measurement Probe

Prior to performing the boundary layer traverse at each individual chordwise location, it was essential to align the hot-wire sensor parallel to the measurement blade surface to avoid non-linear averaging of the velocity profile. The three-dimensional design of the blade made the exact parallel alignment of the sensor a somewhat lengthy process. To achieve this requirement without damaging the sensor wire a method similar to that of Hodson (1983) was adopted. The resistance output of three Ohmmeters was used to establish that both prongs were at the same distance from the blade and that they made contact with the surface simultaneously. When the probe sensor touched the blade surface, a motor shut down command was programmed in the

control software at this precise angular position to eliminate any risk of accidental breakage of the probe during measurement.

Calibration and the alignment procedure could be performed only with the traverse cassette assembly removed from the experimental rig. And due to the LSRC facility's stator ring construction, refitting the cassette assembly onto the rig required that the measurement blade itself be initially loosened and twisted by approximately 15 degrees anti-clockwise. A low tolerance dowel pin was fitted at the root of the blade to ensure it was relocated at the proper stagger angle once the cassette was fixed. Although the dowel system was used as a measure to minimise positional errors, this did not however guarantee that the exact relative distance between the probe and blade surface were restored as during alignment. This uncertainty was overcome by approaching the probe to the blade surface at known increments from a predetermined datum position until the probe sensor literally came in contact with the blade surface. This could be detected easily as the earthing of the probe touching the blade surface resulted in a voltage output of 0 volts.

Two main factors made it not possible to obtain velocity measurements at the blade surface using hot-wire probes. The first was due to the metallic composition of the measurement blade. This was an aluminium alloy (6082 TF Aluminium) with a conductivity of 184 W/m °C (Timmis, 2000). The blade surface, upon contact with the measurement probe caused the circuit to short out resulting in erroneous outputs to the anemometer bridge. The second factor stems from the physical construction of the probe. Although the sensor wire itself was of 5 μm in diameter, it was welded to a probe tip of 0.05 mm nominal radius (Kalfas, 1995). Therefore, the process of locating the boundary layer probe very accurately near the wall introduced a few uncertainties such as proximity effects, which required correction later during post-processing.

It was the author's intention to take measurements along four chordwise positions (see Figure 5.5) at three primary blade heights (i.e. 15%, 50% and 85%). Taking measurements near the end wall regions, particularly at 85% blade height (i.e. near the casing) proved to be considerably difficult and often impossible as the

measurement probe gave erratic outputs when nearing the blade surface and resulted in breakage of the sensor on two occasions. The most probable explanation for these incidences is the violent pressure pulsations that occur in the rotor tip region due to the disturbed flows such as tip clearance flows and tip corner vortices. These fierce pulsations could have caused the measurement probe to reach its resonance vibration and thus causing it to collide with the blade. There were no such occurrences at 15% blade height, though parallel alignment of the sensor was most difficult at this location.

5.4.2 Accuracy of Measurements

Using a measurement probe to traverse the boundary layer that exist in a real turbomachine bring about significant uncertainties due to the much smaller scale in time and space of the phenomena which occur. The following specify the accuracy of the experimental methods applied as well as the non-quantifiable sources of error.

As described previously the difficulty in probe location was overcome by using the technique of moving the probe towards the surface in computer-controlled micro-steps instead of starting from the surface. A 1.8-degree step angle motor with half-step capabilities allowed the micro stepping mode to solve noise and resonance problems and to increase step accuracy and resolution necessary to traverse across the blade boundary layer. The step accuracy is given as ±5% in the stepper motor manufacturer's data sheet but no details could be found about the motor's behaviour when it is used in the micro stepping application. The repeatability of the micro steps was assessed using Anritsu's KL130 series laser displacement meter. This state-of-the art non-contact displacement meter uses the triangulation method for measuring such dimensions as height, difference in level and thickness as well as vibration measurement of rotating shafts. This semiconductor laser displacement meter operated with an accuracy of ±0.01 μm. Ideally with the micro stepping gear operating at a ratio of 12800 steps per revolution, each motor step should give an angular movement of 0.028125 degrees. Given the small size of the movement, this can be translated as a step of 25μm with a 50-mm probe. The displacement meter's laser was focused on the pointer mounted on the rear shaft of the motor to verify the repeatability of the micro steps. Upon recording

several sets of motor step displacements (i.e. 20 * 5 mm), the step accuracy in the micro step electronic gear was determined to be ±9.25 μm per 25 μm step.

One-dimensional flow was assumed when calibrating the single sensor hot wires probes and a fourth order polynomial fit was used for characterising the dual X array probes. Both, the digital data acquisition card and voltmeters were pre-calibrated and configured for the present application. In general, the accuracy of the velocity measurements using the hot wire probes can be considered to be 0.5%.

5.4.3 Proximity Effects

Taking detailed measurements during the boundary layer survey involved approaching the probe to the surface at specified increments until the probe virtually touched the surface. This will introduce errors when obtaining data since the hot-wire sensor is in the vicinity of a wall (i.e. stator blade surface) with a higher conductivity than that of the working fluid. This is because in addition to the heat loss generated from the flow of fluid, conduction will occur and result in a higher voltage output, which will be erroneously interpreted as a higher value of velocity. The requirement for correction in hot-wire measurements near wall has been recognised since the early applications of the technique. Wills (1962) was one of the firsts to deal with the corrections for constant-temperature HWA probes. Corrections were obtained based on the known velocity distribution in a well-defined laminar channel flow. Previous study at Cranfield University has used the method of Wills (1962) where the value of the correction factor for a turbulent boundary layer was deduced to be half of that used for a laminar boundary layer (Kalfas, 1995). No validation had been provided for this. Review on the current state of knowledge concerning the correction used for HWA readings has shown that Wills' assumption provides inconsistent results. A more up to date method suggested by Lange et al (1998) who performed a thorough numerical investigation of the two-dimensional heat transfer and flow around a single heated circular cylinder in the vicinity of a wall has been applied in this investigation. However, the maximum difference between measured and corrected flow velocity was

found to be no more than 2 m/s in the present investigation. A brief discussion on proximity effects of hot-wire measurements can be found in Appendix B.

5.5. Results

Unsteady transitional boundary layer velocity profiles on the suction surface of a stator of an embedded stage have been successfully captured. Although attempts have been made to carry out measurements at three blade heights at each of the four strategic chordwise positions, the time constraints and difficulties described in the previous section have limited the extent of data collected. Table 5.1 below provides a summary of the measurement locations at which collection of velocity profiles have been successful.

		Blade Chord Position			
Flow conditions	Blade Height	C6: 15%	C4: 26%	C3: 37%	C1: 65%
Design	15%	✓	✗	✗	✓
	50%	✓	✓	✓	✓
	85%	✗	✗	✗	✓
Near Stall	15%	✓	✗	✗	✓
	50%	✓	✓	✓	✓
	85%	✗	✗	✗	✗

Table 5.1 Measurement Locations where Data have been Successfully Collected

The time-averaged profiles of velocity at the corresponding measurement locations are shown in figures 5.7 to 5.13. These have been averaged over five wake passing periods of the immediately upstream rotor row. Plots of available near endwall blade height measurements (i.e. at 15% and 85% height) show distinct differences in the flow features. Plots of 15% blade height at both 15% and 65% chord (figures 5.7 & 5.11) indicate less troubled flow. The difference in the state of the boundary layers at each blade height is very evident at 65% chord where the boundary layers at the

remaining heights have already separated (figures 5.11 to 5.13). In contrast, at 85% height at most chord positions the highly disturbed flow that occur near the casing due to the tip clearance flows and endwall boundary layer that have the whole length of the casing to develop, have made it virtually impossible to take measurements.

Example plots of the time varying velocity profiles of unsteady boundary layer data collected in this part of the investigation are presented in Figure 5.14. Each individual plot represents the velocity profile at every 5-step increment in time during one rotor passing cycle. The ordinate has been normalised by the edge of the boundary layer δ and the abscissa is normalised using the boundary layer edge velocity U_{∞}. As can be seen from the plots of Figure 5.14 the state of the boundary layer (either laminar or turbulent) at each time step cannot be easily determined. However, a reference line drawn along the 0.25 mark of the non-dimensionalised velocity scale shows the periodic shifting of the velocity profile with time. To further help the reader appreciate the fluctuating unsteady characteristics of the boundary layer profiles, a collection of boundary layer survey data have been converted into one dimensional vector form and compiled into movie clips using *FieldView (version 6)* graphics software. These AVI files are in the compact disc included with this thesis and can be accessed via a CD ROM drive.

Figure 5.15 presents the results in the log law form as used by Clauser, (1954, 1956) with the normalised velocity U^+ and distance Y^+. As can be seen from this plot the value of Y^+ does not go below the value of 4 reflecting the mechanical and physical limitations associated with measuring the boundary layer using hot wire probes.

5.6. Conclusions

Experimental investigation on the extent of the boundary layer has been conducted on the suction surface of a stator within an embedded stage of a multi-stage compressor. A traverse mechanism specially designed has made it possible to observe the transitional behaviour of the boundary layer exposed to the unsteady environment present in real turbomachinery environment. This is the first time such type of

investigation has been carried out at Cranfield University, where previous related studies have used flat plates in a wind tunnel arrangement.

Despite difficulties associated with the small scale of the measurement section (compared to a large flat plate), unsteady velocity profiles have been captured at four major chord positions at three different radial heights. Hot-wire measurements show that the boundary layer is transitional early on near the leading edge of the blade (i.e. 15% chord) and separation is imminent at 37% chord which is near the region where the pressure gradient reaches zero and becomes positive (i.e. adverse). This may be an indication that the transitional area on the blade may occupy a much larger portion of the blade chord than previously thought. Transitional flow however did not cover as much as 70% of the suction surface as detected by Halstead et al (1995) and Solomon and Walker (1995).

Due to the inconsistency of location caused by the mechanical arrangement and the microscopic scale of the events that are being measured, the results from this experiment should be regarded mostly as a qualitative picture of the behaviour of the boundary layer flows on the stator blade surface.

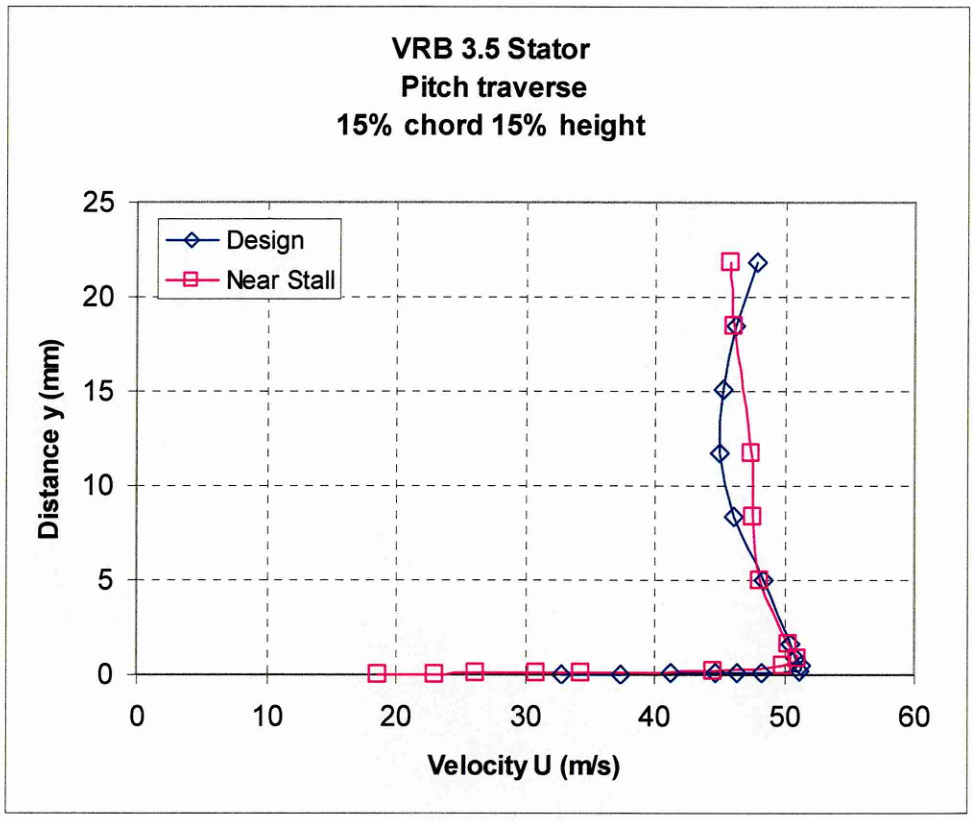

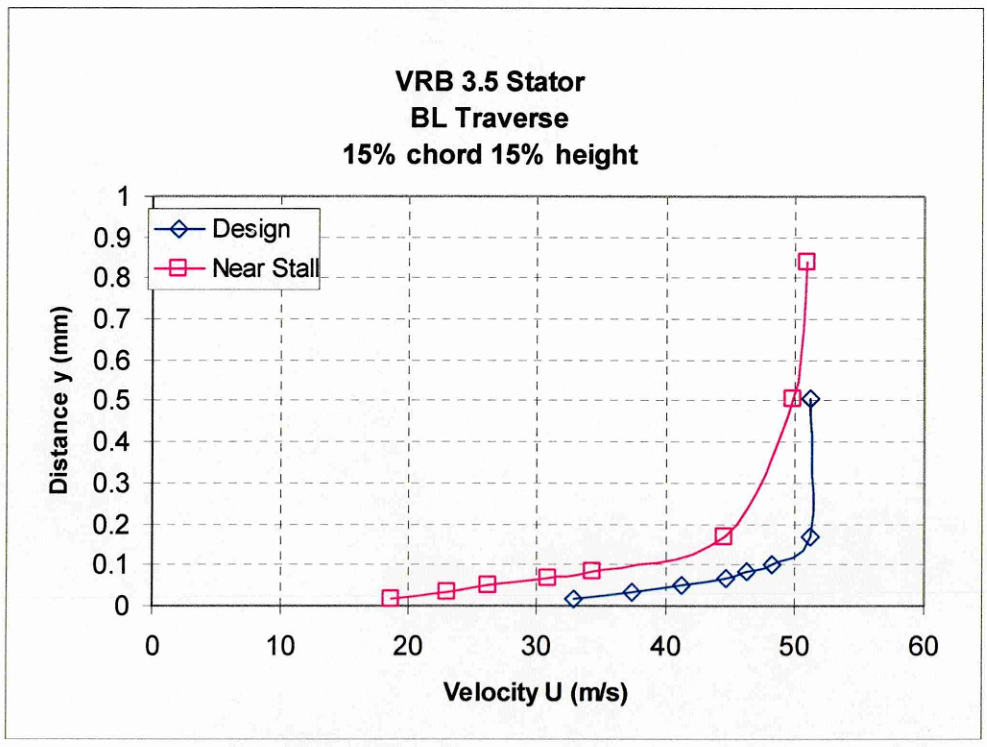

Figure 5.7 Time Averaged Plots of Velocity Profiles at 15% Chord & 15% Height

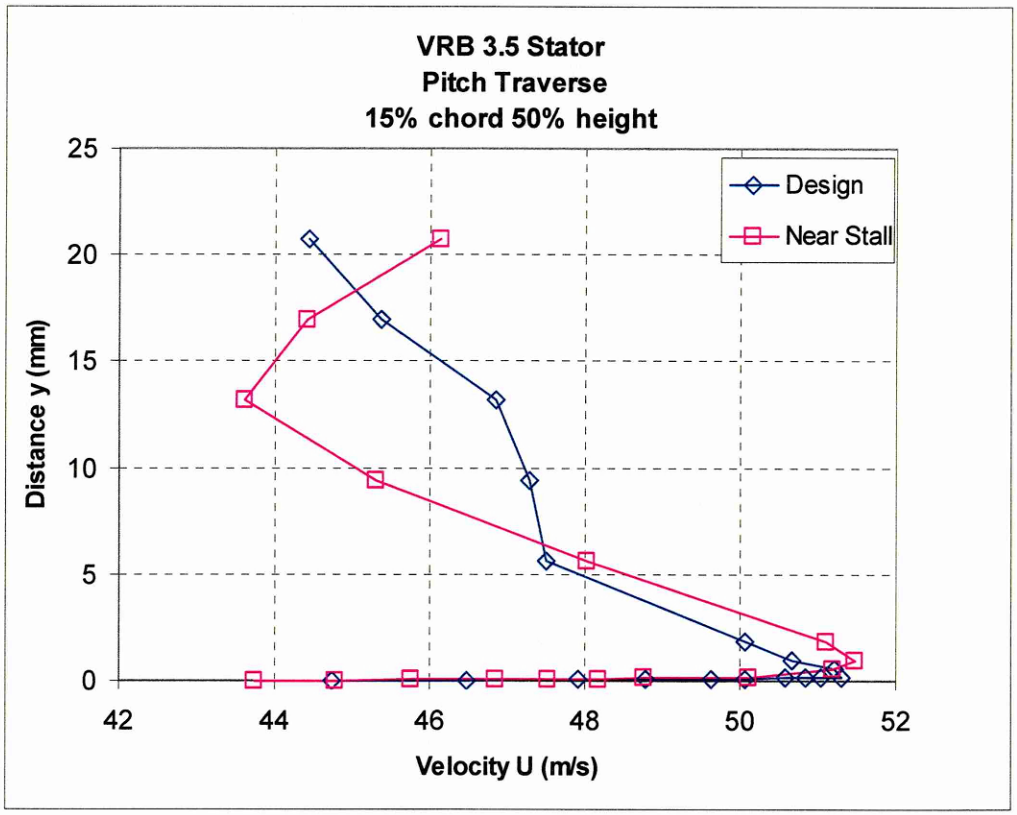

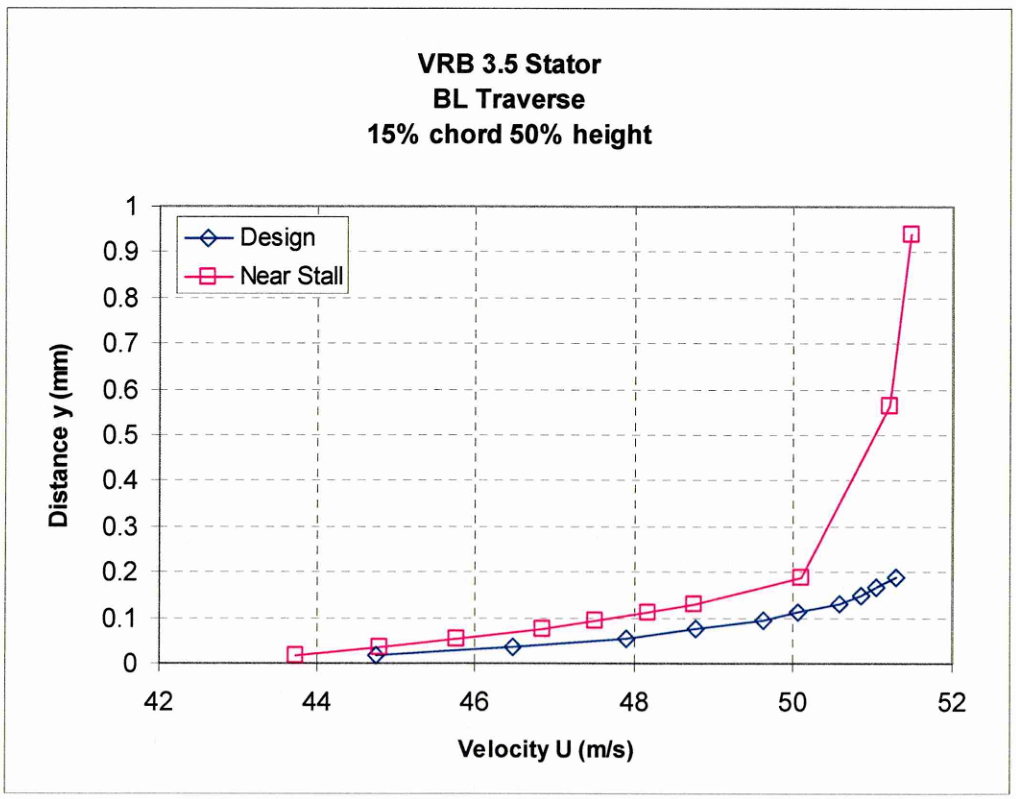

Figure 5.8 Time Averaged Plots of Velocity Profiles at 15% Chord & 50% Height

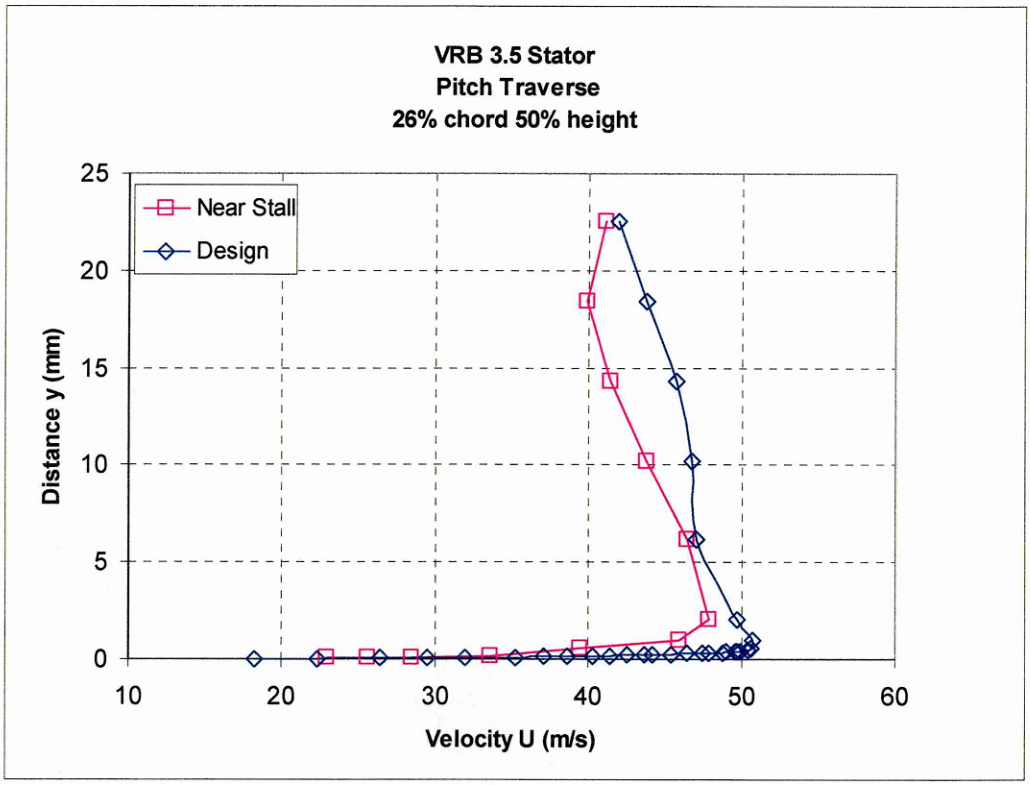

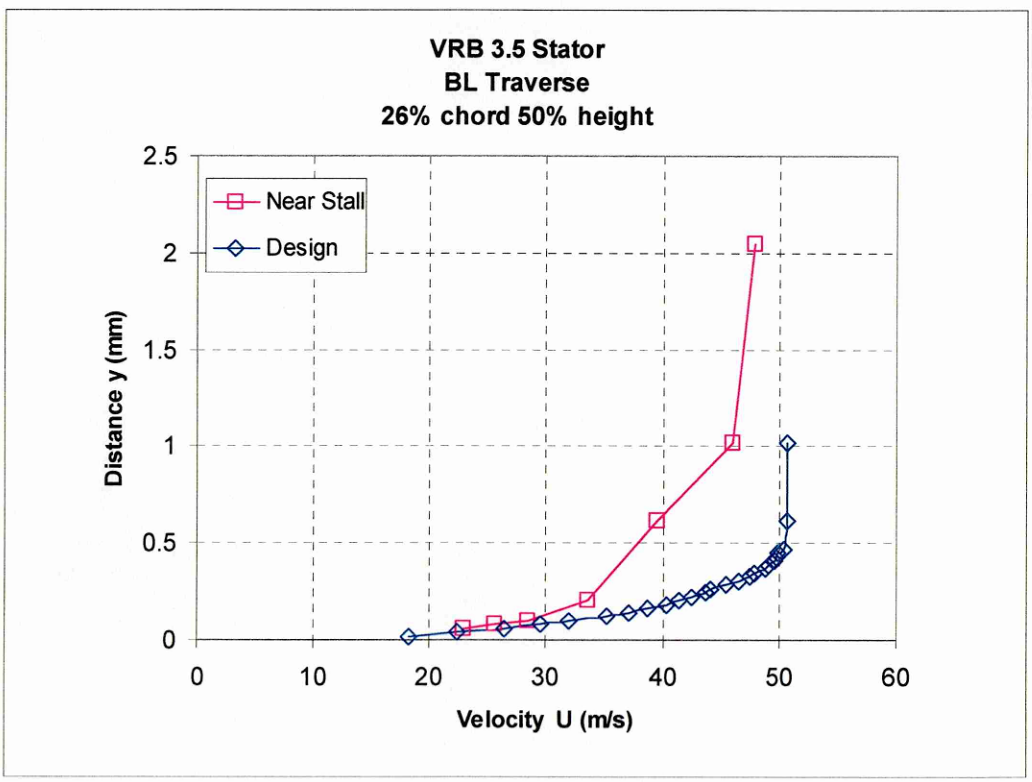

Figure 5.9 Time Averaged Plots of Velocity Profiles at 26% Chord & 50% Height

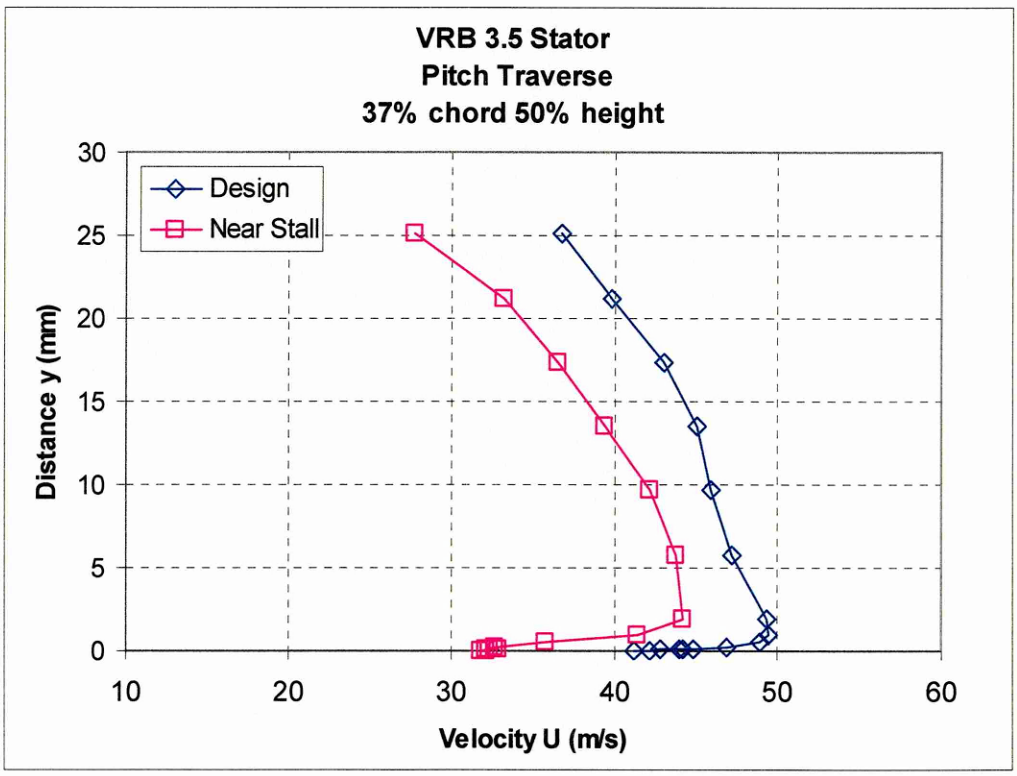

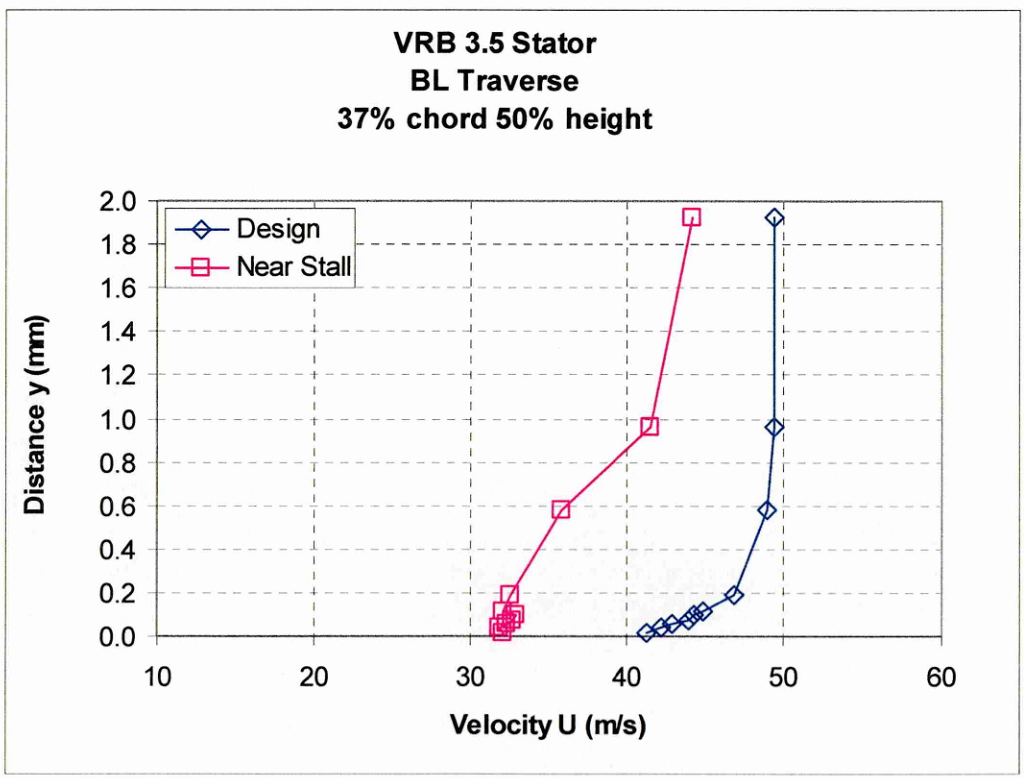

Figure 5.10 Time Averaged Plots of Velocity Profiles at 37% Chord & 50% Height

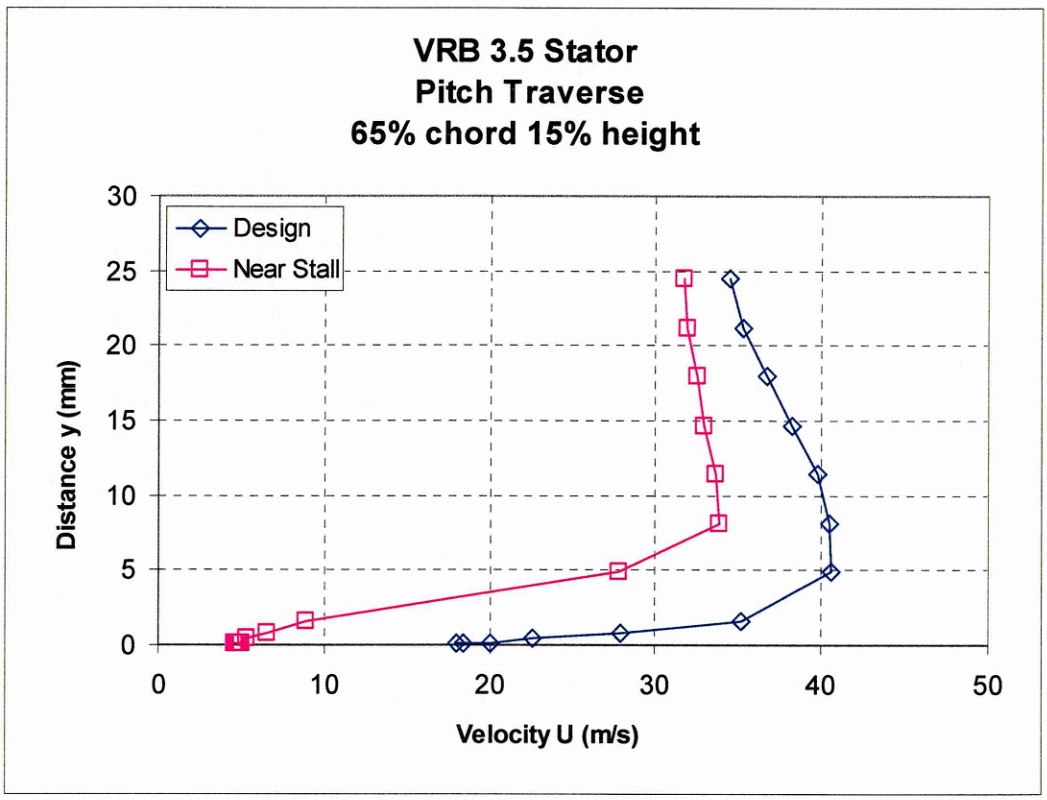

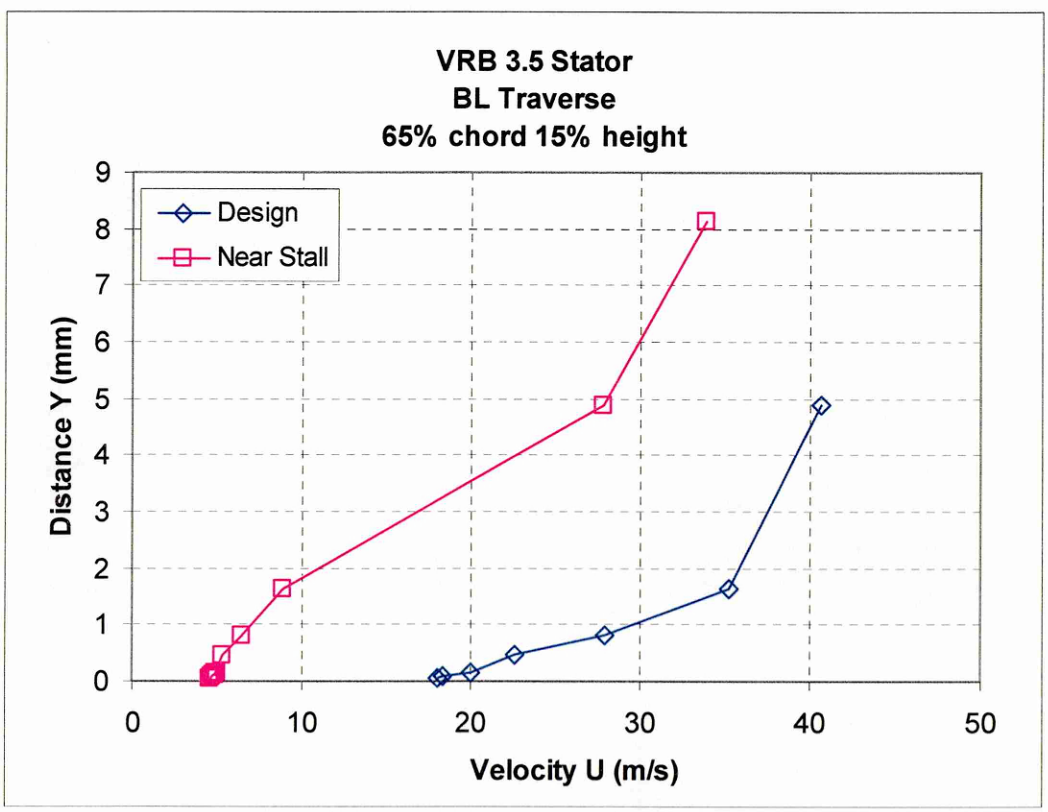

Figure 5.11 Time Averaged Plots of Velocity Profiles at 65% Chord & 15% Height

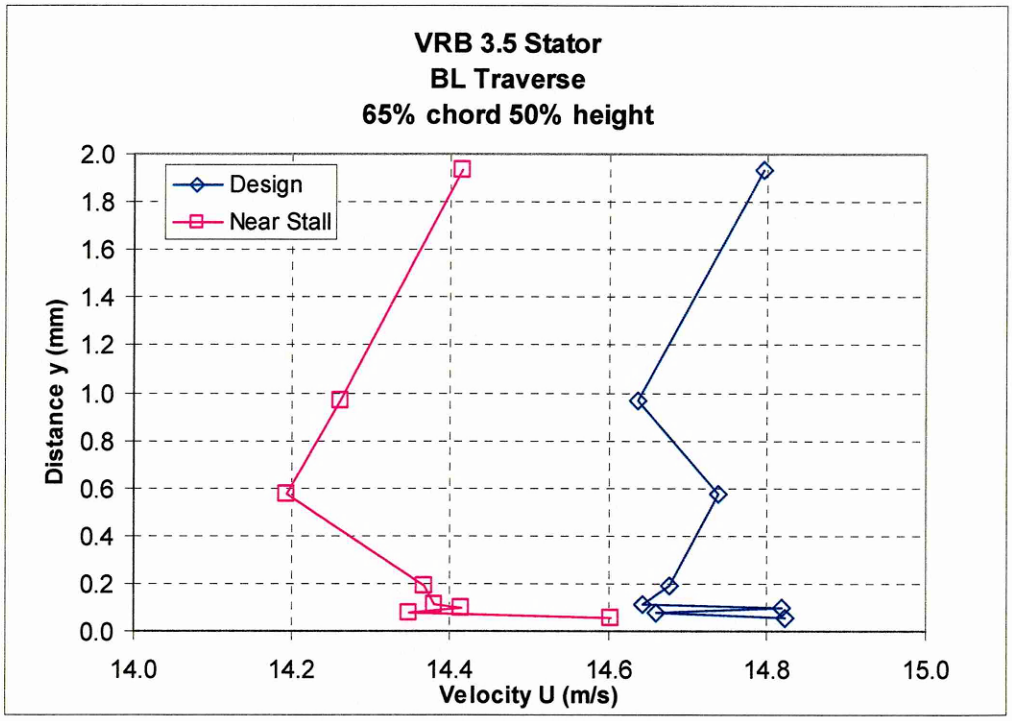

Figure 5.12 Time Averaged Plots of Velocity Profiles at 65% Chord & 50% Height

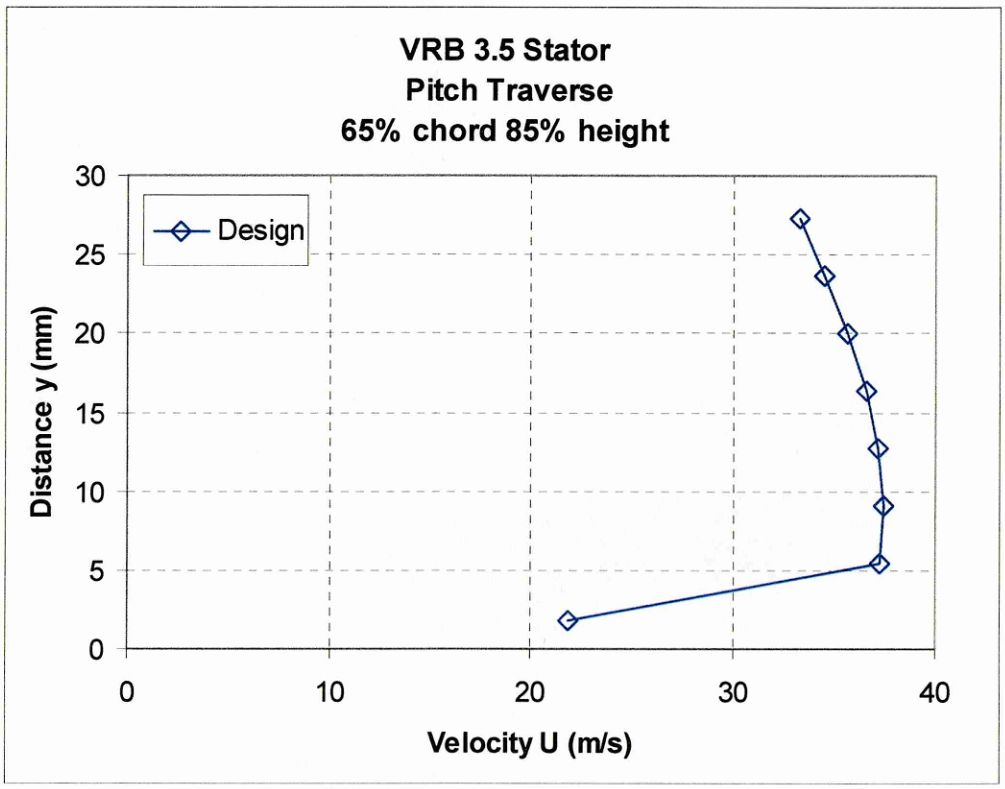

Figure 5.13 Time Averaged Plot of Velocity Profile at 65% Chord & 15% Height

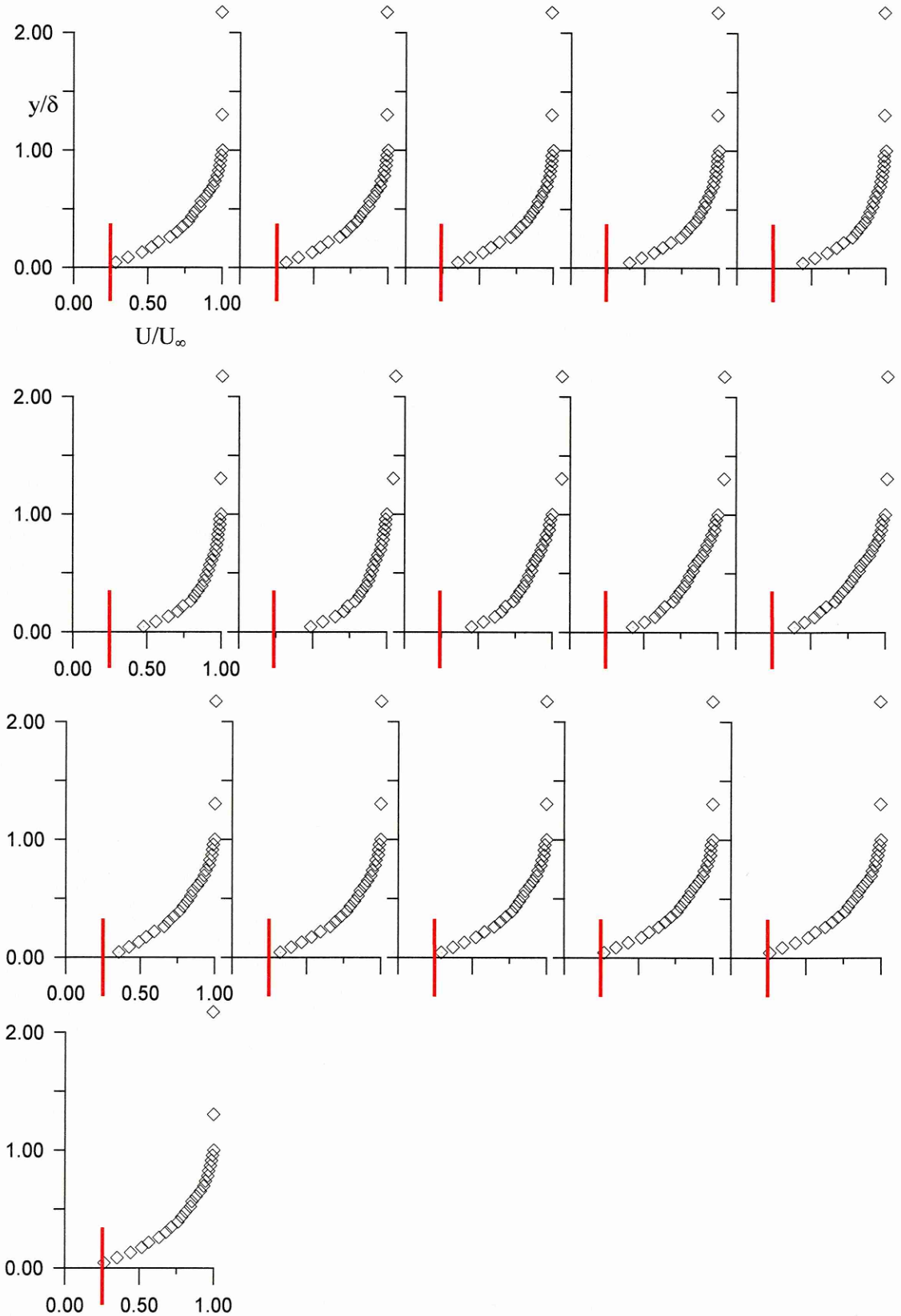

Figure 5.14 Boundary Layer Traverse at Design Conditions (26% chord).

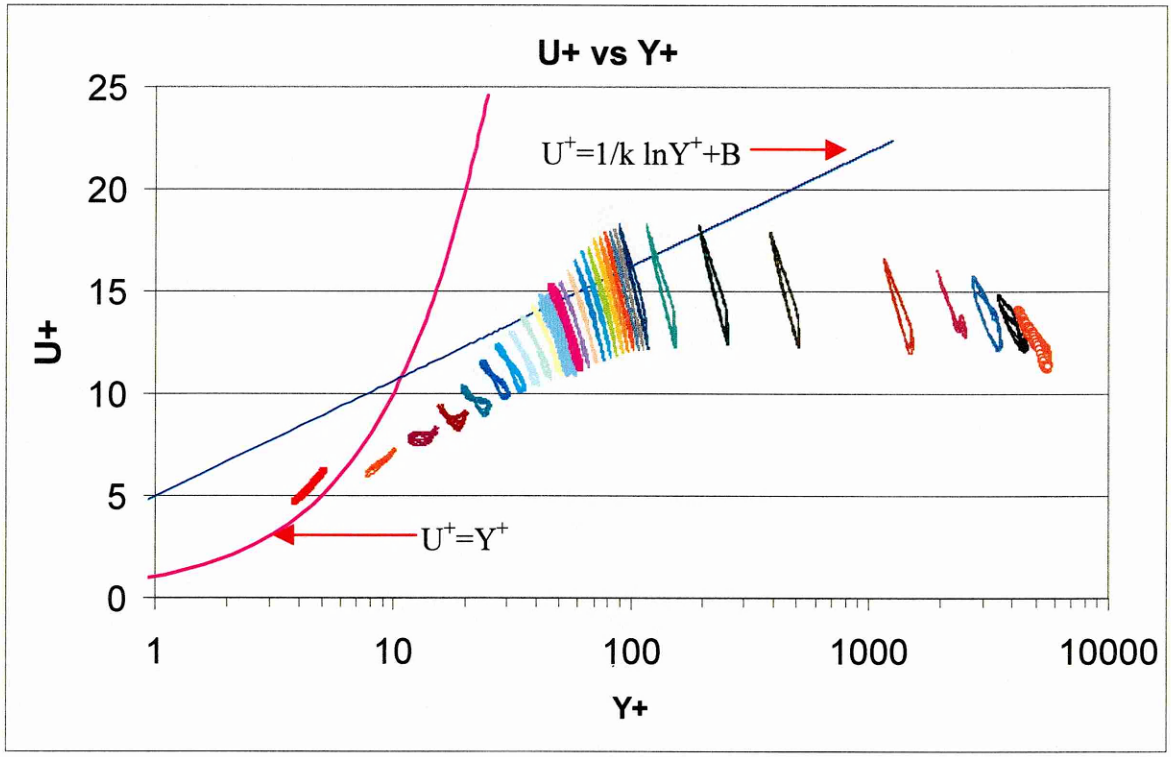

Figure 5.15 Initial Unsteady Plots of Data Using the Log Law

CHAPTER 6

Conclusions and Suggestions for Future Work

6.1. Introduction

Among many factors that contribute to the transition of boundary layers that develop over turbomachinery blading are the influences of turbulent and unsteady free stream flow conditions due to the wakes shed by previous blade rows. Numerous works in the literature report studies undertaken in a quiescent environment with none or very little disturbances in the free stream flow using flat plates and/or cascade arrangements, which do not take into consideration the rotational features of the flow. Previous boundary layer studies at Cranfield University initially concentrated on flows on flat plates with various leading edge geometry (Kalfas 1995) then later introduced pressure gradients representative of modern control diffusion blading (Read 1997). These were conducted in a wind tunnel arrangement in steady flow conditions and with turbulence generating grids delivering quasi-homogeneous and isotropic turbulence levels.

The present research has been the third phase on the study of boundary layer flow behaviour on turbomachinery blading at Cranfield University. The distinctive feature of the present investigation is the considerable step taken from previous experimental arrangement employed at Cranfield University. A first ever attempt has been made at investigating the unsteady boundary layer flow behaviour on real compressor blading within a turbomachinery environment. This was done using Cranfield University's unique low-speed four-stage compressor facility (LSRC) mounted with prototype state of the art 3 D controlled diffusion blades, designed jointly by Rolls Royce PLC and Cranfield University. The first part of this experimental study observed the two-dimensional unsteady flow field generated by previous rotating and stationary blade rows and its interaction with the embedded study

stage. The second part consisted of taking detailed measurements of unsteady velocity profiles of the boundary layer that exist on the suction surface of a stator within an embedded stage.

6.2. Conclusions

Two dimensional flow field measurements within the third embedded stage of Cranfield's four-stage low-speed compressor have shown the distinct characteristics of the wakes present including the turbulence features. The unsteady features captured by the dual X-array hot-wire measurements distinctly show the strong wake features of the rotor row and that of the previous stator row. The rotor wakes exhibit periodic variations in thickness, which indicates blade loss fluctuations. This is more prominent at Near Stall conditions with separation occurring at the casing regions. It can be seen quite clearly that the inlet conditions to the downstream stator blade-row vary considerably along the span, which is a significant consideration in blade design toward the hub and casing region. Strong variations are present in the end-wall regions where corner stall and corner vortex and tip clearance flows dominate. Radial migration of flow deviation was also detected with each passage of a rotor wake. Although this must not be confused with radial components of flow activities, it clearly indicates that there exist significant radial asymmetries in velocity profiles.

It is clearly evident that the wakes cause a velocity deficit and the boundary layer between the wakes is much like the steady flow boundary layer. The effect of these wakes impinging on the immediate downstream stator row was investigated at various chord positions and radial heights on the suction surface of a stator blade of the same embedded stage.

Although boundary layer transition on the stator blade surface was not expected until about midchord, fluctuation between laminar and turbulent of the boundary layer flow was detected even on the forward portion of the stator blade (i.e. 15% chord from leading edge) at 50% height whenever a rotor wake segment was present. This periodic alternating of the boundary layer was apparent also further aft on the blade. The extent of this transitional boundary layer flow varied along the blade span. This variation was

quite evident in the end-wall regions, especially in the casing region where the highly disturbed flow due to tip leakage flows and end-wall boundary layer flows made it virtually impossible to collect velocity data. The frequency of the fluctuation appeared to be more dependent on the state of the boundary layer rather than the passing frequency of the wakes.

Imminent separation was detected on the blade surface at 37% chord and mid-height, at both design and near stall operating conditions followed by complete separation at 65% chord. The occurrence of separation was not anticipated on the VRB 3.5 blading as the 3D design of the blade was aimed at delaying if not eliminating, any such separation until or near the trailing edge. The results from the current study do not agree with those of Halstead et al. (1995), who have indicated that transitional flow may cover as much as 70 percent of compressor airfoil suction surfaces.

6.3. Suggestions for Future Work

It is the author's belief that, although closely related, each of the two investigations described in this dissertation (i.e. flow field measurement and boundary layer survey), merit detailed study on its own.

Firstly, the study of unsteady flow field would reach a much higher potential and certainly bring interesting results with detailed three-dimensional hot-wire measurements upstream and downstream of both rotor and stator rows of an embedded stage. Several studies on the effects of IGV and stator indexing have been documented in the literature but the effects of varying the axial gap between blade rows at different flow coefficients have received scant attention. Investigating this should certainly improve the understanding of the effect of wake mixing on compressor performance and the relation between the wake recovery and the change in kinetic energy of the unsteady velocity field across a blade row. In addition to hot-wire anemometry methods, optical instrumentation such as Doppler Global Velocimetry (DGV), which enables full field measurement as opposed to the point measurement of LDA, would be ideal in providing a picture of the troubled flow present especially in the tip clearance region.

An immediate recommendation for the boundary layer study is the creation of an access window on the LSRC facility solely dedicated for boundary layer traverse arrangement. Eliminating the complications encountered in the current study with fixing and removing the traverse assembly to and from the rig will help greatly in reducing testing time and ensure repeatability. Implementing a motorised system enabling the probe to traverse along the chord would help provide valuable information by allowing detailed measurements to be taken at an infinite number of chord positions.

The proportionally large scale of the blading could make it possible for pressure tappings to be instrumented along the chord of the blade at strategic heights, particularly near the end-wall regions. This would enable the analysis of the Mach number distribution along the chord length and provide useful information for comparative purposes in parallel with thermal anemometry. Further work is recommended using a measurement blade made of non-conducting material (i.e. Perspex), which would minimise if not eliminate the proximity effects on hot-wire measurements.

BIBLIOGRAPHY

- Abu-Ghannam, B. J. and Shaw, R. (1980)
  "Natural Transition of Boundary Layers-The Effects of Turbulence, Pressure Gradient and Flow History"
  Journal of Mechanical Engineering Sciences, Vol. 22, pp. 213-228.

- Adamczyk, J. J. (1996)
  "Wake Mixing in Axial-Flow Compressors"
  ASME Paper 96-GT-29.

- Barankiewicz, W. S. and Hathaway, M. D. (1997)
  "Effects of Stator Indexing on Performance in a Low Speed Multistage Axial Compressor," ASME Paper 97-GT-486.

- Bennett, I. (1999)
  Private Discussions, Cranfield University

- Bhatia, J. C., Durst, F., and Jovanovic, J. (1982)
  "Corrections of hot-wire anemometry measurements near walls"
  Journal of Fluid Mechanics., Vol. 122, pp. 411-431.

- Bradshaw, P. (1971)
  "An Introduction to Turbulence and its Measurement," Pergamon Press, Oxford.

- Bruun, H. H. (1995)
  "Hot-wire Anemometry Principles and Signal Analysis," Oxford University Press.

- Camp, T. R., Shin, H. W. (1995)
  "Turbulence Intensity and Length Scale Measurements in Multistage Compressors," ASME *Journal of Turbomachinery*, Vol. 117, pp. 38-46.

- Champagne, F. H., Sleicher, C. A., and Whermann, O. H. (1967)
  "Turbulence Measurements with Inclined Hot-wires." Part 1, Heat transfer experiments with inclined hot-wire." *J. Fluid Mech.,* 28, pp. 153-175.

- Chen, K. K., Thyson, N. A. (1971)
  "Extensions of Emmons' Spot Theory to Flows on Blunt Bodies"
  AIAA Journal, Vol. 9, No. 5, pp. 821-825.

- Clauser, F. H. (1954)
  "Turbulent Boundary Layers in Adverse Pressure Gradients"
  Journal of the Aeronautical Sciences, February 1954, Vol. 21, pp. 91-108.

- Clauser, F. H. (1956)
  "The Turbulent Boundary Layer," Advances in Applied Mechanics,
  Vol. IV, pp. 1-51.

- Cohen, H., Rogers, G. F. C., Saravanamuttoo, H. I. H.
  "Gas Turbine Theory," 4th Edition, Longman, 1996.

- Collis, D. C. and Williams, M. J. (1959)
  "Two-dimensional Convection from Heated Wires at Low Reynolds Numbers"
  Journal of Fluid Mechanics, Vol. 6, pp. 357-384.

- Cumpsty, N. A. (1989)
  "Compressor Aerodynamics," Longman Scientific & Technical, New York, U.S.A.

- Cumpsty, N. A., Dong, Y., Li, Y.S. (1995)
  "Compressor Blade Boundary Layers in the Presence of Wakes"
  ASME Paper 95-GT-443.

- DANTEC Measurement Technology
  Probes for Hot-Wire Anemometry, Catalogue

- DANTEC Measurement Technology
  56C17 Anemometer Bridge Instruction Manual.

- DISA 56C01 CTA and 56B10/56B12 Main frame Instruction Manual.

- Dean, R. C. (1959)
  "On the Necessity of Unsteady Flow in Fluid Machines"
  Journal of Basic Engineering, March 1959, pp.24-28.

- Denton, J. D. (1993, October)
  "Loss mechanisms in turbomachines"
  Journal of Turbomachinery, Vol. 115, pp 621-656, 93-GT-435.

- Dixon, S. L. (1975)
  "Fluid Mechanics, Thermodynamics of Turbomachinery," Pergamon Press.

- Doeblin, E. D. (1990)
  "Measurement Systems: Application and Design," 4th Edition McGraw Hill International Editions.

- Dong, Y., Cumpsty, N. A. (1989)
  "Compressor Blade Boundary Layers: Part I: Test Facility and Measurements with No Incident Wakes, Part II: Measurements with Incident Wakes"
  ASME Papers 89-GT-50 and 89-GT-51.

- Dring, R. P., Spear, D. A. (1991)
  "The Effects of Wake Mixing on Compressor Aerodynamics"
  ASME *Journal of Turbomachinery,* Vol. 113, October 1991, pp. 600-607.

- Emmons, H. W. (1951)
  "The Laminar-Turbulent Transition in a Boundary Layer – Part 1"
  Journal of the Aeronautical Sciences, Vol. 18, No. 7, pp. 490-498.

- Evans, R. L. (1975)
  "Turbulence and Unsteadiness Measurements Downstream of a Moving Blade Row," ASME *Journal of Engineering for Power,* pp. 131-139.

- Evans, R. L. (1978)
  "Boundary-Layer Development on an Axial-Flow Compressor Stator Blade"
  ASME *Journal of Engineering for Power,* Vol. 100, April 1978, pp. 287-293.

- Foley, A. C. (1995)
  "Tip Clearance Effects in Low Speed, Axial Flow Compressors," PhD Thesis Cranfield University.

- Funazaki, K. (1996a)
  "Unsteady Boundary Layers on a Flat Plate Distrubed by Periodic Wakes: Part I-Measurement of Wake-Affected Heat Transfer and Wake-Induced Transition Model," ASME *Journal of Turbomachinery,* Vol. 118, April 1996, pp. 327-336.

- Funazaki, K. (1996b)
  "Unsteady Boundary Layers on a Flat Plate Distrubed by Periodic Wakes: Part II-Measurements of Unsteady Boundary Layers and Discussion," ASME *Journal of Turbomachinery,* Vol. 118, April 1996, pp. 337-346.

- Gaster. M. (1969)
  "The Structure and Behaviour of Laminar Separation Bubbles"
  Aeronautical Research Council. R&M No. 3595.

- Gostelow, J. P. (1977)
  "New Approach to the Experimental Study of Turbomachinery Flow Phenomena"
  ASME *Journal of Engineering for Power,* Vol. 99, January 1977, pp. 97-105.

- Gostelow, J. P. (1984)
  "Cascade Aerodynamics," Pergamon Press, First Edition.

- Gostelow, J.P., Walker, G.J., Solomon, W.J., Hong, G., Melwani, N. (1996)
  "Investigation of the Calmed Region Behind a Turbulent Spot"
  ASME Paper 96-GT-489.

- Gresh, M. Theodore, P.E. (1991)
  "Compressor Performance," Butterworth-Henemann

- Halstead, D.E., Wisler, D.C., Okiishi, T.H., Walker, G.J., Hodson, H.P., Shin, H.W., "Boundary Layer Development in Axial Compressor and Turbines," Part 1; Composite picture, Part 2; Compressors, Part 3; LP Turbines, Part 4; Computations and Analysis. ASME Paper 95-GT-461, 95-GT-462, 95-GT-463 and 95-GT-464.

- Hansen, J. L., Okiishi, T. H. (1987)
  "Rotor Wake Segment Influence on Stator-Surface Boundary Layer Development in an Axial-Flow Compressor Stage," AIAA-87-1741, 1987/San Diego, California

- Hinze, J. O. (1959)
  "Turbulence," McGraw-Hill, New York.

- Hodson, H. P. (1983)
  "The Detection of Boundary Layer Transition and Separation in High-Speed Turbine Cascades," *Measurement Techniques for Transonic and Supersonic Flow Proceedings of the 7th Symposium held in Aachen, Sept. 21-23, Cascades and Turbomachinery.*

- Horlock, J. H. (1968)
  "Unsteady Flows in Turbomachines," Paper no. 2674, Third Australasian Conference on Hydraulics and Fluid Mechanics, Syndey.

- Howard, M. A, Ivey, P. C., Barton, J. P. and Young, K. F.(1994)
  "Endwall Effects at Two Tip Clearances in a Multistage Axial Flow Compressor With Controlled Diffusion Blading," ASME *Journal of Turbomachinery*, Vol. 116, pp. 635-647.

- Hourmouziadis, J. (1989),
  "Aerodynamic Design of Low Pressure Turbines," AGARD Lecture Series, No. 167.

- Ivey, P. C., Swoboda, M. (1998)
  "Leakage Effects in the Rotor Tip-Clearance Region of A Multistage Axial Compressor Part 1: Innovative Experiments," ASME Paper 98-GT-591.

- Joslyn, H. D., Dring, R. P. (1985)
  "Axial Compressor Stator Aerodynamics"
  ASME *Journal of Engineering for Gas Turbines and Power,* Vol. 107, pp. 485-493.

- Kalfas, A. I. (1995)
  "Transition to Turbulence in the Boundary Layer of Turbomachinery Blading," PhD Thesis, Cranfield University.

- Keithley Metrabyte, DAS-1800ST/HR Series User's Guide

- Kerrebrock, J. L., Mikolajczak, A. A. (1970)
  "Intra-Stator Transport of Rotor Wakes and Its Effect on Compressor Performance," ASME *Journal of Engineering for Power*, Vol. 92, pp. 359-368.

- Lange, C. F., Durst, F., Breuer, M. (1998)
  "Wall Effects on Heat Losses from hot-wires," *International Journal of Heat and Fluid Flow* 20 pp. 34–47.

- Lockwood, C. (1999)
  "Comparison of Average-Passage Equation Closures Through Simulation of Single and Multi-Row Axial Compressors; The Limitations of Using A Commercial CFD Code," PhD Thesis, Cranfield University.

- Lomas, C.G., (1986)
  "Fundamentals of Hot-Wire Anemometry," Cambridge University Press, Cambridge, U.K.

- Massey, B. S. (1989)
  "Mechanics of Fluids," 6th Edition, Chapman & Hall, 1989

- Mayle, R. E. (1991)
  "The Role of Laminar-Turbulent Transition in Gas Turbine Engines," ASME *Journal of Turbomachinery*, Vol. 113, pp. 509-537. ASME 91-GT-261.

- Mayle, R. E. & Schulz, A. (1996)
  "The Path to Predicting Bypass Transition," ASME 96-GT-199.

- Michelassi, V. (1997)
  "Shock-Boundary Layer Interaction and Transition Modelling in Turbomachinery Flows," *Proc Instn Mech Engrs,* Vol. 211 Part A pp. 225-234.

- McNally, W. D. & Sockol, P. M. (1982)
  "REVIEW-Computational Methods for Internal Flows With Emphasis on Turbomachinery," *Journal of Fluids Engineering*, Vol. 107 pp. 6-22.

- Narasimha, R. (1957)
  "On the Distribution of Intermittency in the Transition Region of a Boundary Layer," *Journal of Aerospace Science,* Vol.24, pp. 711-712.

- Narasimha, R. (1985)
  "The Laminar-Turbulent Transition Zone in the Boundary Layer," *Progress in Aerospace Science,* Vol. 22, pp. 29-80.

- Orth, U. (1993)
  "Unsteady Boundary Layer Transition in Flow Periodically disturbed by Wakes," *Journal of Turbomachinery*, Vol. 15, pp. 707-713.

- Pfeil, H., Herbst, R., Schröder, T. (1983)
  "Investigation of the Laminar-Turbulent Transition of Boundary Layers Disturbed by Wakes," ASME *Journal of Engineering for Power*, Vol. 105, pp. 130-137.

- Read, S. (1997)
  "Transition to Turbulence in Turbomachinery Environment," PhD Thesis, Cranfield University.

- Robinson, C. J. (1991)
  "End-Wall Flows and Blading Design for Axial Flow Compressors," PhD Thesis, Cranfield Institute of Technology, United Kingdom.

- RS Components Ltd (1999)
  Stepper Motor RS 440-458 Specifications Sheet

- Schlichting, H. (1979)
  "Boundary Layer Theory," 7th edition, McGraw Hill, New York.

- Schubauer, G. B., & Klebanoff, P. S. (1955)
  "Contributions on the Mechanics of Boundary Layer Transition," NACA TN 3489.

- Schulte, V. (1995)
  "Unsteady Separated Boundary Layers in Axial-flow Turbomachinery," PhD Dissertation, Cambridge University.

- Smith, L. H., Jr. (1966)
  "Wake Dispersion in Turbomachines"
  ASME *Journal of Basic Engineering,* Vol. 88, pp. 688-690.

- Solomon, W. J., & Walker, G. J. (1995)
  "Observation of Wake-Induced Transition on An Axial Compressor Blade"
  ASME Paper 95–GT–381.

- Steinert, H., Starken, H. (1996)
  "Off-Design Transition and Separation Behaviour of a CDA Cascade"
  ASME *Journal of Turbomachinery*, Vol. 118, pp. 204-210.

- Timmis, P. (2000)
  Private Discussions, Cranfield University

- Turan, Ö, Azad, R. S., Atamanchuk, T. M. (1987)
  "Wall Effect on the Hot-Wire Signal Without Flow"
  J. Phys, E: Sci. Instrum Vol. 20 pp. 1278-1280.

- Vagt, J. D., Fernholz, H. H. (1979)
  "A discussion of probe effects and improved measuring techniques in the near-wall region of an incompressible three-dimensional turbulent boundary layer"
  AGARD Conf. Proc., 271, 10.1-10.17.

- Walker, G. J. (1993)
  "The Role of Laminar-Turbulent Transition in Gas Turbine Engines: A Discussion," *Journal of Turbomachinery*, Vol. 117, pp. 207-217.

- Walker, G. J., Hughes, J. D., Köhler, I., Solomon, W. J. (1998)
  "The Influence of Wake-Wake Interactions on Loss Fluctuations of a Downstream Axial Compressor Blade Row"
  ASME *Journal of Turbomachinery,* Vol. 120, October 1998, pp. 695-704.

- Walker, G. J., Hughes, J. D., Solomon, W. J. (1998)
  "Periodic Transition on An Axial Compressor Stator-Incidence and Clocking Effects," Part 1-Experimental Data, Part 2-Transition Onset Predictions
  ASME Papers 98-GT-363, 98-GT-364.

- White, F. M. (1974)
  "Viscous Fluid Flow," McGraw Hill, New York, U.S.A.

- Wills, J. A. B. (1962)
  "The Correction of Hot-Wire Readings for Proximity to a Solid Boundary,"
  Journal of Fluid Mechanics, Vol. 12, pp. 388-396.

- Wisler, D. C. (1985)
  "Loss Reduction in Axial-Flow Compressors Through Low-Speed Model Testing,"
  ASME *Journal of Engineering for Gas Turbines and Power*, Vol. 107, April 1985, pp. 354-363.

- Wisler, D. C., Bauer, R. C., Okiishi, T. H. (1987)
  "Secondary Flow, Turbulent Diffusion, and Mixing in Axial Flow Compressors"
  ASME *Journal of Turbomachinery*, Vol. 109, October 1987, pp. 455-482.

- Young, A. D. (1989)
  "Boundary Layers," BSP Professional Books, Oxford, U.K.

APPENDIX A

Hot Wire Calibration and Measurement Techniques

A.1. Introduction

This appendix opens with a general introduction to the principles of Constant Temperature Hot-wire Anemometry, the primary tool used in this study. Detailed descriptions of the calibration methods applied prior to and after carrying out measurements of the unsteady flow-field and stator blade boundary layer characteristics are given accompanied by example calibration curves for the two types of probes used. The problems associated with the temperature drift of the calibration curve, as a side effect of the measurement, and how this obstacle was minimised are also discussed.

A.2. Hot-Wire Anemometry

A.2.1 Principles

Constant Temperature Anemometry (CTA) has been widely accepted as a tool for investigations in fluid dynamics and has been applied as such for over 50 years (Lomas, 1986). Its ease of operation and cost effectiveness has established itself as a popular technique for obtaining information about flow velocity. The continuous output in voltage makes it suitable for digital sampling and data reduction. The CTA's notable advantages over other methods are the high spatial and temporal resolution, which makes it particularly suitable for measuring highly fluctuating velocity components at a particular point. Hinze (1975) and Bradshaw (1971) have documented in detail the important features of hot-wire anemometry for applications to turbulence measurements.

The electronic package of a constant temperature anemometer contains a Wheatstone bridge with the sensor situated as one arm of the bridge. As shown in Figure A.1, two fixed resistors and one adjustable resistor complete the circuit. The

hot-wire acts as one resistor and the feedback amplifier automatically adjusts the current to maintain the bridge balance. The current through the wire is adjusted automatically to keep the wire temperature constant.

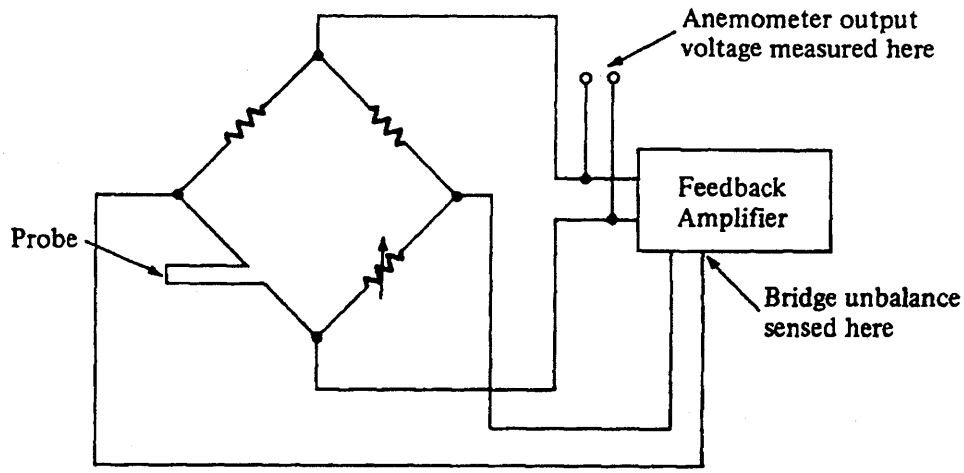

Figure A.1 Block diagram of a Constant Temperature Anemometer (Lomas, 1986)

The sensor is a thin wire made of platinum or tungsten of about five microns in diameter with a length to diameter ratio ranging from 200 - 600. The electrically heated sensor wire is convection cooled by the fluid passing over it, and this cooling effect is a measure of the fluid velocity. Any increase in velocity cools the sensor and unbalances the bridge. The differential feedback amplifier senses the bridge unbalance and responds by adding current to hold the sensor temperature constant and bring the bridge back into balance. The fast response of the feedback amplifier maintains the sensor temperature virtually constant as the fluid velocity changes. The anemometer output therefore represents the instantaneous velocity in the flow. The application of the hot wire sensor's small thermal inertia in conjunction with a very high servoloop amplification system allows flow fluctuations of up to several hundred kHz to be captured.

Assuming forced convection as the main heat transfer mechanism, an energy balance for the wire can be derived at equilibrium conditions.

$$I^2 R_w = hA(T_w - T_f) \tag{A.1}$$

The terms on the right side describe the cooling effect and the left hand side terms describe the current added to keep a constant temperature. (Doeblin, 1990)

Where
- I = wire current
- R_w = wire resistance
- T_w = wire temperature
- T_f = temperature of flowing fluid
- h = heat transfer coefficient
- A = heat transfer area

The heat transfer coefficient is mainly a function of the flow velocity for a given fluid density.

$$h = C_0 + C_1\sqrt{V} \tag{A.2}$$

where C_0 and C_1 are constants and V is the velocity.
The wire's surface area A and the temperature gradient (T_w-T_f) is approximately constant under the calibration. Adding Equations (A.1) and (A.2) gives a relation between the velocity and the voltage called the King's Law:

$$E^2 = A + BV^n \tag{A.3}$$

The voltage across the bridge is proportional to the fluid velocity and thus the velocity can be determined. A is the voltage at zero flow (also written as E_0) and the constants B and n (within 0.4-0.5) can be determined using the calibration data by linearising the calibration curve. Examples of the calibration techniques used on both single and dual sensor hot wire probes are shown in the following section.

A.3. Calibration of Hot-wires

As stated previously, the relationship between the CTA anemometer voltage output and velocity is exponential in nature. This results in very non-linear system but gives an almost constant relative sensitivity over a large range of velocity, which makes it suitable for measuring velocities from a few m/s to above the speed of sound.

The complex heat transfer function of the CTA system makes calibration a must prior to its application. Hotwire probes must be calibrated in the fluid in which it is to be used and exposed to known velocities. An existing calibration unit (DISA 99D90) was used for this purpose. Compressed air first passes through a filter and an integrated valve regulates the mass flow. The flow then enters the nozzle unit of varying diameters and emerges as a free laminar jet. The pressure drop (Δp) across the nozzle is measured by a differential pressure micro-manometer.

Prior to exposing the hot-wire probe to the flow from the calibration unit, the bridge must be balanced. Also, the adjustable resistor in the Wheatstone bridge must be adjusted to hold the sensor's operating temperature at a desired value via the selection of an overheat ratio a, defined as R_w/R_a (see Chapter 3). The length-to-diameter ratio of the probes used in this experimental work dictated the overheat ratio to be between 0.8 and 1 for optimum performance.

The total resistance must also be determined by adding the contributing resistance in the CTA system. The procedure for calculating the resistance is given in detail in DANTEC's '56C17 Anemometer bridge system instruction manual.'

Briefly, the steps for calculating the total resistance are as follows:

1. Cable resistance R_C and lead resistance R_L
2. Measurement of sensor resistance at zero flow conditions
3. Calculation of operating resistance with overheat selection
4. Adjustment of resistance setting taking into account the above contributions

The velocity of the flow exiting the nozzle can be calculated using Bernoulli's equation for an incompressible frictionless flow.

$$\Delta p_{nozzle} = \frac{1}{2}\rho v^2 \tag{A.4}$$

The velocity from the above equation can be calculated using the universal gas equation for density.

$$p = \rho RT \tag{A.5}$$

thus

$$V = \sqrt{\frac{2\Delta p_{nozzle} RT_{amb}}{P_{amb}}} \tag{A.6}$$

where R is the Gas constant and P_{amb} and T_{amb} are the ambient pressure and temperature respectively.

The hot-wire is exposed to a flow having a known velocity from the calibration unit and a voltage output signal is displayed on the voltmeter and/or computer. This procedure is followed for different velocities and at different flow angles if the yaw characteristic is also desired (e.g. for dual sensor X array probes). A characteristic curve is then plotted for each wire. The micromanometer should be calibrated periodically to ensure consistency in the calibration data.

Although the fundamental principles are the same, the methods of calibration (i.e. characterisation) of the two types of hot-wire sensors used in this investigation varied. This was especially the case with the X array dual sensor probe mainly due to the orientation of the probe axis relative to the flow. The differences in applications of the probes are briefly described below.

A.3.1. Single Sensor

Single sensor probes (e.g. DANTEC's 55P01 & 55P05), were used for the boundary layer survey on the stator blade (see Chapter 5) and were orientated so that the flow approached the hot-wire sensor normal to its axis. This method is normally used when the flow can be considered one-dimensional without taking into account any yaw effects. Thus the calibration equation used for characterising the single sensor was the conventional King's Law relation. This relation is commonly used for velocity calibration.

A.3.2. Dual Sensor

The application of a dual sensor probe is primarily for simultaneously capturing both the magnitude and direction of a two-dimensional flow field in a measurement plane. X array probes (e.g. DANTEC's 55P52) were used in the present study for capturing two components of velocity, U and V downstream of an embedded rotor stage (see Chapter 4). The perpendicular orientation of the probe axis relative to the flow made it necessary to take into account the effects of the support prongs. The wakes from the neighbouring support prongs made it not feasible to consider each sensor separately and a modified method of probe characterisation was necessary.

A.4. Examples of Hot Wire Calibration

A.4.1 Single Sensor Probe

- Probe Type 55P01 single sensor
- Sensor Resistance at 20°C R_{20} 3.1 Ω
- Lead Resistance R_L 0.5 Ω
- Sensor TCR a_{20} 0.36 %/C
- Measure Total Probe Resistance, R_{TOT}, at Ambient Temperature, T_0
- Select Sensor Operating Temperature T_{sensor}<300°C
- Calculate Operating Resistance

$$R = R_{TOT} + (a_{20} \times R_{20}(T_{sensor} - T_0)$$

- Ambient Pressure: 0.99587 Bar
- Ambient Temperature: 286 K

Meter	Dp (Bar)	Velocity	Voltage	Log Vel	Log (Eb^2-E0^2)
0	0	0	1.449	N/A	N/A
10	0.00098	12.7166	2.047	1.104372	0.320272608
20	0.00196	17.984	2.15	1.254887	0.401899865
40	0.00392	25.4333	2.269	1.405402	0.484123238
50	0.00491	28.4353	2.307	1.453857	0.508212871
60	0.00589	31.1493	2.337	1.493448	0.526593575
80	0.00785	35.9681	2.388	1.555917	0.556657391
90	0.00883	38.1499	2.409	1.581493	0.568633456
100	0.00981	40.2135	2.428	1.604372	0.579278493
110	0.01079	42.1763	2.45	1.625068	0.591387313
120	0.01177	44.0517	2.466	1.643963	0.600052719
150	0.01472	49.2513	2.508	1.692418	0.62226201
170	0.01668	52.432	2.536	1.719597	0.63665787
200	0.01962	56.8705	2.57	1.754887	0.653723619
210	0.0206	58.2749	2.58	1.765482	0.658659872
220	0.02158	59.6463	2.591	1.775583	0.664047469
240	0.02354	62.2985	2.608	1.794478	0.672288444
250	0.02453	63.5832	2.617	1.803342	0.676610217
280	0.02747	67.2901	2.641	1.827951	0.687999563
300	0.02943	69.6519	2.656	1.842933	0.695020432

Table A.1 Calibration Data for Single Sensor Probe

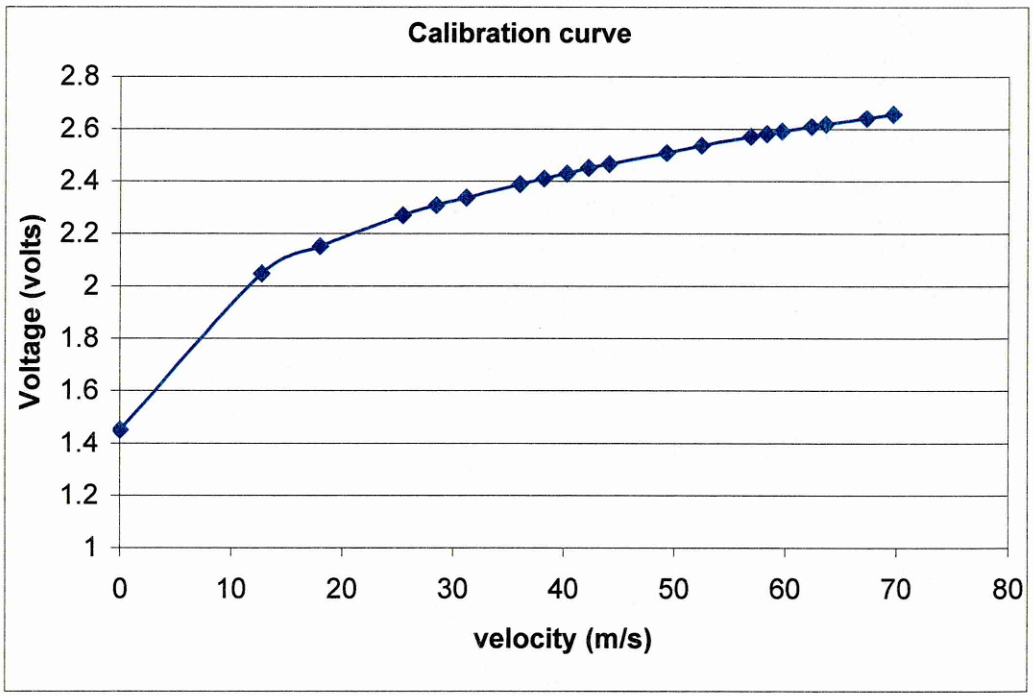

Figure A.2 Calibration Curve of Hot-wire Probe type 55P01 (single sensor)

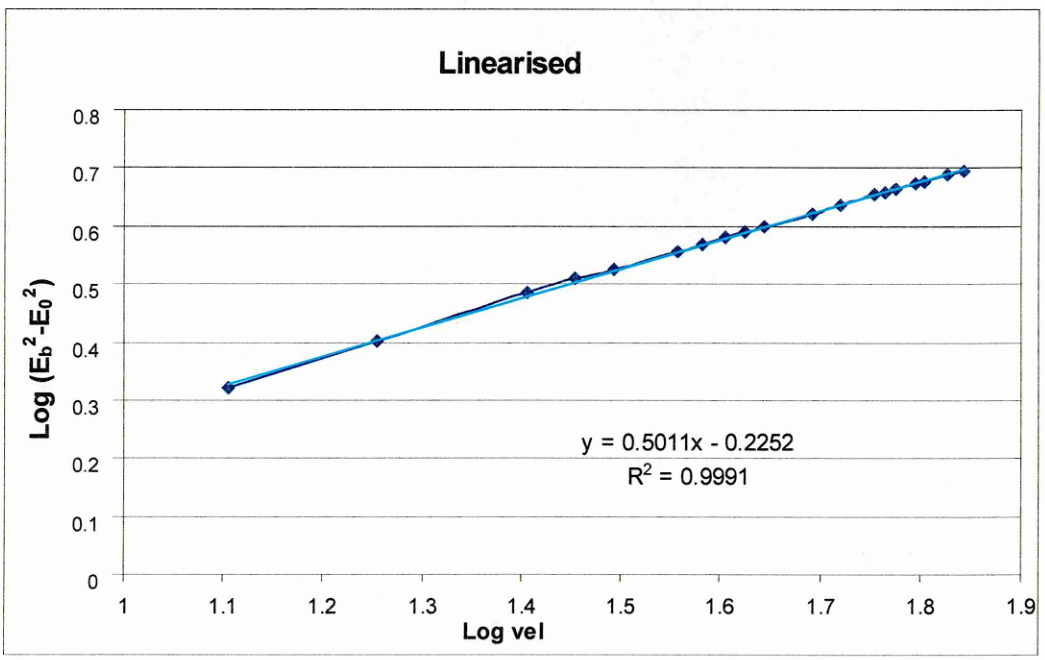

Figure A.3 Linearised Calibration Curve

Therefore:

$$E^2 = 1.449^2 + 0.59538 \times V^{0.5011} \qquad \text{(A.10)}$$

Using the above equation, the fluid velocity V can be deduced from the voltage output E displayed on the voltmeter and/or PC monitor.

A.4.2 X Array Dual Sensor Probe

The calibration method for a single sensor probe using the King's Law equation has been described above. Taking detailed measurements of the complex flows that exist within turbomachines often requires for more than one component of the velocity to be captured. X array dual sensor probes allow simultaneous measurement of two dimensional velocity components and this requires that the directional sensitivity of the wires be known. Normal component or cosine law cooling is generally assumed, but this is true for wires of infinite length. For finite wire lengths, the non-uniform wire temperature distribution causes a deviation from the cosine law. The effects of the wakes from the support prongs mentioned earlier also contribute to peculiarities, which require care during characterisation of the probes. The physical differences of two versions of X array probes are shown in Figure A.4. DANTEC's 55P52 is copper and gold plated at the ends to a diameter of approximately 15 μm making its overall length 3mm. The copper and gold plated features have shown to be crucial in the present application as it reduced the conduction of heat to the prongs and minimised the effects of wakes from the prongs. A comparison of the characteristics of these two versions of probes is given providing an assessment of their suitability to this investigation.

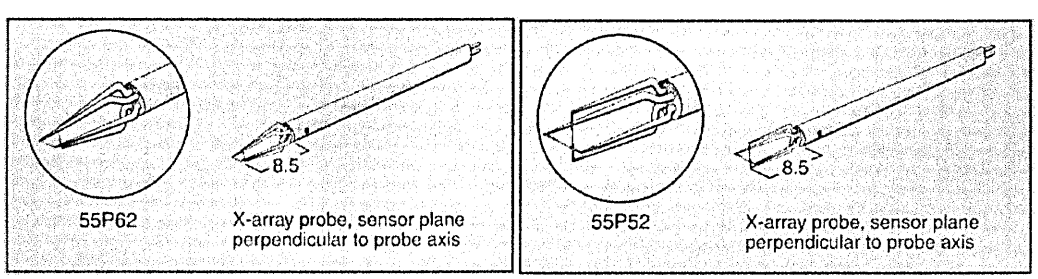

Figure A.4 DANTEC's' Miniature' and 'Gold Plated' X Array Probes

Hinze's yaw-angle relationship gives:

$$U_{eff}^2 = U_x^2 + k^2 U_y^2 \tag{A.11}$$

where ***k*** is the yaw factor which takes into account the additional cooling by the tangential component of velocity. Champagne et al (1966) performed heat transfer experiments with inclined hot wires to investigate the directional sensitivity. The value of ***k*** has been determined to be approximately 0.2 for wires of length to diameter ratio l/d=200, and decreasing with higher l/d, effectively reaching zero at l/d=600.
The above equation can be rewritten as:

$$U_{eff}^2 = U^2(\cos^2\theta + k^2 \sin^2\theta) \tag{A.12}$$

This expression is also known as the 'Champagne's Law' where the angle θ is taken as the angle between the normal of each wire to the mean flow. So from the above:

$$\begin{aligned} U_{normal} &= U\cos\theta \\ U_{parallel} &= U\sin\theta \end{aligned} \tag{A.13}$$

Ignoring the third dimension *and assuming* that the wires are *orthogonal* to each other.

$$U_{normal\ 1} = U_{parallel\ 2}$$

or (A.14)

$$U_{parallel\ 1} = U_{normal\ 2}$$

and

$$\begin{aligned} U_{eff\,1}^2 &= U^2{}_{normal\,1} + k_1{}^2 U^2{}_{parallel\ 1} \\ U_{eff\,2}^2 &= U^2{}_{normal\ 2} + k_2{}^2 U^2{}_{parallel\ 2} \end{aligned} \tag{A.15}$$

Then, substituting the parallel components of one wire with the normal components of the other we obtain:

$$U_{eff\,1}^2 = U^2{}_{normal\ 1} + k_1{}^2 U^2{}_{normal\ 2}$$
$$U_{eff\,2}^2 = U^2{}_{normal\ 2} + k_2{}^2 U^2{}_{normal\ 1} \qquad \text{(A.16)}$$

the above gives a linear relation of the squared values of velocities and can be represented in a matrix form as follows:

$$\begin{bmatrix} U_{eff\,1}{}^2 \\ U_{eff\,2}{}^2 \end{bmatrix} = \begin{bmatrix} 1 & k_1^2 \\ -k_2^2 & 1 \end{bmatrix} \begin{bmatrix} U^2_{normal\ 1} \\ U^2_{normal\ 2} \end{bmatrix} \qquad \text{(A.17)}$$

Therefore:

$$\begin{bmatrix} U^2{}_{normal\ 1} \\ U^2{}_{normal\ 2} \end{bmatrix} = \frac{1}{1 - k_1{}^2 k_2{}^2} \begin{bmatrix} 1 & -k_1{}^2 \\ -k_2{}^2 & 1 \end{bmatrix} \begin{bmatrix} U_{eff1}{}^2 \\ U_{eff2}{}^2 \end{bmatrix} \qquad \text{(A.18)}$$

Calibration of both versions of X array probes was carried out using 15 velocities from 0 m/s to a maximum of 70 m/s and varying the angle of approach over a range of 180 degrees (-90 to 90 degrees) at 5 degree increments. To avoid confusion, prior to the angular calibration, the datum position was set so that the probe was orientated with the lower wire 'normal' to the flow exiting the nozzle as illustrated in Figure A.5. A protractor, which formed part of the radial traverse assembly, was used as a guide to rotate the probe along its stem axis to the desired angle. It should be noted that the lower wire could be effectively considered as a single sensor probe as the prong effects of the neighbouring sensor do not generally affect it.

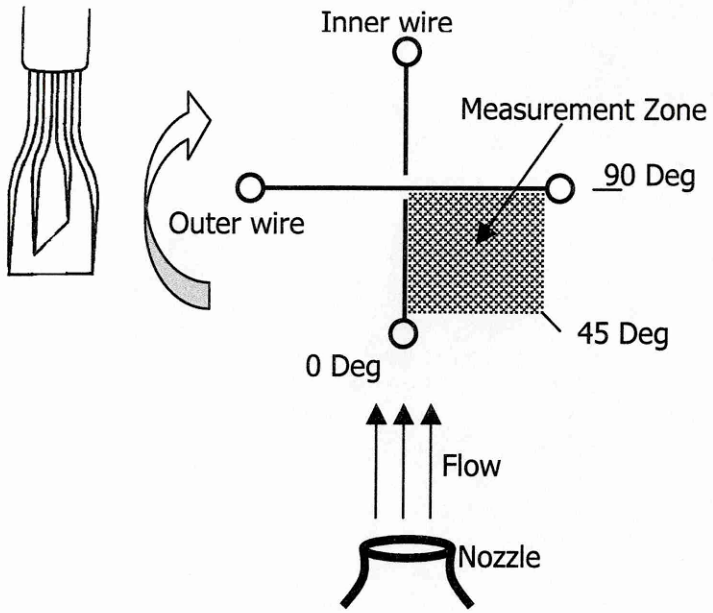

Figure A.5 Datum Position of X Array Probe

Figures A.6 and A.7 show the characteristic maps "***E1***" vs. "***E2***" (i.e. voltage output of Outer vs. Inner wire). The maps show the range of angle of approach from 0 to 90 degrees at 5-degree increments, where near 0 and 90 degrees the deviation from

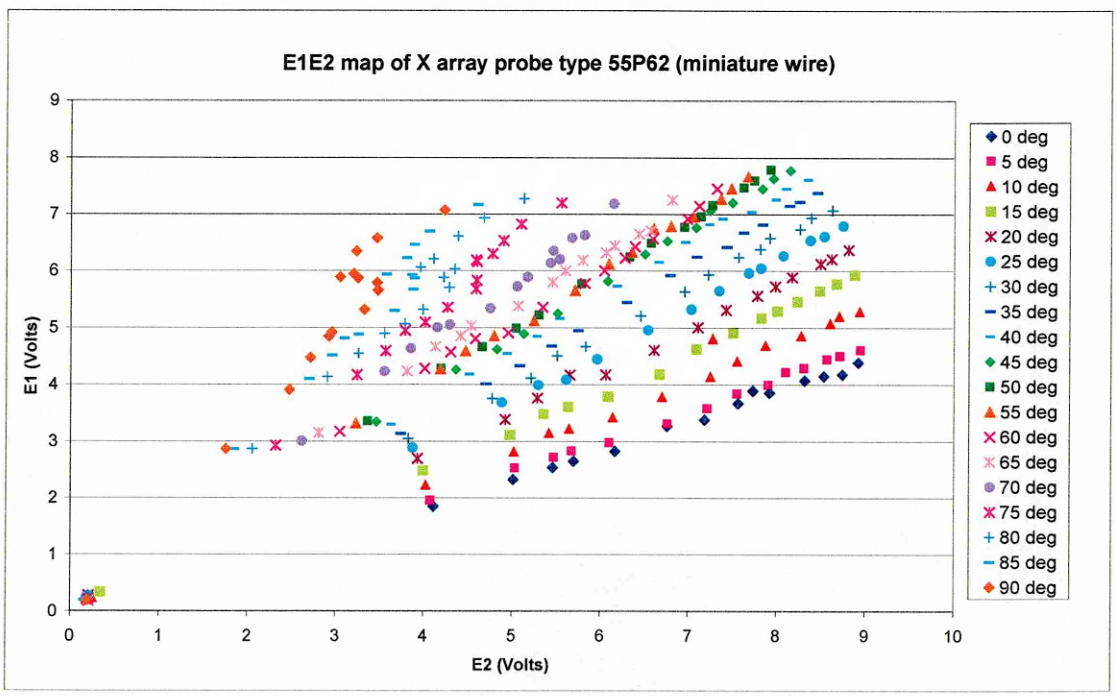

Figure A.6 Voltage Map of X Array Probe 55P62 (Miniature)

the pattern is significant, particularly with the 55P62 miniature version. This is due to the prong interference.

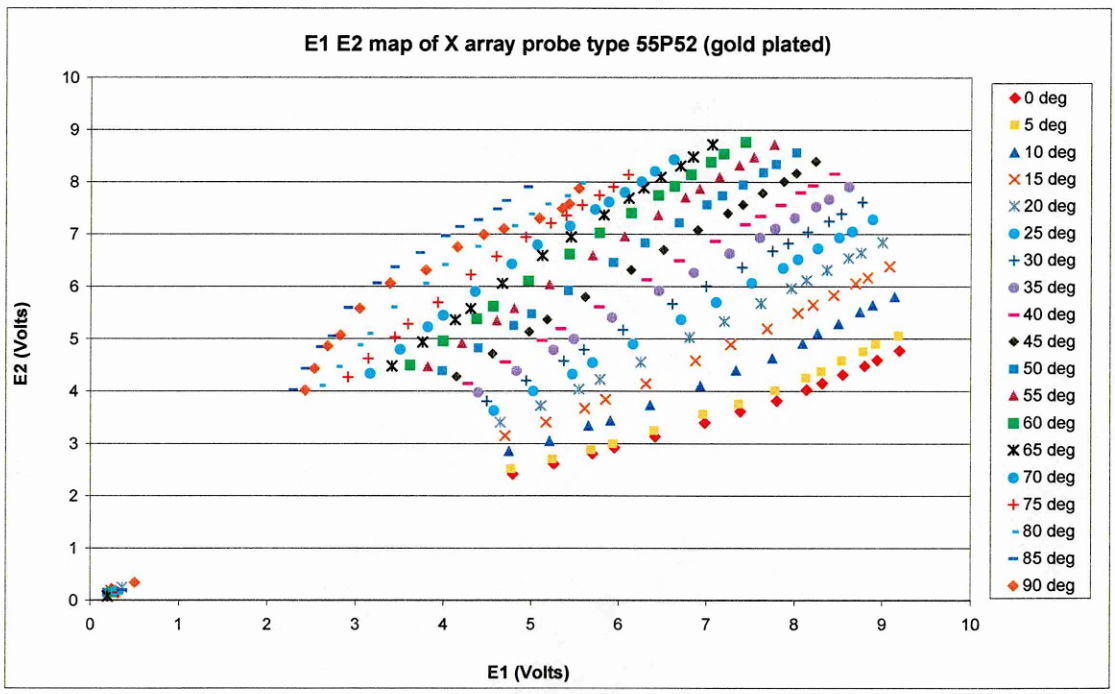

Figure A.7 Voltage Map of X Array Probe 55P52 (Gold Plated)

The voltage maps clearly indicate that the gold-plated probe, 55P52 gives a better operating range. Although the gold-plating feature does not exempt the probe from prong interference, the effects are minimised to a more acceptable level. Since it was anticipated that the mean angle of the flow to be measured would deviate no more than 10 ±2 degrees, probe type 55P52 was selected as the most appropriate version for the flowfield study.

The graphs in Figures A.8 – A.11 show the characteristics of each sensor wire (i.e. outer and inner) of the two version of X array probes where effective cooling velocities at selected angles of approach are plotted. The effects of prong interference on both probes are clearly evident and further highlight the influence of probe orientation.

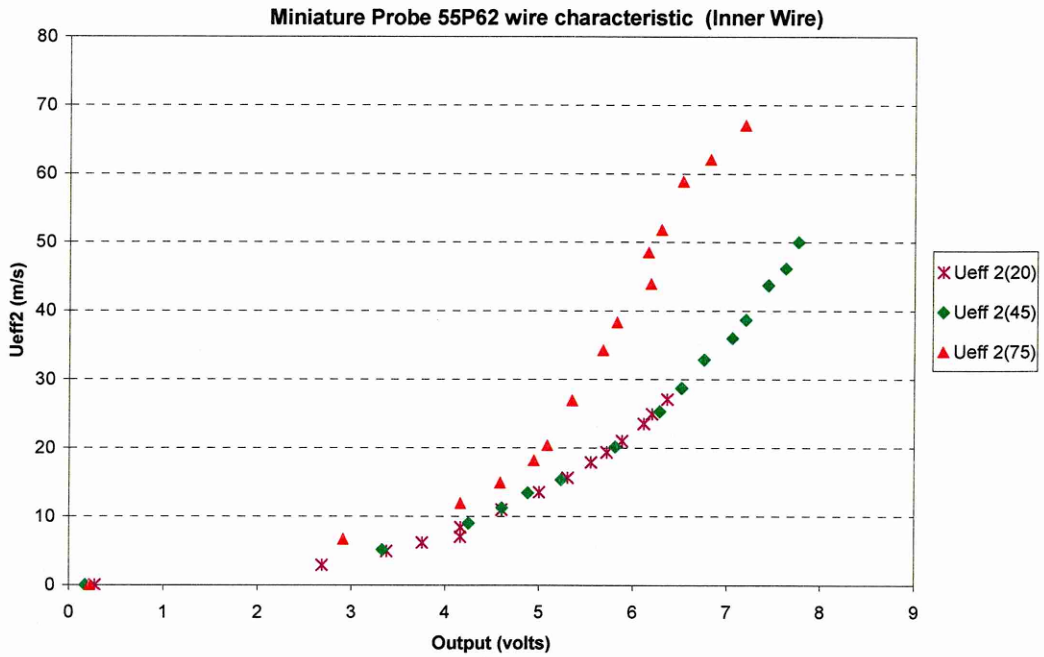

Figure A.8 Characteristic Plot of Probe 55P62 Inner Wire

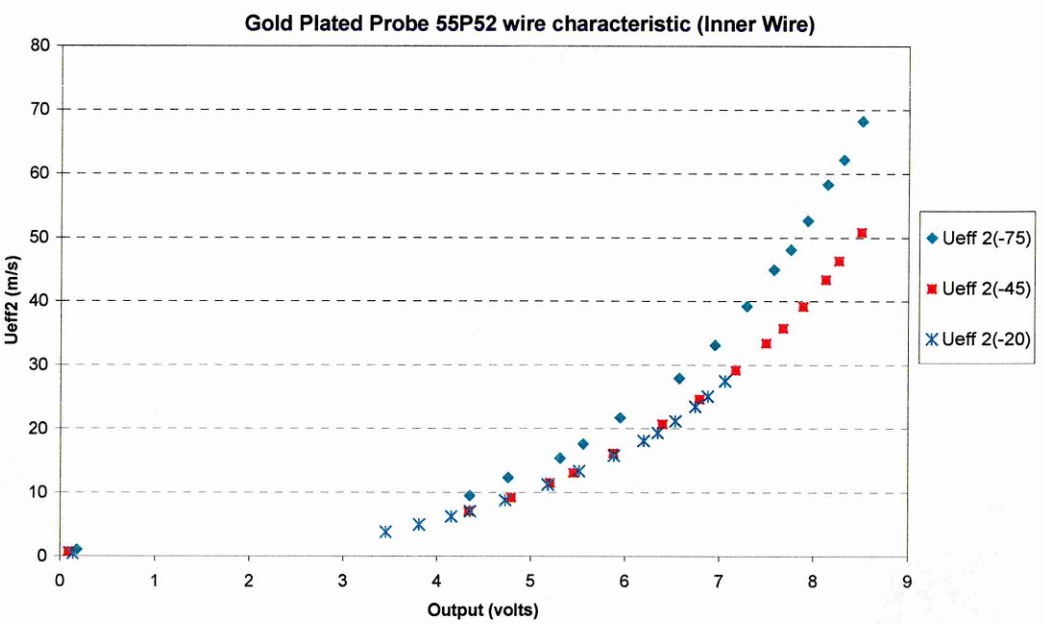

Figure A.9 Characteristic Plot of Probe 55P52 Inner Wire

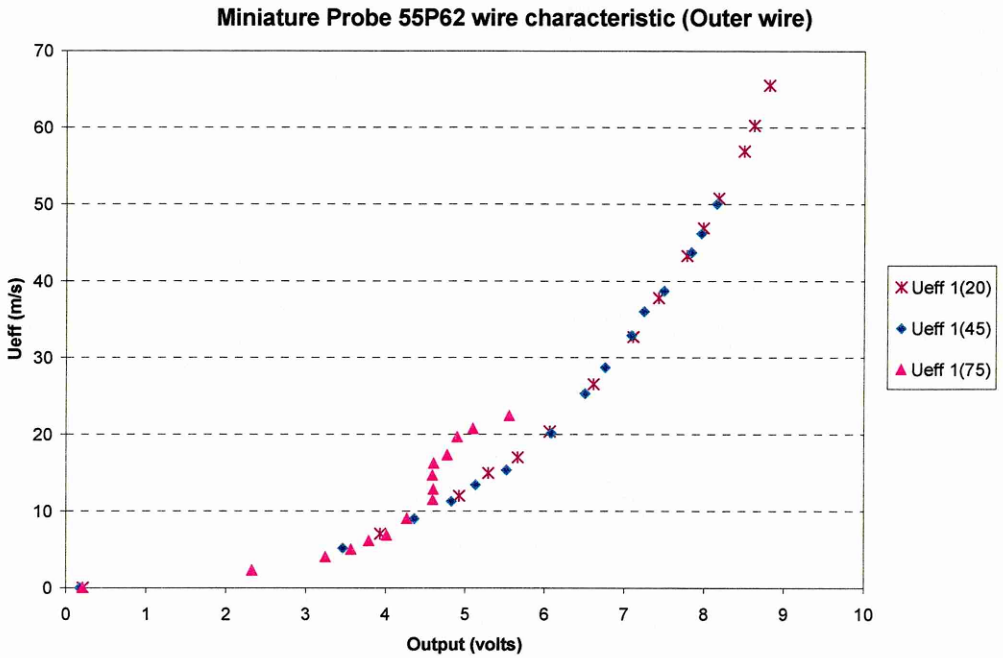

Figure A.10 Characteristic Plot of Probe 55P62 Outer Wire

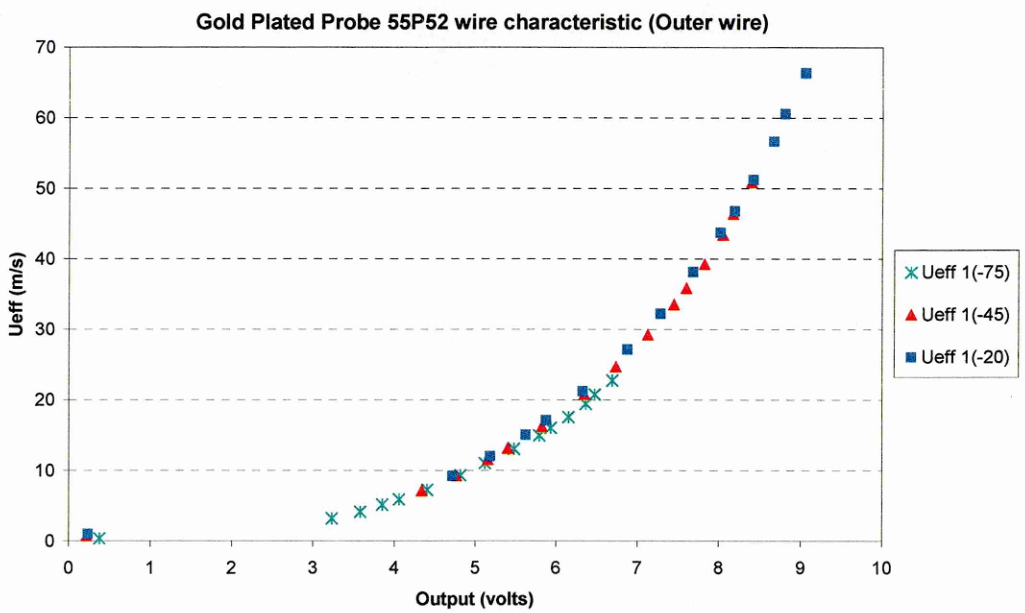

Figure A.11 Characteristic Plot of Probe 55P52 Outer Wire

A fourth order polynomial curve fitting procedure was used to characterise each wire of the probe. An example of these curve fits applied on a 55P52 probe are shown below in Figures A.12 and A.13.

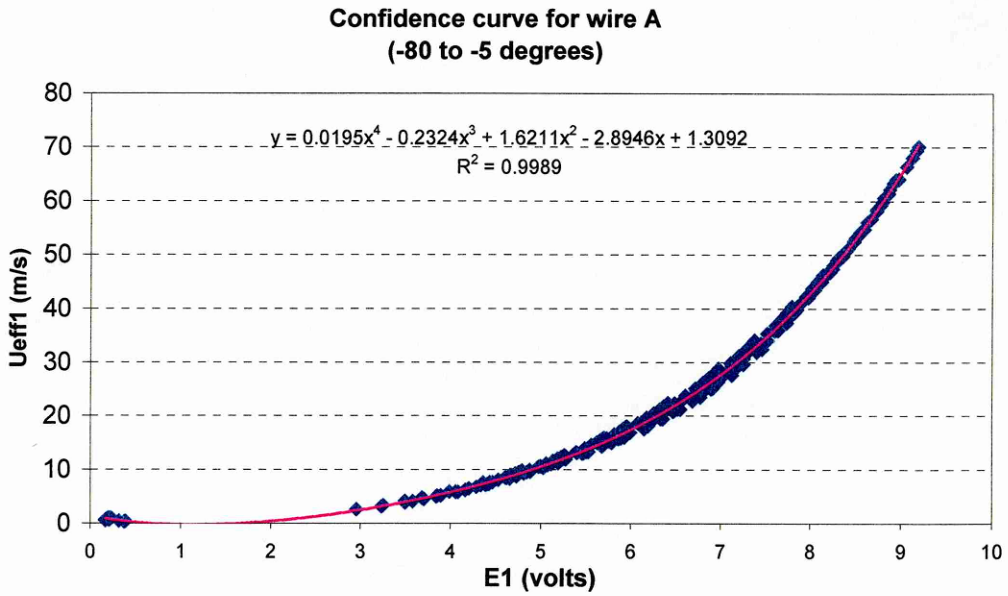

Figure A.12 Polynomial Curve fit for Outer wire of 55P52 Probe

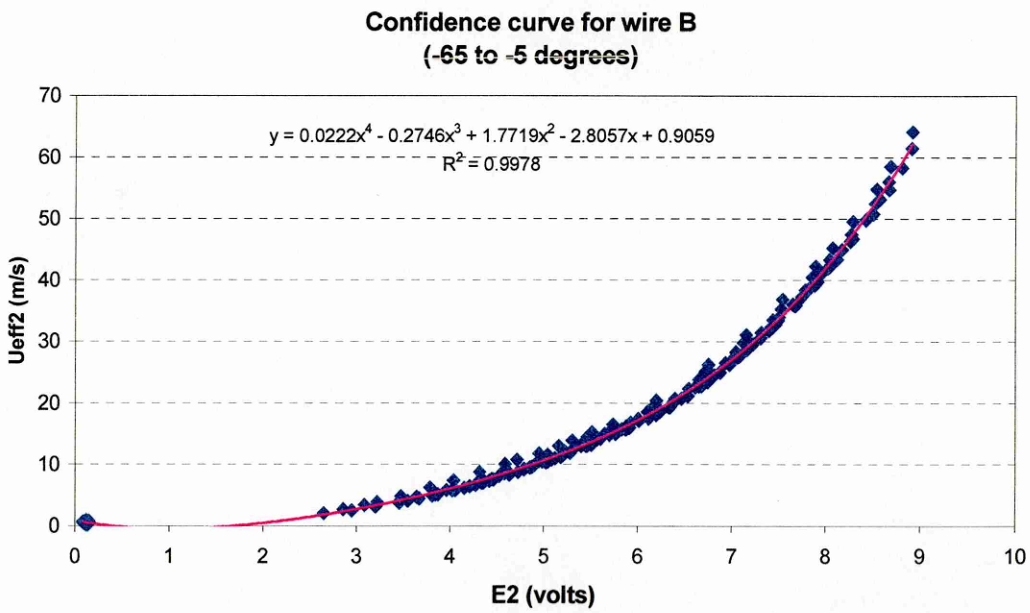

Figure A.13 Polynomial Curve fit for Inner wire of 55P52 Probe

Combining the characteristic or 'confidence curve' of the two sensors effectively reduces the measurement region in the 'quadrant' of the X array probe sensor plane. The reduction in measurement zone requires that the probe must be yawed along its axis so that the mean flow is aligned with the centre region of this zone. Figure A.14 illustrates the reduced measurement region.

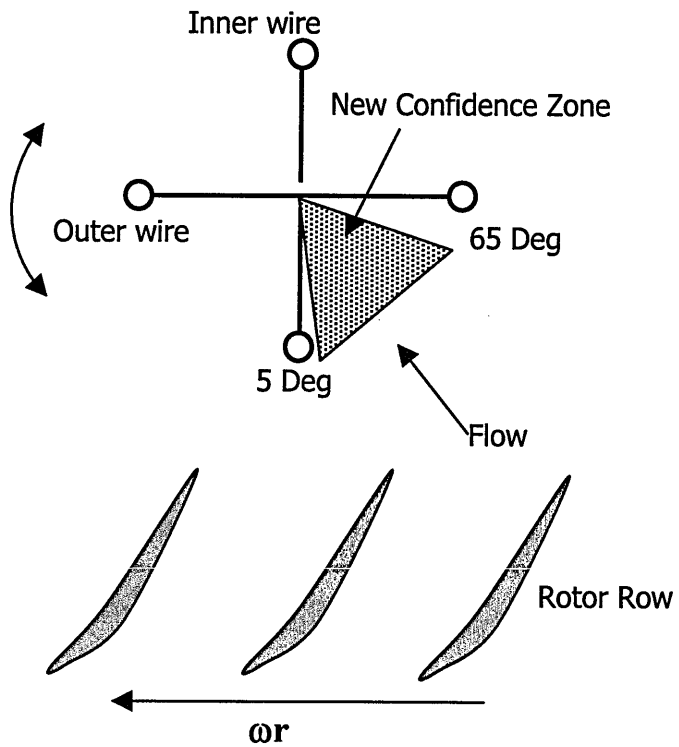

Figure A.14 Reduction in Measurement Area Due to Probe Interference

A.5. The Effect of Fluid Temperature

One of the main difficulties in the use of hot wires is the effect of fluid temperature changes on the heat transfer. A 1 °C temperature change in air may produce an error of 2 per cent in measured velocity Bradshaw (1971). As Cranfield University's LSRC facility drew air from the atmosphere, temperature gradients were large particularly during wintertime and a longer time was required to stabilise the operational temperature. A lift of the calibration curve was frequently encountered during testing. Bradshaw (1971) gives a correlation of King's Law for the hot-wire calibration:

$$\frac{H_f}{T_w - T_f} \propto \frac{I^2 R_w}{R_w - R_f} = A_1(T_f) + BU^n \qquad \text{(A.19)}$$

where H_f is the heat transfer per unit time and A_1 is a function of the fluid temperature T_f but B is not. Therefore the slope of the heat transfer curve remains unaltered, but a positive temperature change causes a lift of the curve as shown in Figure A.15 below.

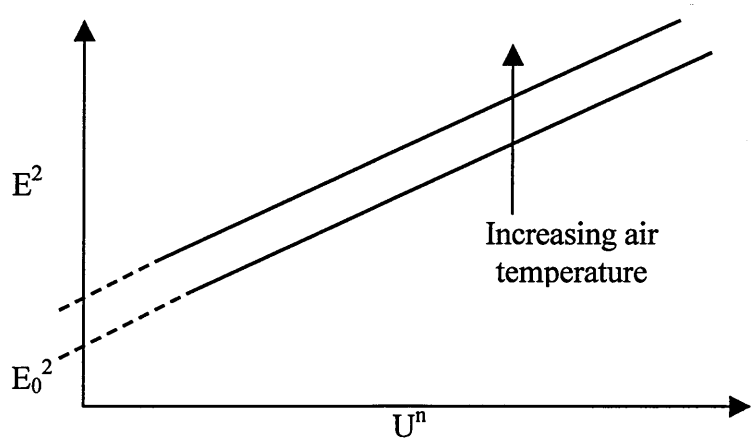

Figure A.15 Effect of Air Temperature On a Wire Calibration

Because the hot wire responds to fluctuations in both temperature and velocity and since the process of extracting these is rather complicated, it is worth going to some trouble to suppress temperature fluctuations within the fluid. The voltage/velocity calibration can be made independent of fluid temperature over a small range through the use of a temperature-compensating element, exposed to the fluid. However, such equipment was not available during the course of study and thus efforts were made to minimise the temperature gradient between the test house and the outdoors.

As the testing period sometimes lasted several hours temperature drift within the experimental rig was inevitable. Therefore performing calibrations before and after the test sessions and using the calibration that best fits the temperature conditions under the investigation cannot be done with accuracy. In an effort to minimise errors inlet temperature readings were taken periodically during test sessions to monitor the fluctuations. These readings were then applied in the following correction prior to converting the output to flow velocity.

$$E_{corr} = \left(\left(T_w - T_{ref}\right) / \left(T_w - T_{acq}\right)\right)^{0.5} E_{acq} \qquad \text{(A.20)}$$

but this gives an under-compensation of approximately 0.4 %/°C in velocity.

An improved correction:

$$E_{corr} = \left(\left(T_w - T_{ref}\right) / \left(T_w - T_{acq}\right)\right)^{0.5(1\pm m)} E_{acq} \qquad \text{(A.21)}$$

Selecting the proper m, "load factor" (m=0.2 typically for wire probe at over heat ratio a=0.8) improves compensation to better than ±0.05%/°C.

APPENDIX B

Discussion on Proximity Effects on Hot Wire Readings

B.1 Introduction

Hot wire anemometry (HWA) has been recognised to be the most versatile measurement system for investigating the mean and fluctuating fluid velocities. Aside from the absence of the need for seeding particles the primary characteristics of HWA, which make it suitable for turbulence measurements are the small size of the sensing element, the fast response to high frequency fluctuations and the suitability of the output signal for treatment with electronic instrumentation.

Obtaining accurate near-wall measurements often requires complex signal analysis methods complemented with advanced experimental techniques. Usually the HWA probes are calibrated in a laminar free stream with controlled velocity and the coefficients of a correlation equation are adjusted for the particular probe sensor. Using this correlation, the measured values of the heat flux from the wire are converted into precise velocity data. This method assumes that the flow and heat transfer conditions during the actual experiment remain similar to the conditions at calibration. This similarity can no longer be assumed in the vicinity of a wall, where during operation the hot-wire sensor is kept at a higher temperature than the neighbouring solid boundary and correction of the measured data is required due to the additional heat losses to the wall. This is because operating the hot-wire sensor near an infinitely large solid boundary with a much higher thermal conductivity than the working fluid results in considerable alteration of the thermal and velocity fields in the surrounding region. This essentially means that heat is conducted to the solid from the surrounding fluid that is heated by the hot-wire sensor.

The extra heat loss due to the wall proximity is perceived by the electronic signal processing system as an increased velocity in the vicinity of the solid boundary.

This effect becomes more prominent as the sensor approaches the wall. It is difficult to account for these errors if calibration data used are those obtained from calibration test rigs without walls.

Accurate velocity measurements in the near wall region can only be obtained by applying a correction procedure. This appendix briefly reviews the documented information in the literature and outlines the correction method employed in this investigation.

B.2 Brief Review of Literature

In airflow analysis near a solid boundary, the thermal conductivity k_w, of the wall is higher than that of the measurement fluid for both conducting and non-conducting wall materials. The consequence of this is that in the proximity of a solid wall the heat transfer from the heated element increases due to changes in the velocity and temperature field around the sensor (Bruun, 1995). Table B.1 illustrates the ratio of thermal conductivity of different wall materials to that of air.

Type of Wall Material	Material	k_w/k
Conducting	Copper	14,382
	Aluminium	6,400
	Brass	4,582
	Steel	1,400
	Granite	136
Non-conducting	Glass	32
	Plexiglass	8
	Plywood	4.5

Table B.1 The ratio of the thermal conductivity, k_w, of wall materials to the Thermal conductivity of air, (k =0.02559 W m^{-1} K^{-1}) (Turan et al. 1987)

The problem of hot wire anemometer-signal interpretation for near-wall measurements has been recognised for many years and a substantial number of theoretical and experimental studies have been carried out. Among them the best known is the investigation by Wills (1962), who obtained the relationship

$$Nu\left(\frac{T_w}{T_a}\right)^{-0.17} = A + K_w\left(\frac{2y}{d}\right) + B\,\mathrm{Re}_d^{0.45} \qquad \text{(B.1)}$$

based on the calibration results of Collis and Williams (1959). The function K_w *(2y/d)* in equation B.1 was introduced to account for the wall effects. The above equation implies that heat transfer from the wire to the wall is by conduction only. From this Wills (1962) proposed that an appropriate correction to hot-wire measurements in wall proximity can be obtained by subtracting the constant K_w, which is dependent on the non-dimensional distance from the wall *(y/r)*, from the value Re^n, where n is one of the constants involved in the King's Law calibration equation. The variation of K_w with *y/r* is illustrated in Figure B.1 below.

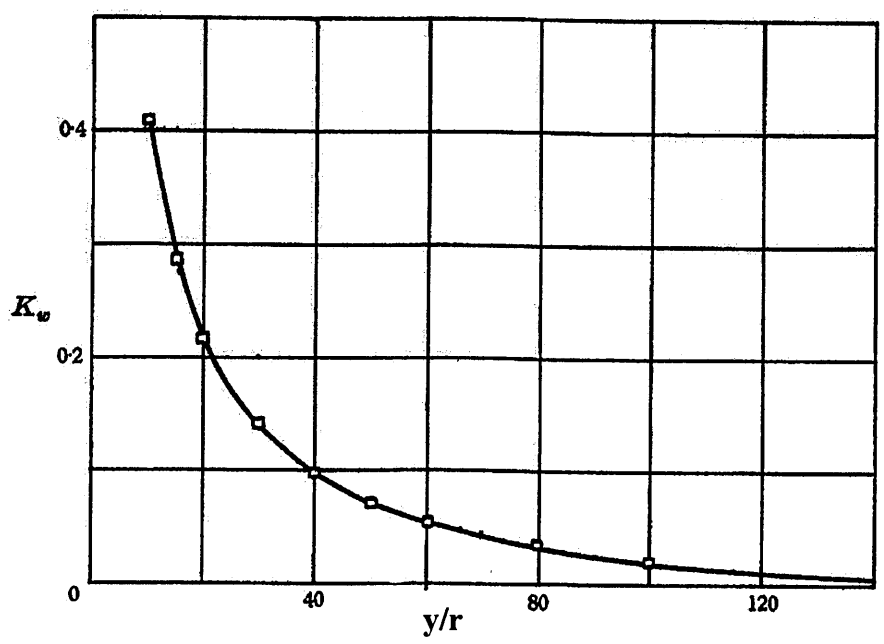

Figure B.1 Correction to Measured Values of $Re_w^{0.45}$ for Proximity to Wall (after Wills 1962)

The correction value to the measured velocity can be obtained using the following:

$$U^n = \left[\frac{\nu}{2r}\left(\frac{T_w}{T_a}\right)^{0.17}\right]^n \mathrm{Re}_w^n \qquad \text{(B.2)}$$

where T_w and T_a represent the temperature of the sensor wire and the working fluid (air in this case) respectively and Re_w^n is the correction value obtained from Figure B.1. Although the physical properties of a gas vary with temperature, it is assumed here that the kinematic viscosity of air ν will have a value close to its value at ambient temperature. It was also assumed to a certain extent, that the temperature of air in the vicinity of the hot-wire is closer to ambient than to the temperature of the wire itself. Wills (1962) found that equation B.1 could not be applied for turbulent flow and suggested that half of the laminar correction be used. This method of correction has been used by a previous investigator at Cranfield, both for laminar and turbulent boundary layers (Kalfas, 1995). Later studies have shown that this method gives unsatisfactory corrections (Bruun, 1995).

There have been contradictory views in the literature on the effect of different wall materials, and thus on the cause of the wall proximity effect. Although Bhatia et al (1982) stated that no wall effect would be expected in the proximity of a non-conducting wall, Vagt & Fernholz (1979) disproved this observation by using the gradual increase in the hot-wire signal as the probe approached a non-conducting wall to determine the distance of the probe from the wall. Turan et al (1987) conducted practical investigations on the wall effect on hot-wire signal at no flow using four conducting and four non-conducting wall materials. It was found that the effect of the wall on the hot-wire signal at a given distance from the wall increased with wall thermal conductivity up to a relative thermal conductivity, k_w/k, of 100, and beyond this the signal due to proximity effect remained at this asymptotic value. Furthermore, it was observed that wall effects became negligible for distances greater than 0.5 mm from the wall.

B 3 The Present Correction Method

The present experimental study involved traversing the boundary layer that occur on the suction surface of a stator blade using a hot-wire probe and approaching the solid boundary as close as 50 μm. The wall material was an aluminium alloy for aeronautical applications with a high thermal conductivity. Appropriate correction procedure has been applied to the unsteady velocity measurements collected in the vicinity of the blade surface to obtain corrected velocity profiles.

This part of the appendix briefly outlines the correction method that has been employed based on a recent numerical investigation by Lange et al (1998) of the two-dimensional heat transfer and laminar flow around a single circular cylinder. A very efficient finite volume Navier-Stokes solver enhanced by multigrid and local refinement techniques ensured accuracy of results.

The friction velocity U_T is defined as:

$$U_T = (T_w)^{0.5}/\rho \tag{B.3}$$

where T_w is the molecular momentum transport term at the wall, also known as the shear stress. Traditionally, the friction velocity is applied to normalise the velocity and the distance y from the wall in turbulent flows. The non-dimensionalised quantities are then,

$$U^+ = U/U_T \tag{B.4}$$

$$Y^+ = yU_T/\nu \tag{B.5}$$

where U is the velocity component parallel to the surface, y the perpendicular distance from the wall and ν is the kinematic viscosity of the fluid. If the variation of U with y is linear as in the near-wall part of the laminar boundary layer, the following relationship applies

$$U^+ = Y^+ \tag{B.6}$$

This linear variation of velocity also occurs in the laminar sublayer of a turbulent boundary layer. On this basis, Wills (1962) found his laminar correction factor to be too large to be applied to turbulent flow measurements and concluded only half of the laminar correction should be employed in the sublayer. However, no justification was provided for this.

The proposed correction factor C_u developed by Lange et al (1998) has the advantage of being bounded between 0 and 1 and readily shows the relative magnitude of the influence of the wall on the measured apparent velocity with less dependence on the temperature loading of the hot-wire.

The actual local velocity U_0 normalised to the apparent velocity U_{meas} is plotted against the non-dimensionalised distance Y^+. The correction, defined as

$$C_U = U_0/U_{meas} \tag{B.7}$$

represents a factor that is to be simply multiplied to the measured velocity U_{meas} in order to obtain the actual local velocity U_0. Figure B.2 below shows the different values of C_u obtained from computations for different temperature loadings with results from experimental results.

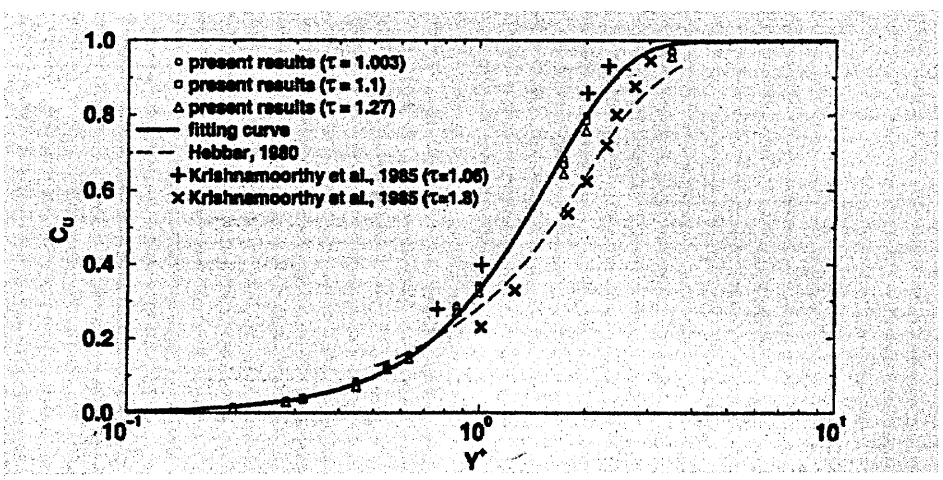

Figure B.2 Numerical and Experimental Values of the Velocity Correction Factor C_U for Different Temperature Loadings (after Lange et al, 1998)

With a good approximation, the calculated values of the correction factor C_U can be fitted by a relatively simple formulation

$$C_U = 1.0 - \exp(-0.4Y^{+^2}) \tag{B.8}$$

the resulting curve of the above equation is also shown in Figure B.2.

APPENDIX C

BL Traverse Mechanism Technical Drawings

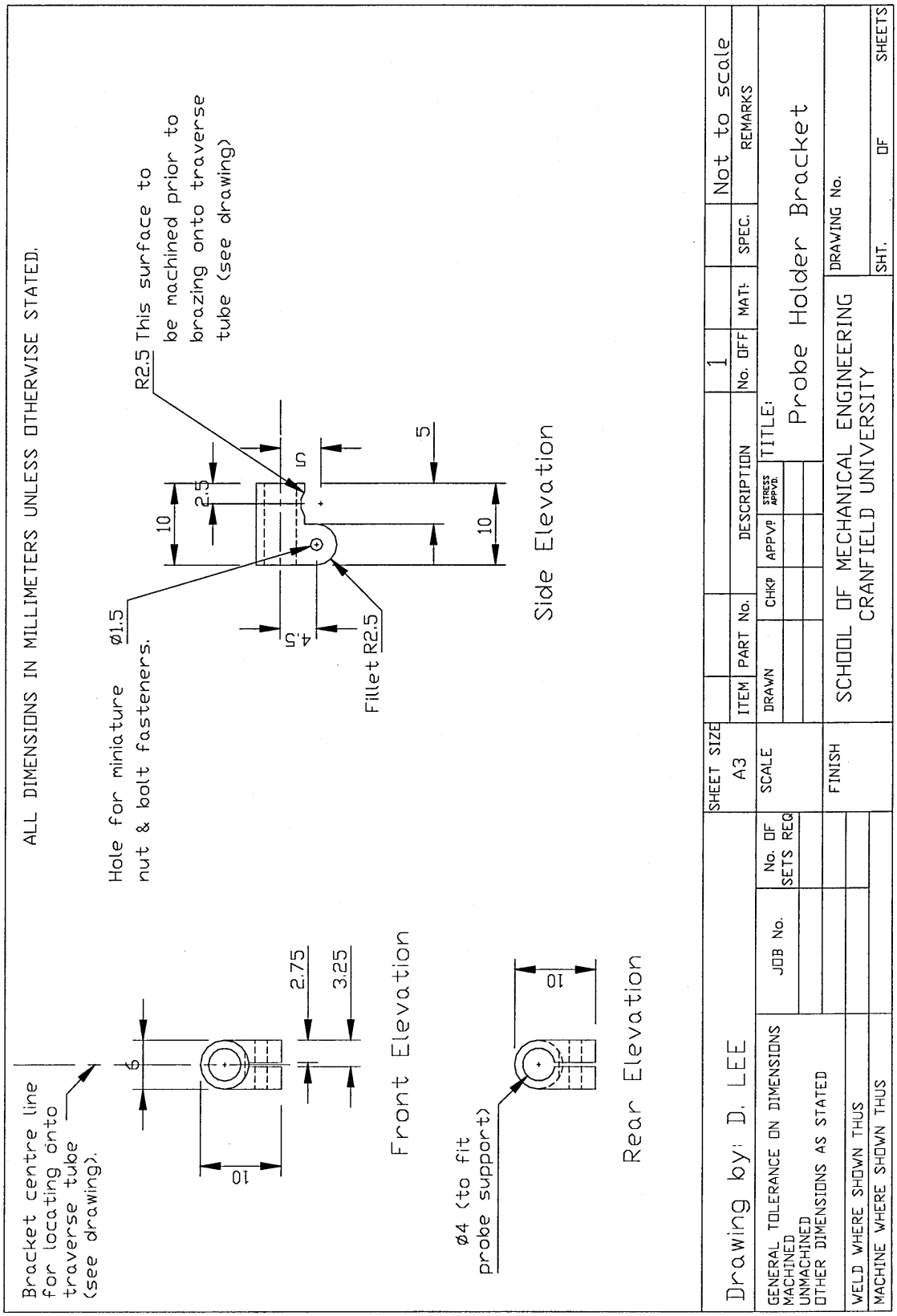

Figure C1 Probe Holder Bracket

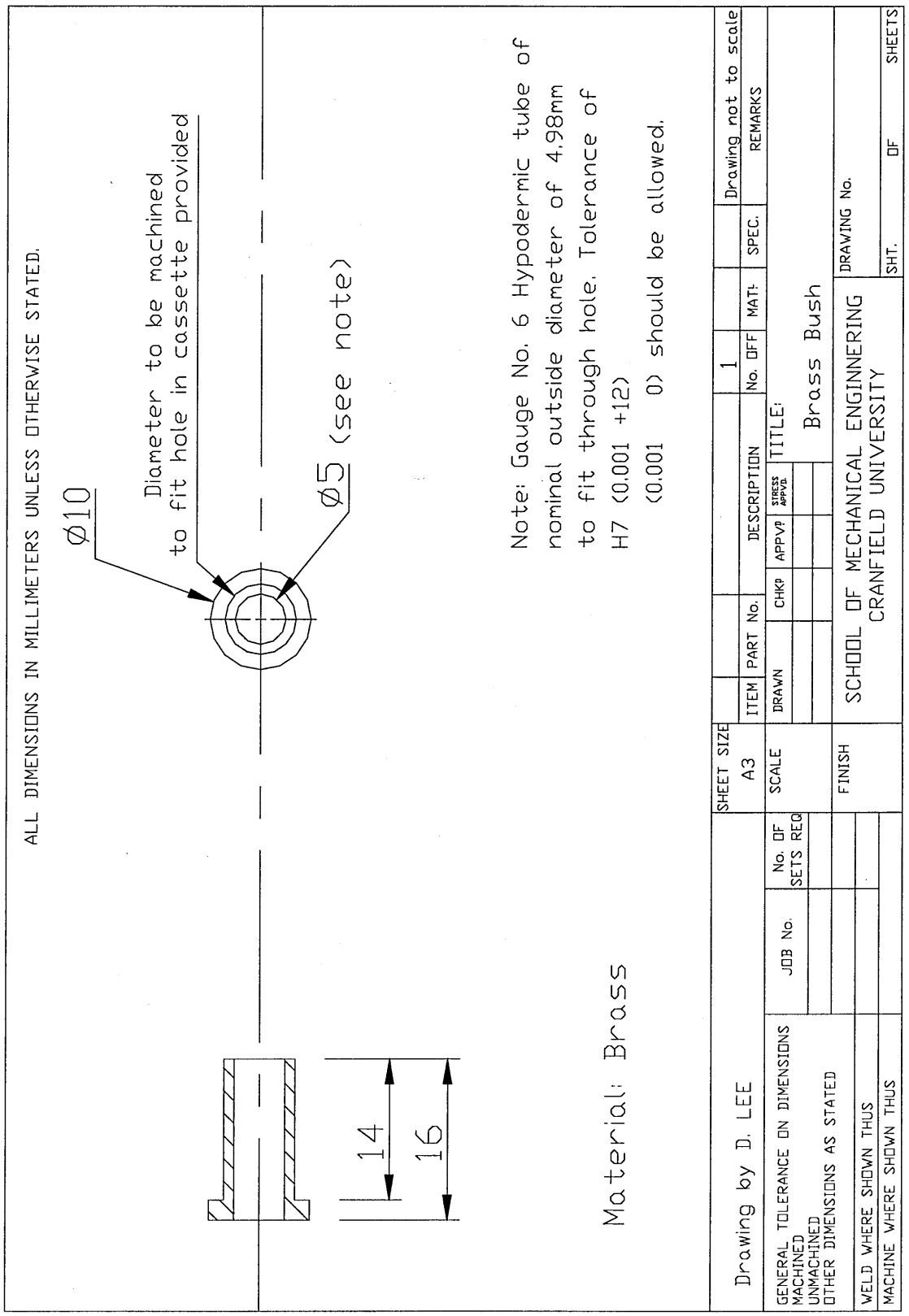

Figure C2 Brass Bush

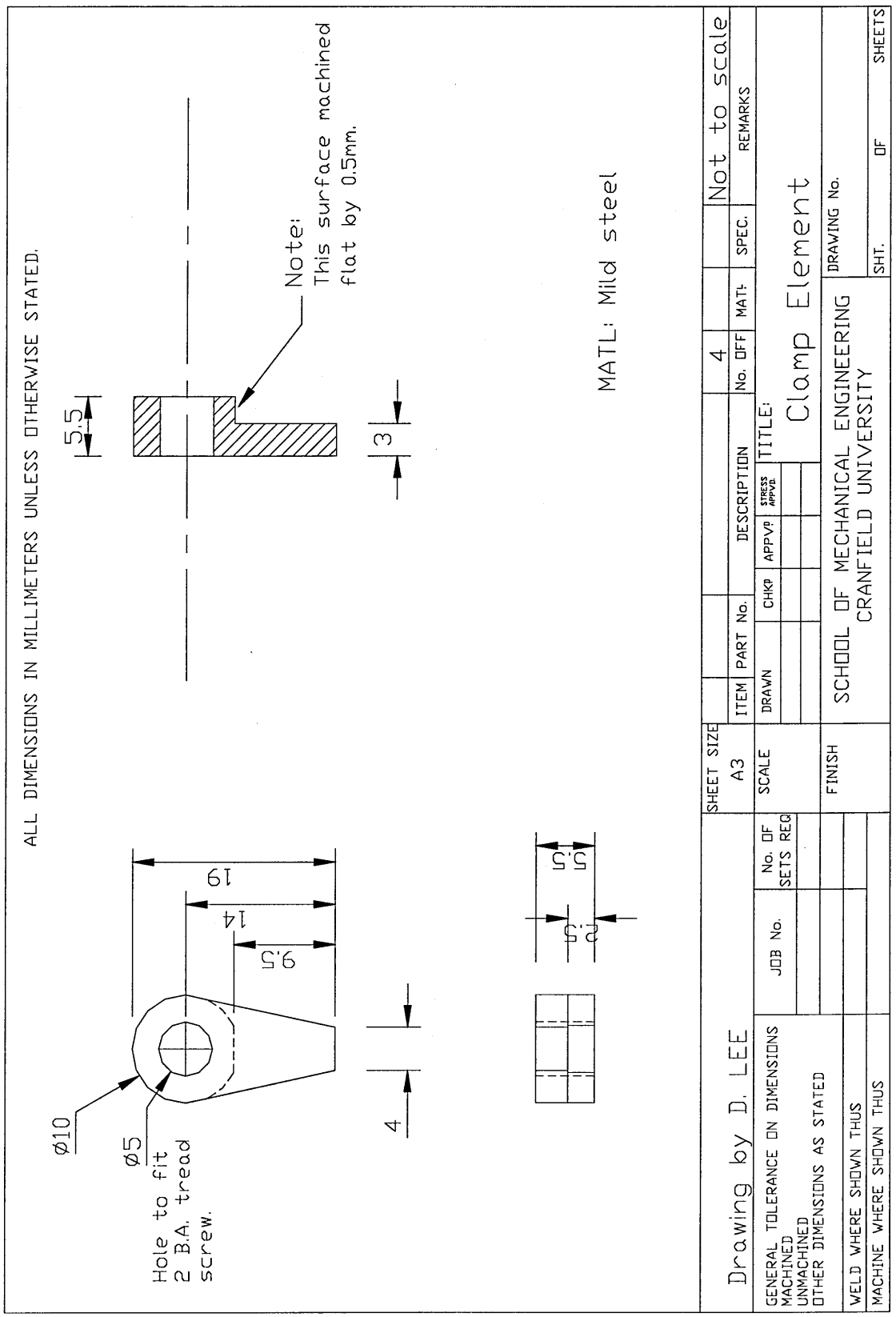

Figure C3 Clamp Element No.1

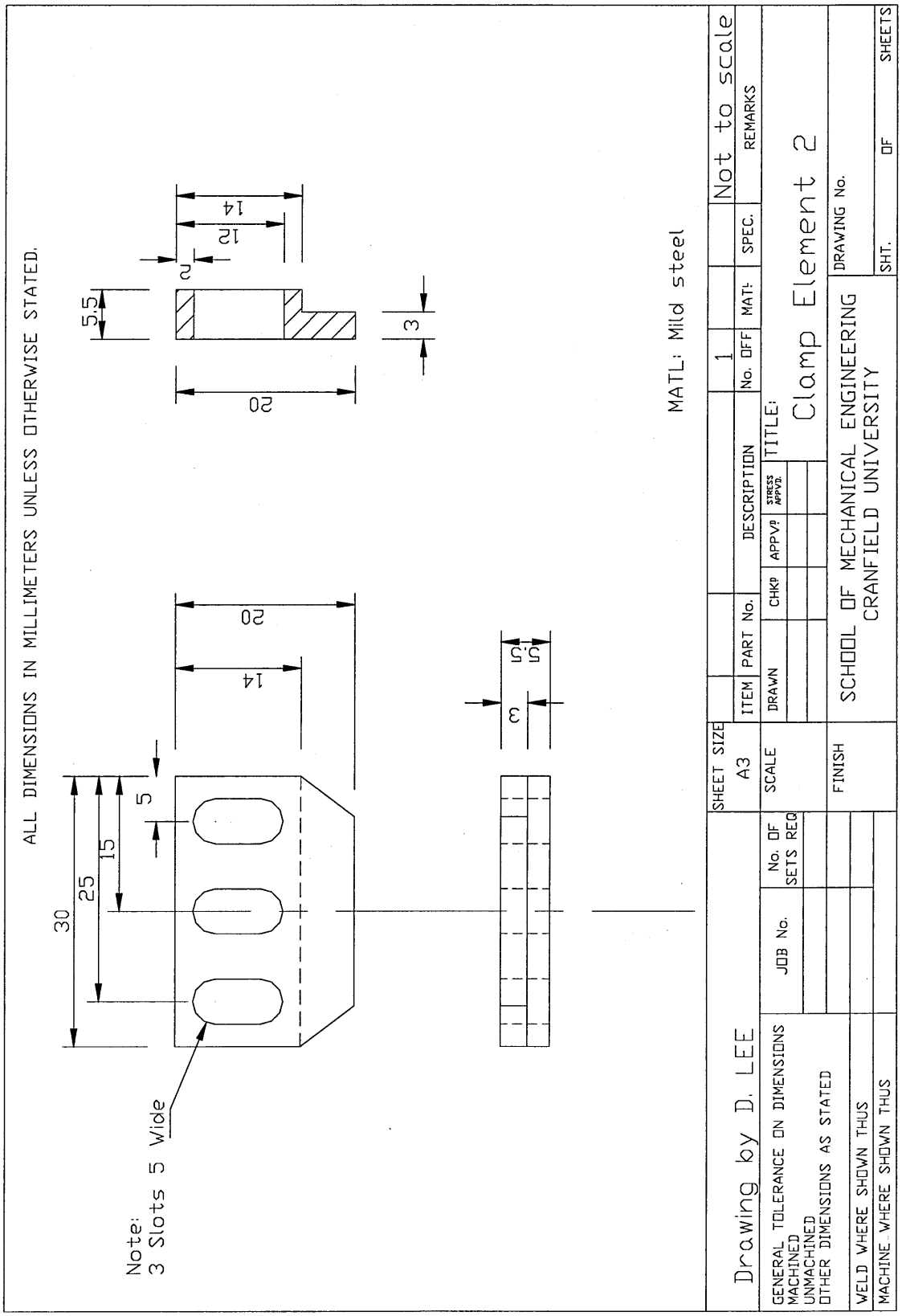

Figure C4 Clamp Element No.2

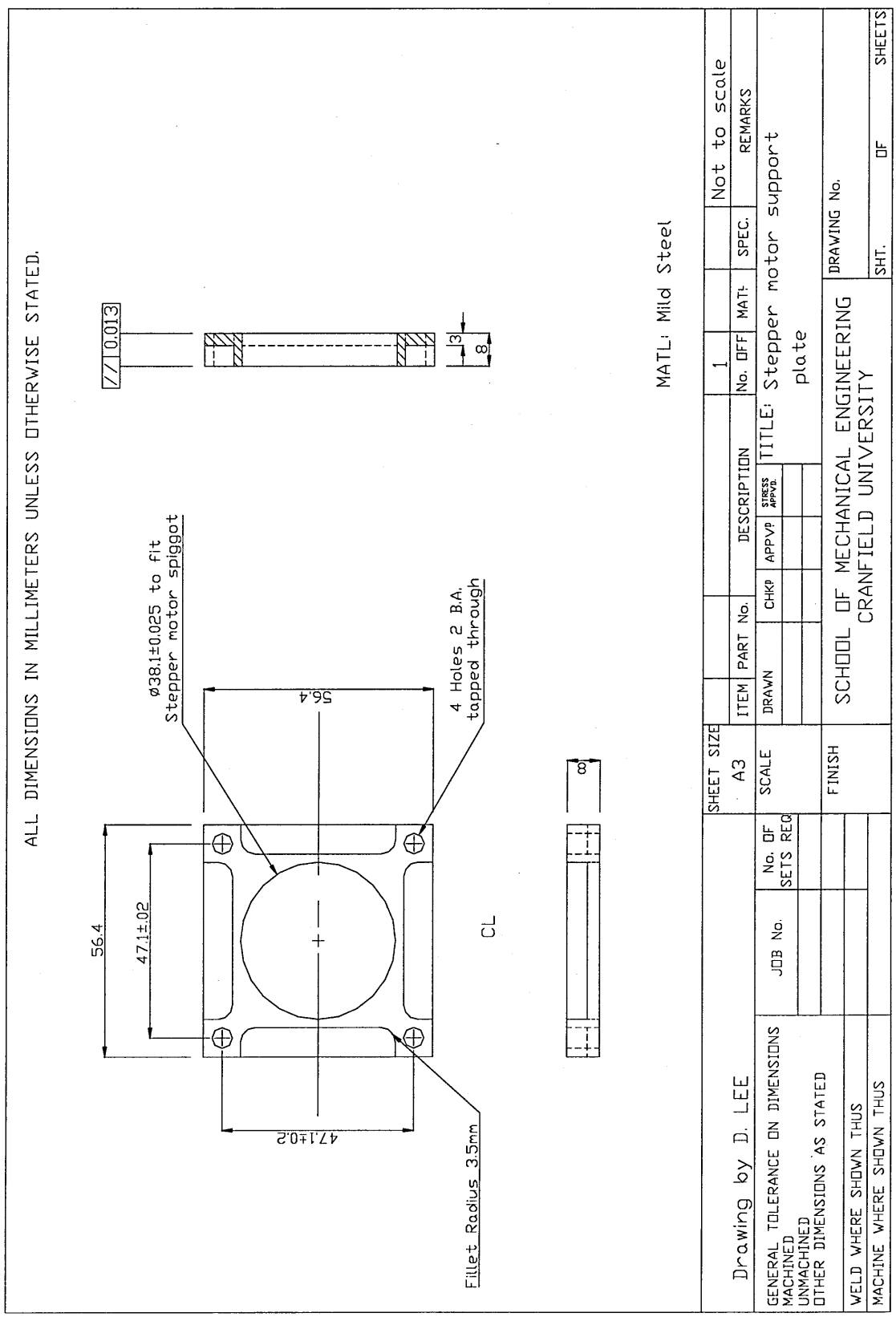

Figure C5 Stepper Motor Support Plate

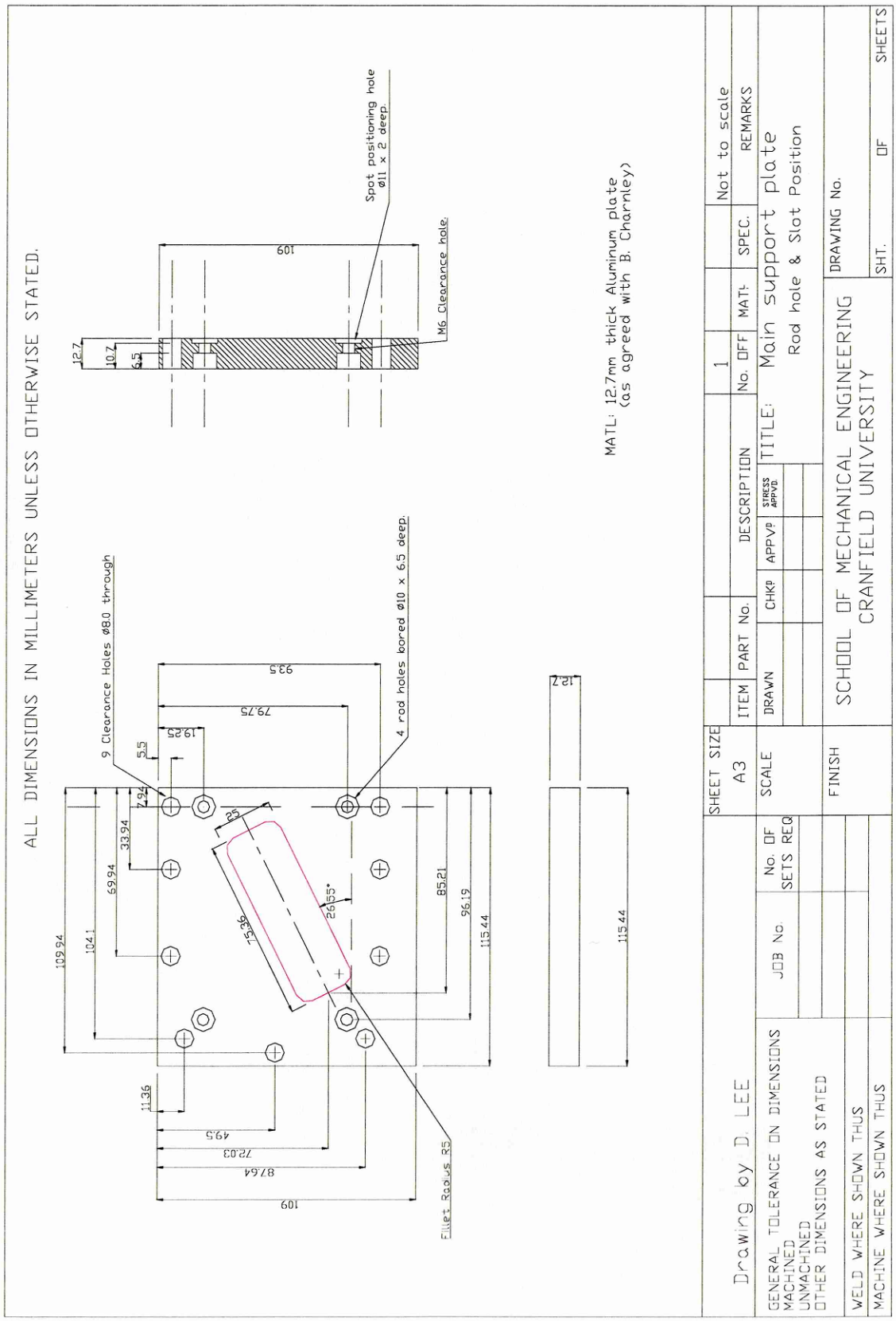

Figure C6 Main Support Plate (Rod hole & Slot Position)

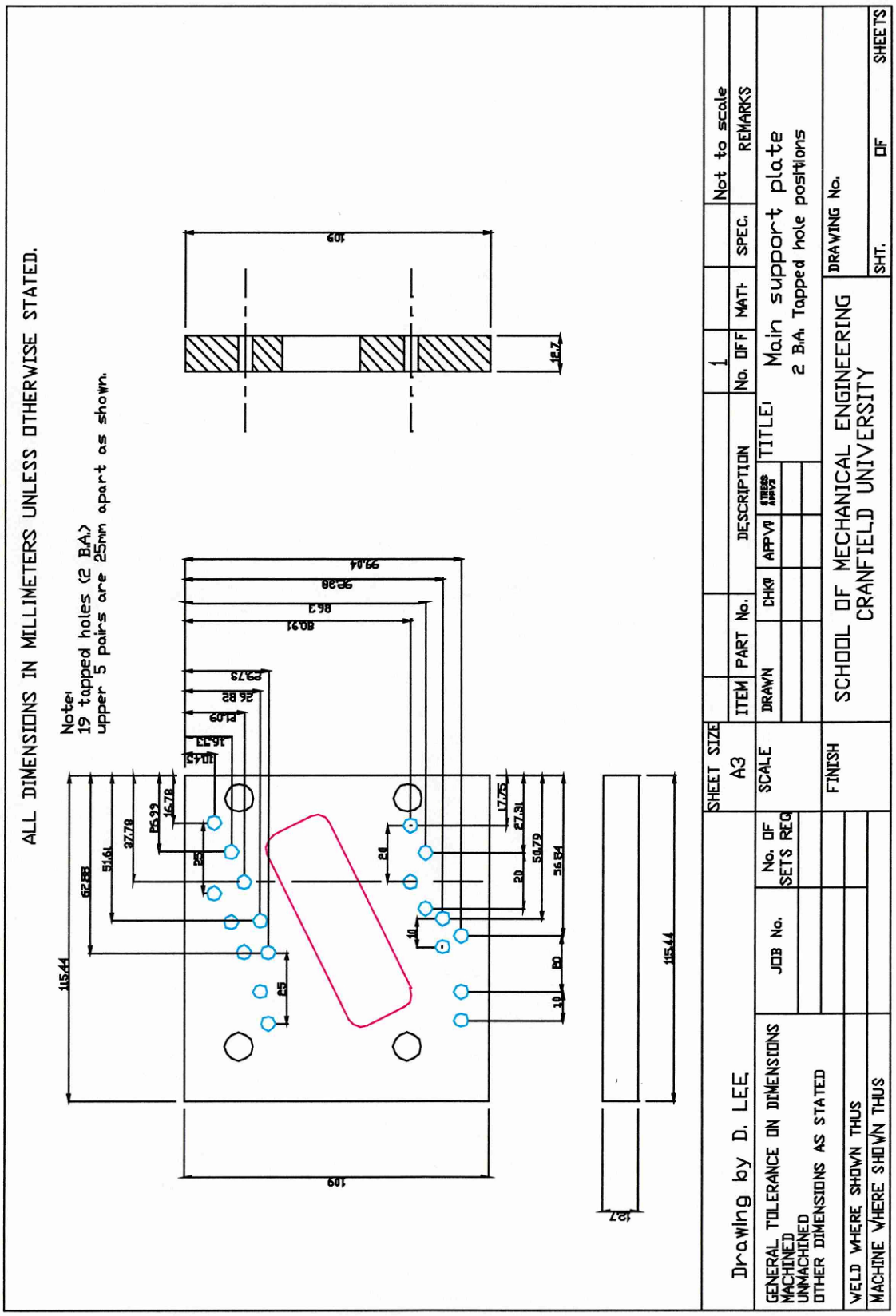

Figure C7 Main Support Plate (2 BA tapped hole positions)

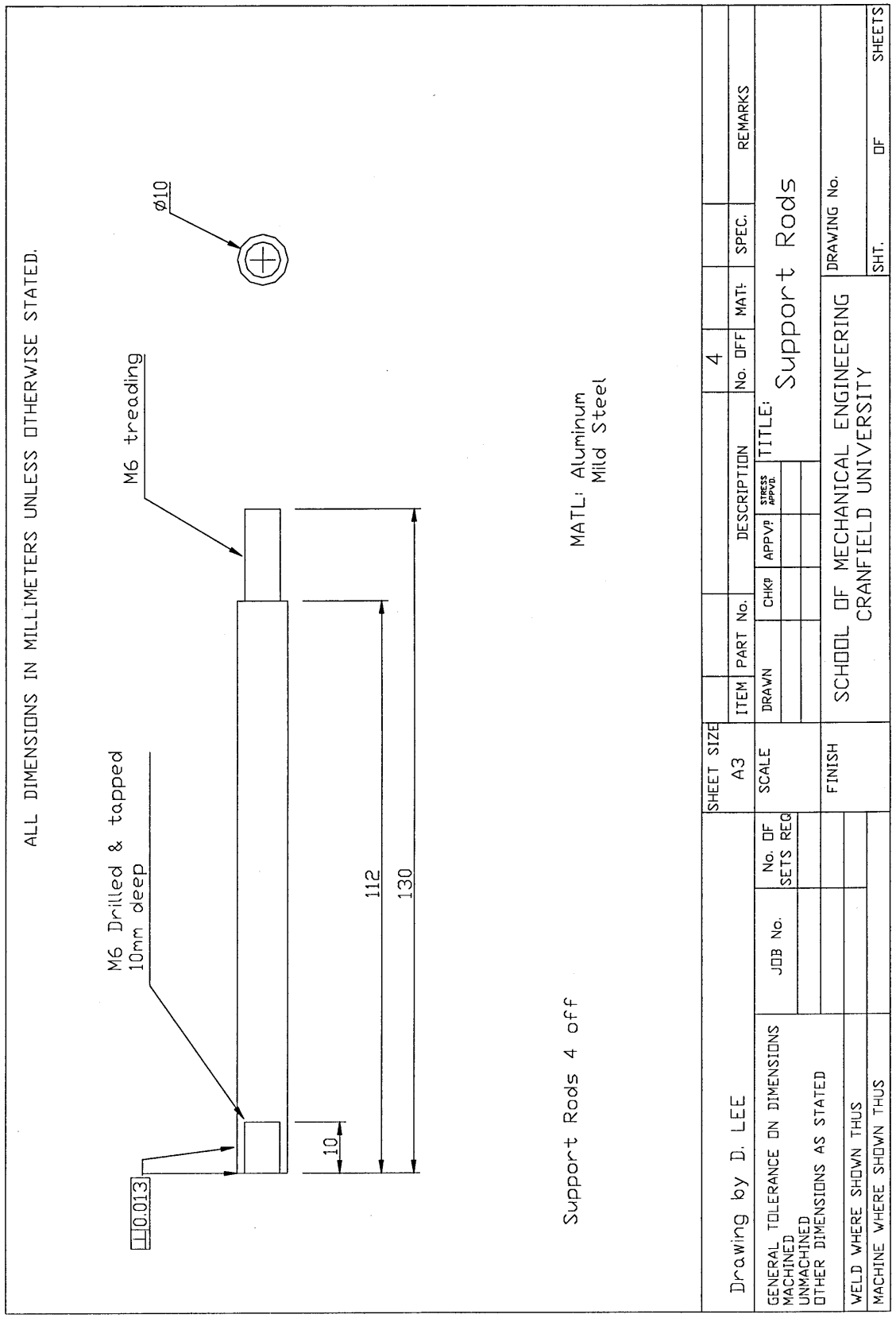

Figure C8 Support Rods

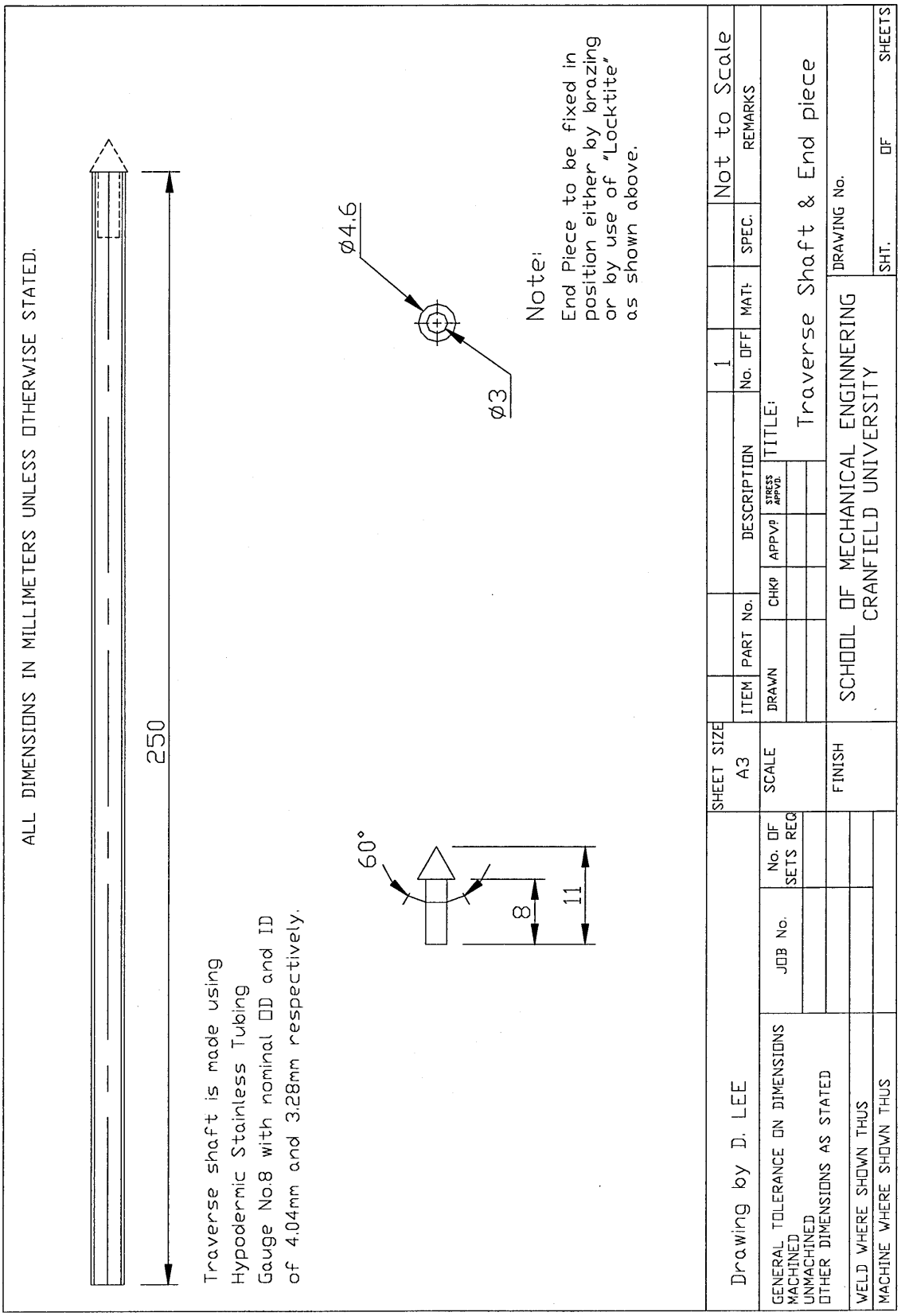

Figure C9 Traverse Shaft and End Piece No.1

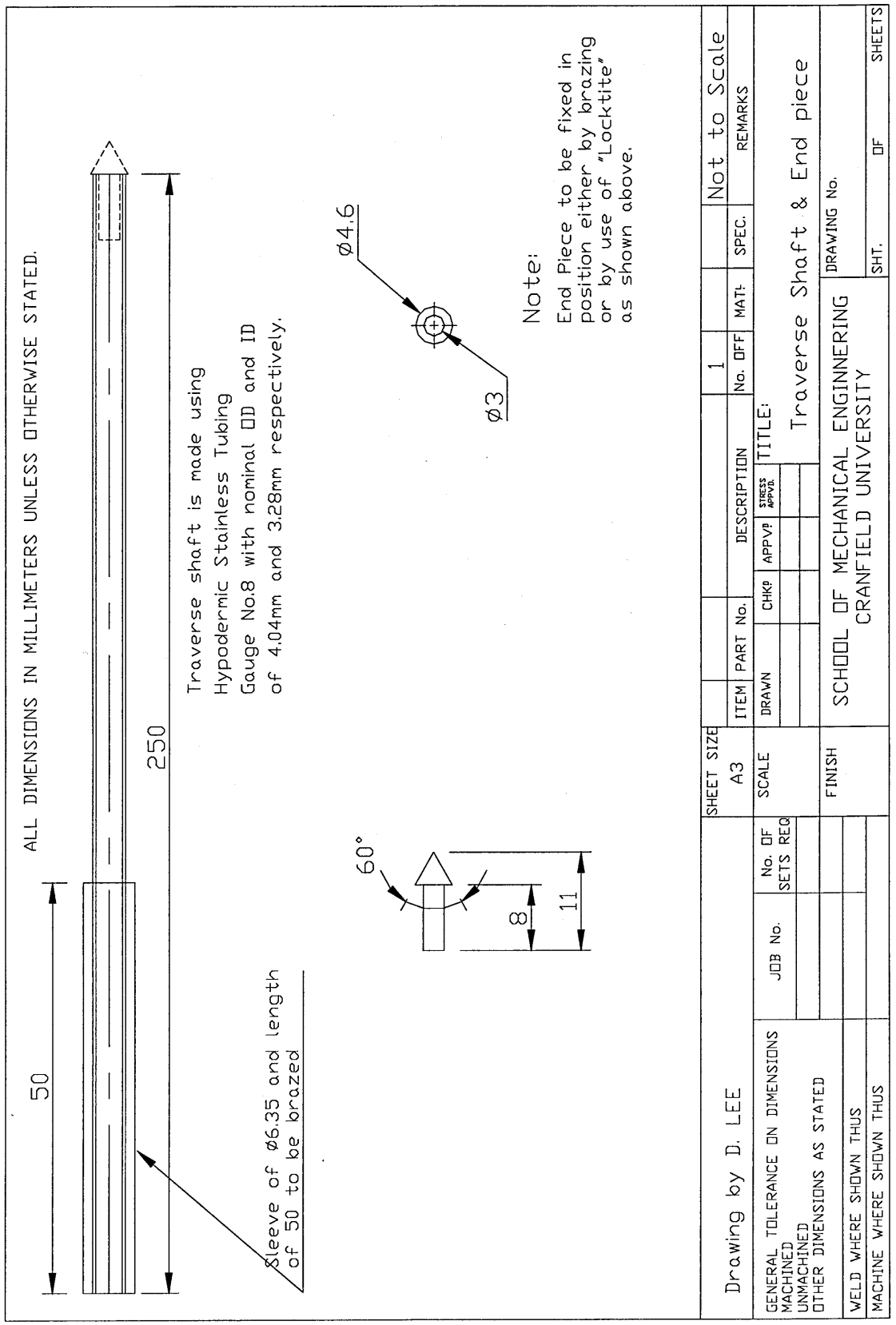

Figure C10 Traverse Shaft and End Piece No.2

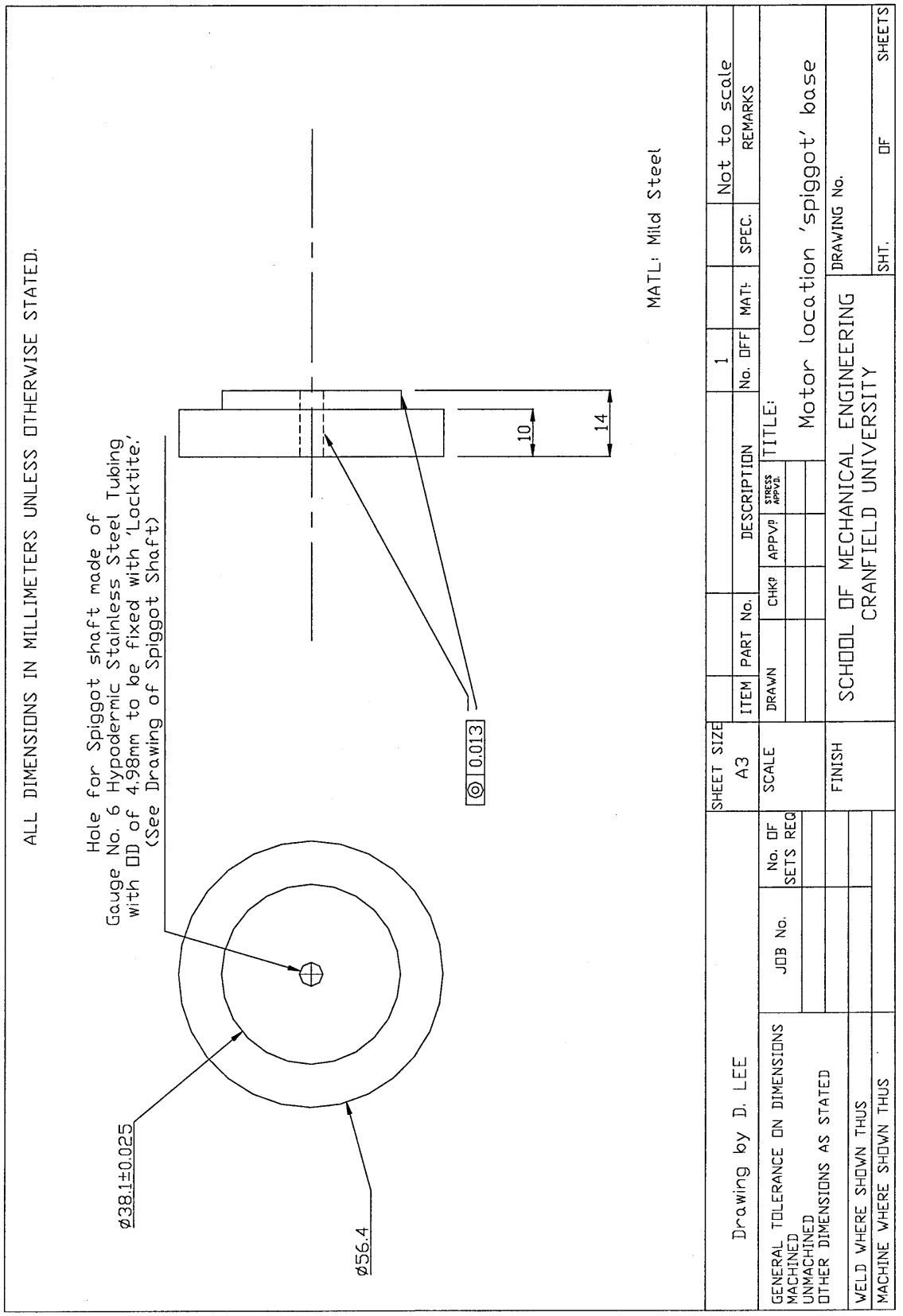

Figure C11 Spigot Base for Motor Location

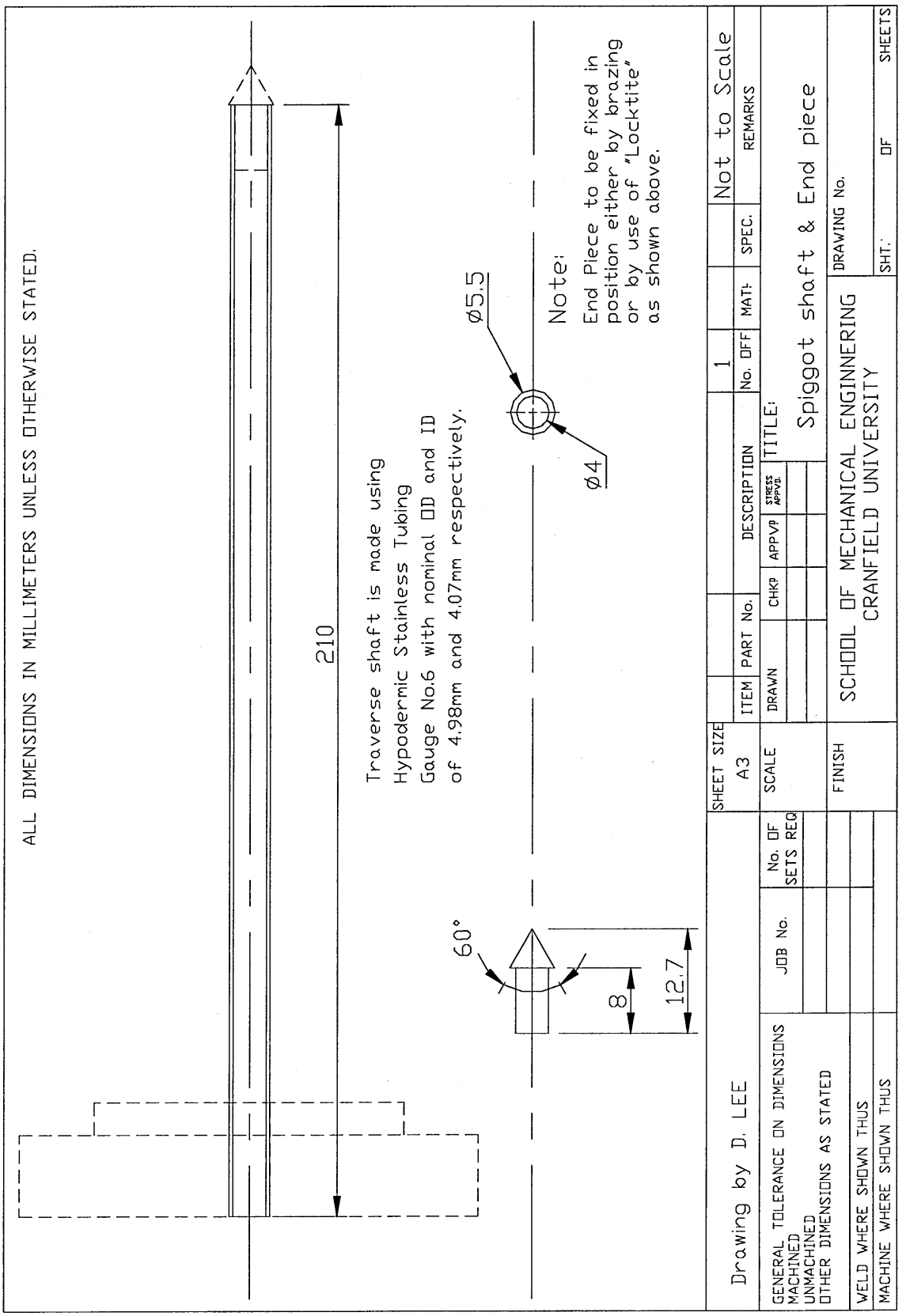

Figure C12 Spigot Shaft and End Piece

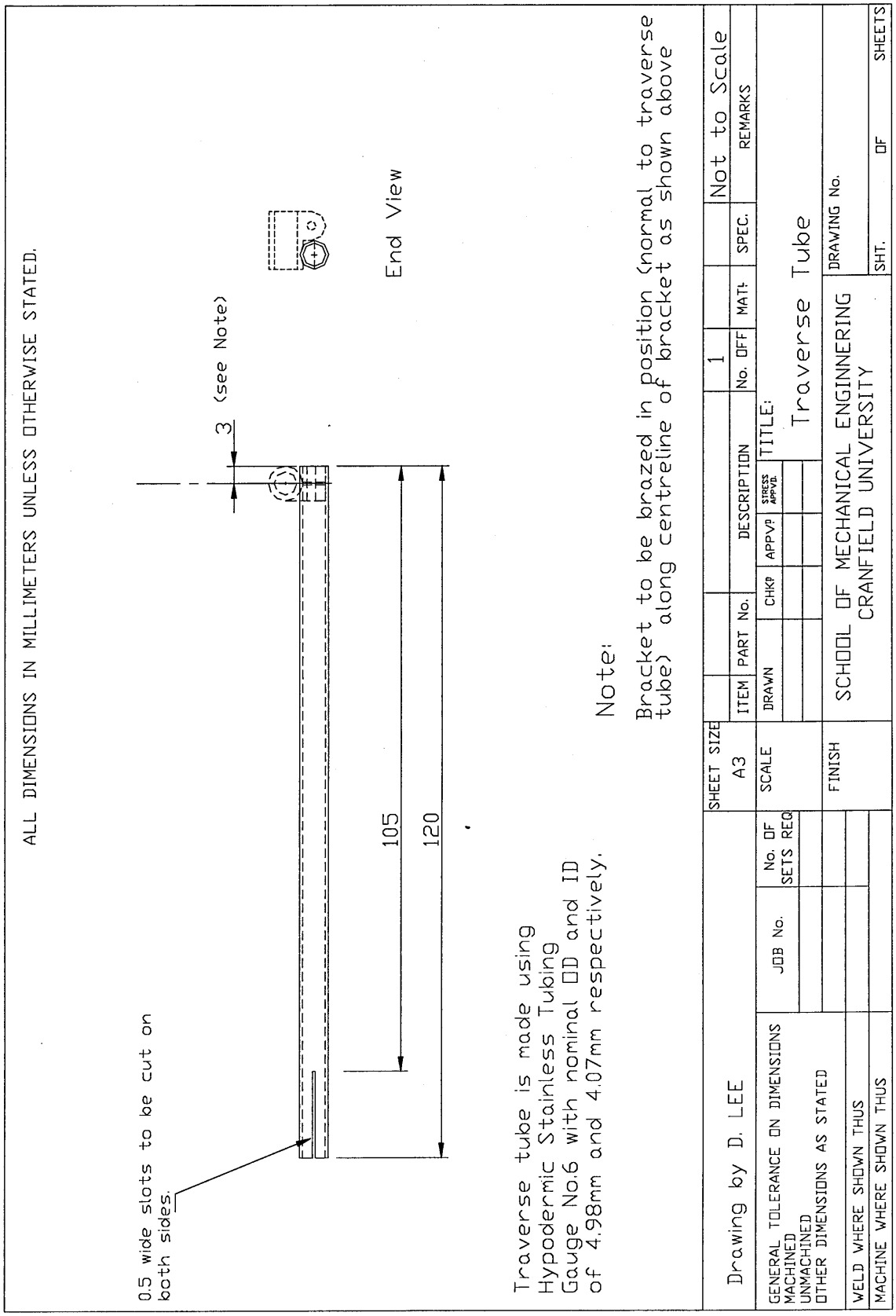

Figure C13 Traverse Tube

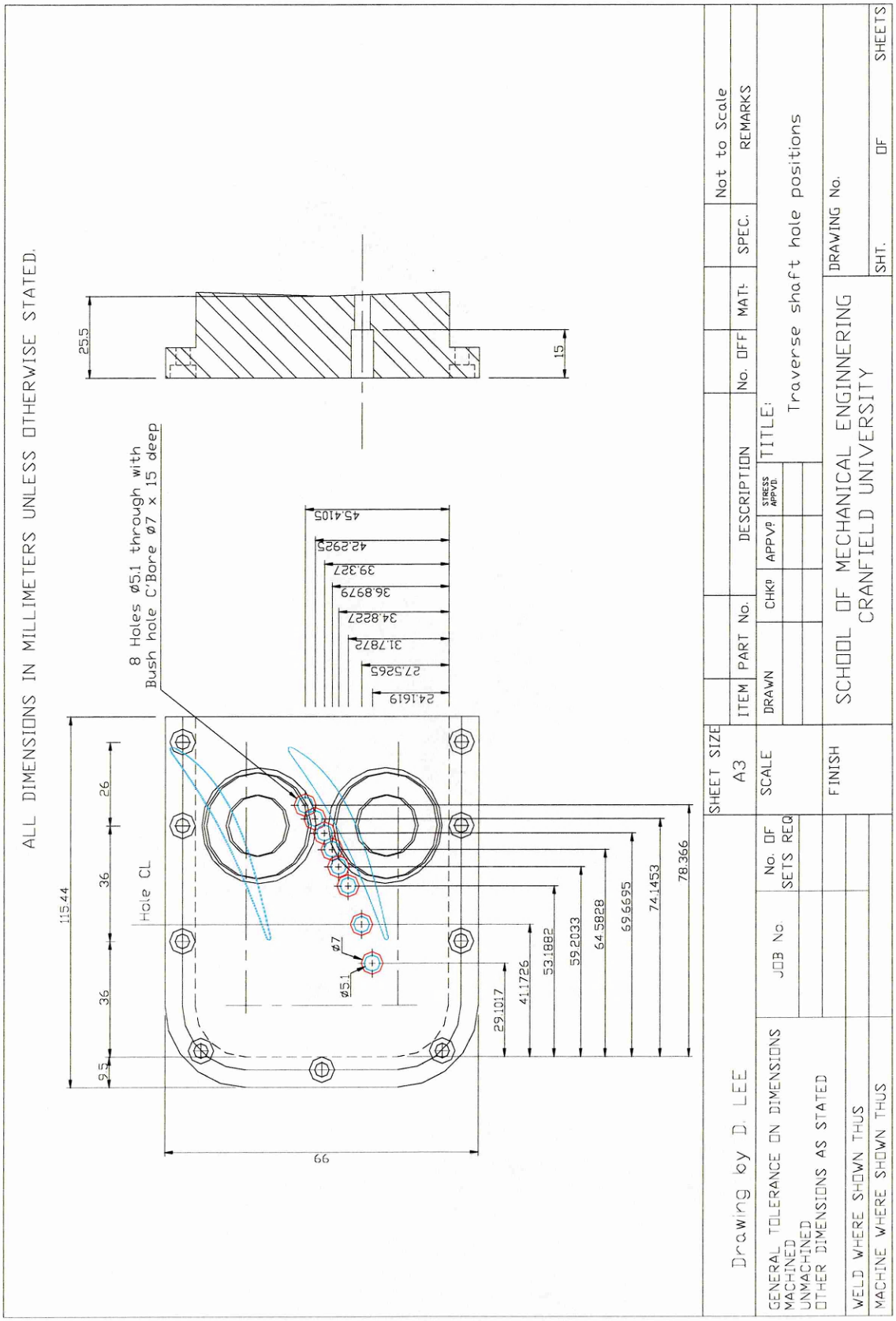

Figure C14 Traverse Shaft Hole Locations

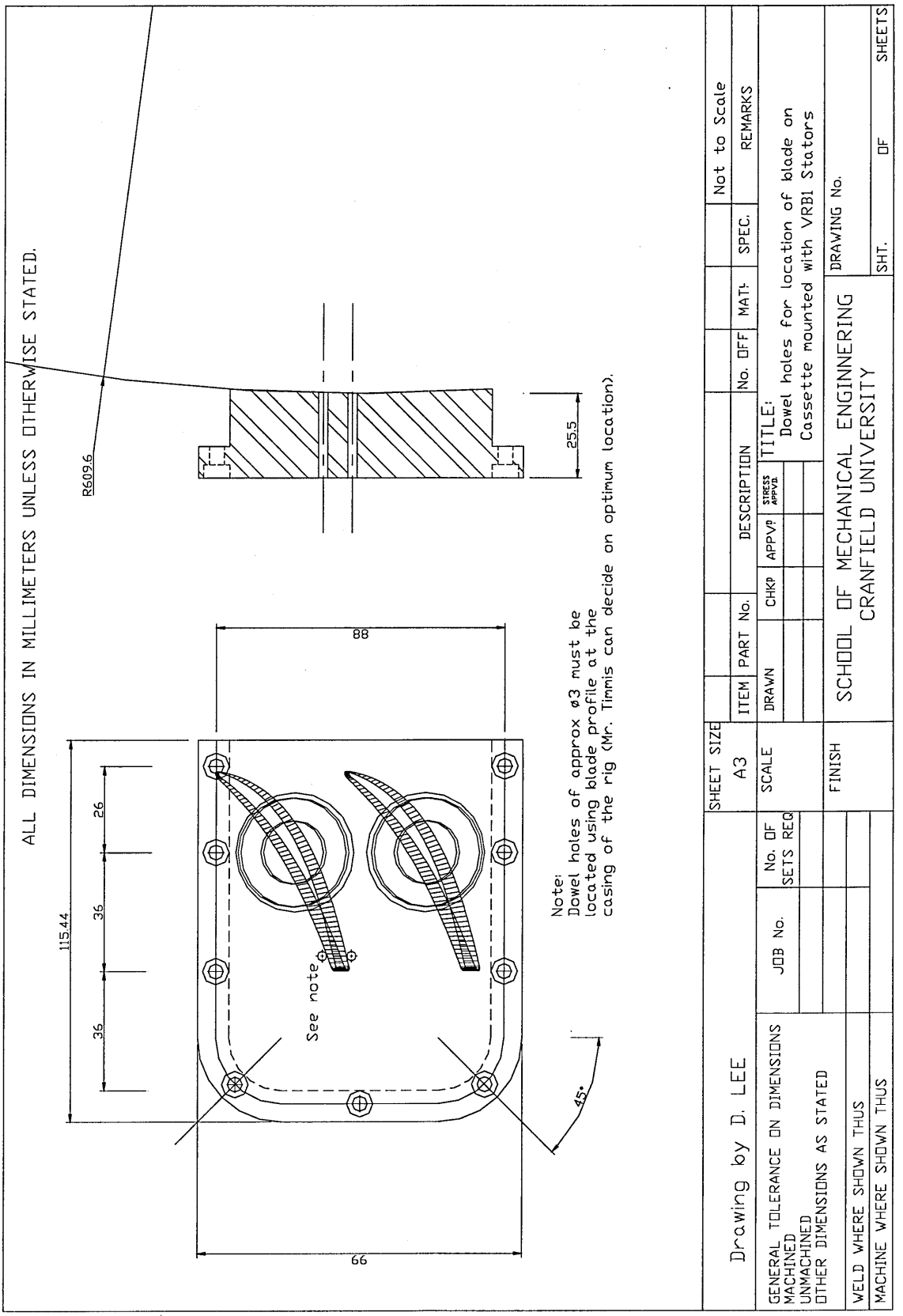

Figure C15 Dowel Holes for Location of Stator Blade

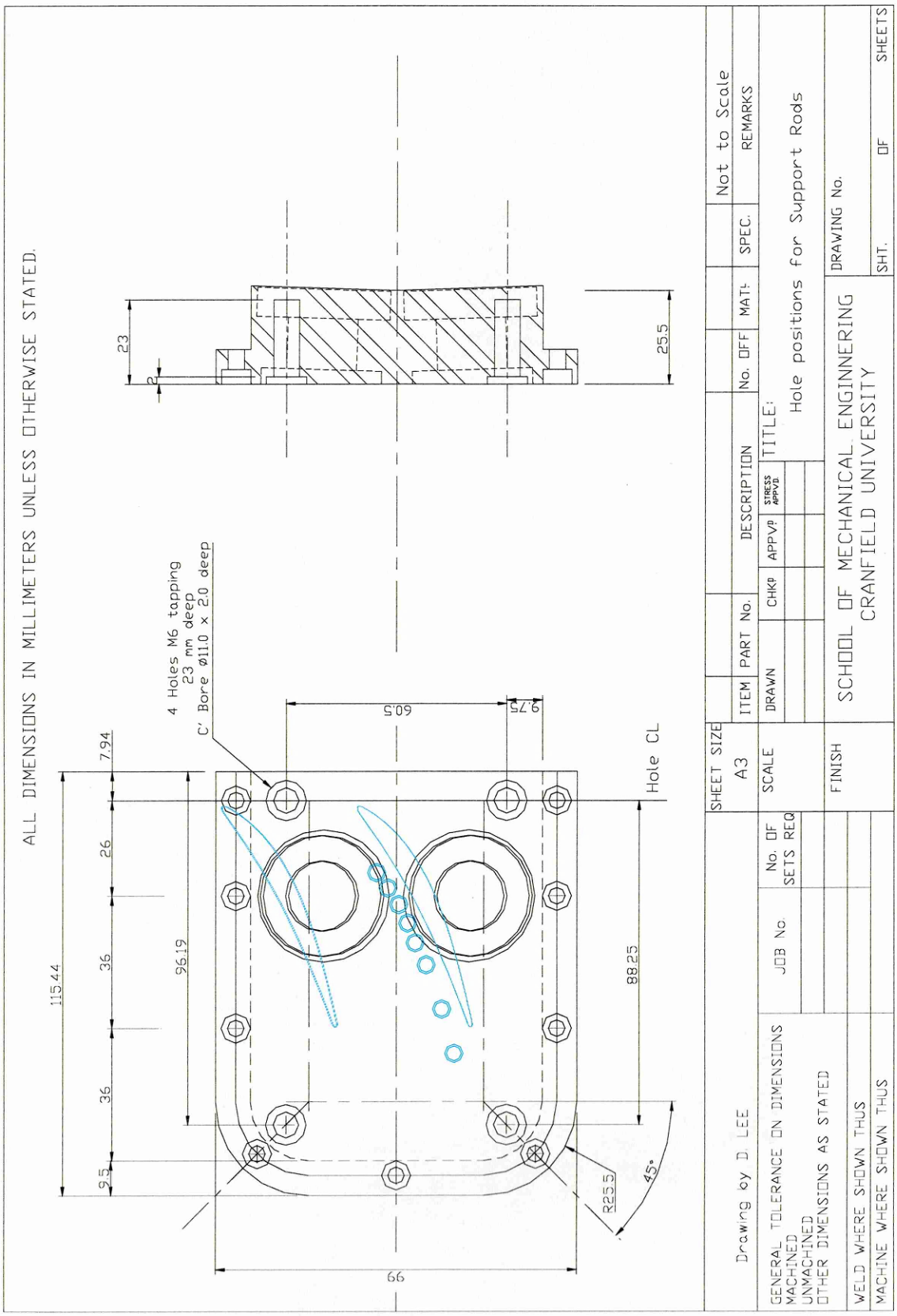

Figure C16 Support Rods Positioning Holes

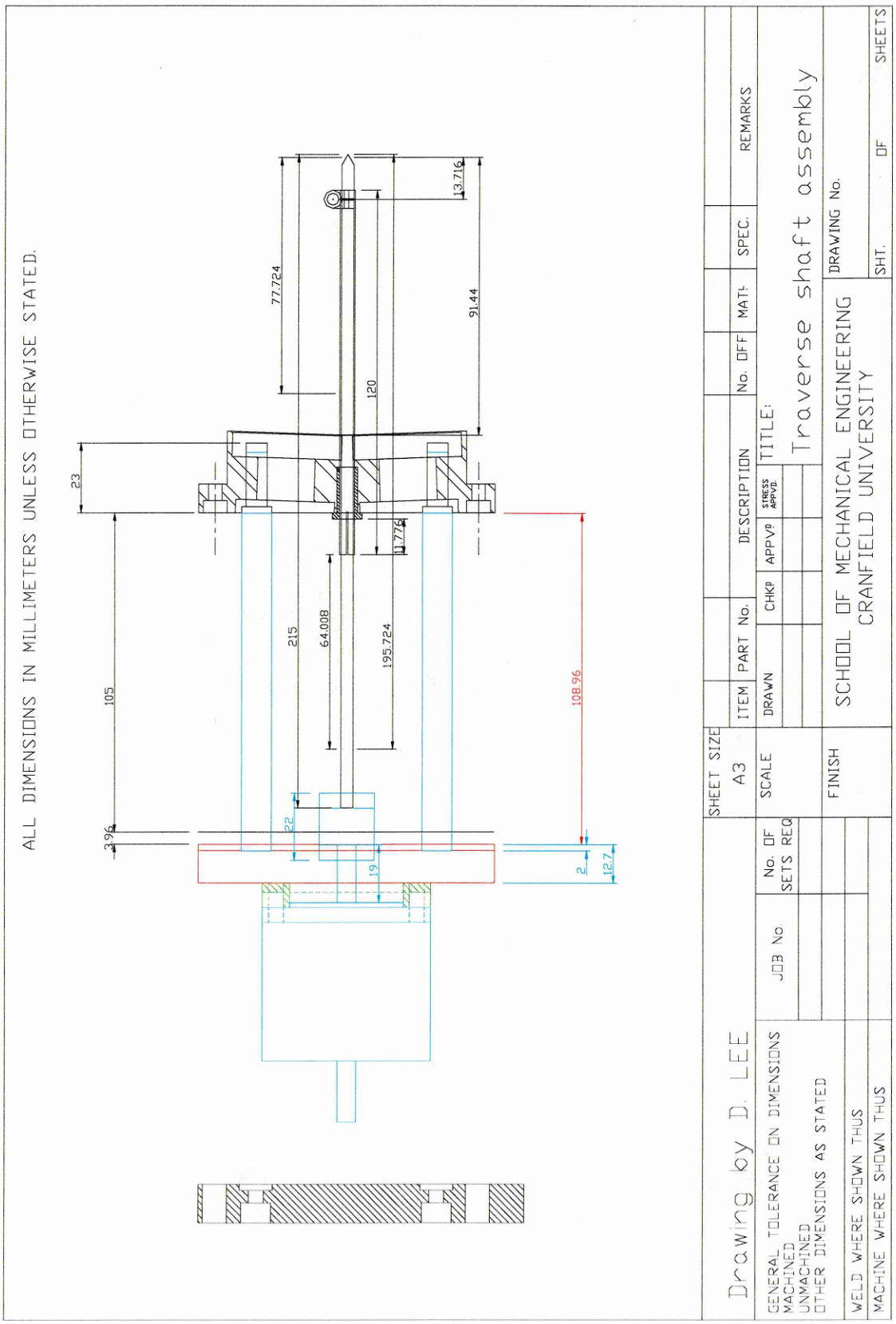

Figure C17 Traverse Assembly